Development and Characterization of GM2 Gangliosidoses Mouse Models

By

Emily Barker

A Thesis submitted to the Faculty of Graduate Studies of the University of Manitoba in partial fulfilment of the requirements for the degree of Master of Science

Department of Biochemistry and Medical Genetics
Max Rady College of Medicine
Rady Faculty of Health Science
University of Manitoba
Winnipeg, Manitoba

Abstract

GM2 gangliosidoses are a group of rare lysosomal storage disorders (LSDs) characterized by lysosomal accumulation of GM2 ganglioside in the nervous system, resulting in a range of neurodegenerative disorders. These disorders result from mutations in the genes encoding the α- or β-subunits of the enzyme β-hexosaminidase A (HexA), or more rarely the GM2-activator protein. Loss-of-function mutations in *HEXA,* encoding the α-subunit, cause Tay-Sachs disease (TSD) whereas mutations in *HEXB,* encoding the β-subunit, cause Sandhoff disease (SD). Successful therapies are available for many lysosomal storage disorders, however none of these are available for treatment of GM2 gangliosidosis. While mice models of SD with juvenile onset have been available for many years, attempts to create similar TSD models have failed due to a sialidase bypass that degrades GM2 in mice. Juvenile-onset TSD mice have since been created by knocking out both *Neu3* and *Hexa* genes. Late-onset GM2 gangliosidosis models in mice have yet to be successfully created.

In this study we attempted to create a late-onset GM2 gangliosidosis model using the most common adult onset *HEXA* mutation in humans, c.805 G>A p. G269S combined with $Neu3^{-/-}$. The resulting $HexA^{G269S/G269S}$ knock-in, $Neu3^{-/-}$ animals, referred to as the knock-in knock-out model (KIKO) were compared with a previously reported juvenile-onset $Hexa^{-/-}$ $Neu3^{-/-}$ double KO model (dKO) and controls. Monitoring of disease onset, signs of illness and changes to behaviour or neurological phenotype using a variety of methods were undertaken to assess if differences could be detected between these models. dKO and KIKO mice did not display any significant differences in phenotype when compared to each other but did model juvenile GM2 gangliosidoses compared to controls. Motor deterioration, tremors, gait disturbances and behavioural changes were observed in both models. Enzyme activity of HexA in both models was reduced, and no increase in residual activity was observed in KIKO animals. Histological and gross anatomical investigations confirmed widespread accumulation of GM2 throughout the brains of both dKO and KIKO animals. Decreased survival of KIKO and dKO compared to controls was consistent with previously reported dKO models.

Acknowledgements

I have many people to thank for supporting me through my academic journey. These people have help train me in laboratory techniques and given me the knowledge base to succeed in this field, but most importantly they've fostered my curiosity, built my confidence, and improved my critical thinking beyond what I expected during my time here.

First, I'd like to thank my supervisor Dr. Barbara Triggs-Raine, who has been an instrumental mentor throughout my journey into research. I first started in her lab as an undergraduate co-op student working on the HYAL2 project. I didn't have any lab experience outside of my university classes, but Barb was willing to take me on and train me. In addition to training me, she was eager to hear my ideas and encouraged me to conduct my own experiments once I had a grasp of the project. She guided me through this, giving adjustments when needed but also motivated me to search the literature for my own answers. Whether or not these experiments were successful, her willingness to let me try something new fostered my curiosity, allowed me to think about my results in a meaningful way and developed the skills I needed to present my research to a group of peers. I'm so grateful for the opportunities she gave me to learn during my undergraduate degree, it truly gave me the confidence I needed to begin a graduate degree. This mentorship only continued to grow throughout my graduate degree, and her suggestions for both personal and professional development have been greatly appreciated. The opportunities she provided for me to mentor and train other students allowed me to grow my confidence further and develop teaching skills. Despite her busy schedule as department head, there's never been a time I've felt neglected. The supportive environment she provides has made all the difference during these last few years and has allowed me to grow in countless ways.

Secondly, I'd like to thank our research associate Dr. Richard Hemming, who has been vital to my successes in the lab. Rick has been truly invaluable; the guy to go to when google didn't have the answers to my questions anymore. He has dedicated countless hours to my training, provided much needed technical advice and is always willing to lend a hand to anyone who needs it. He's kept the lab a happy place, always cracking jokes with us between helpful remarks about our experiments and techniques.

I'd also like to thank Dr. Elaine Anjos (post-doctoral fellow), Mehrafarin Ashiri (graduate student), Agnes Fresnoza (transgenic services technician) and Betselot Betemariam (undergraduate student technician) for their support, direction, and all the advice they've provided me, whether through helping directly with experiments and genotyping or simply grabbing a coffee with me.

Third, I'd like to thank my committee members, Dr. Marc Del Bigio and Dr. Brian Mark, who have asked thought provoking questions and provided perspectives to the project I hadn't thought of. Their thoughts on how to improve my presentation skills and research have been truly insightful.

Fourth, I'd like to thank all past members of the Triggs-Raine Lab, Dr. Wafa Kammouni, Promita Ghosh, Steven Cooper, Deanne Nixie Miao, Nik Furletti, and Shirley Yu for their support. The advice, training, help with experiments, or the teaching opportunities you provided me have helped me greatly to grow as a researcher.

Fifth, I'd like to thank our Department of Biochemistry and Medical Genetics faculty and students for their input during seminars and classes, you've all taught me something along the way. I'd like to especially thank Dr. Hao Ding and Xiaoli Wu for their assistance in histology and use of their equipment. I'd also like to thank our office staff, Lisa Zhang (past), Chloe Lepage (past), Philip Dufresne, Annan Sher, and Fadumo Osman for their assistance and guidance during this program. I'd like to acknowledge the Canadian Institute of Health Research, the University of Manitoba and Dr. Triggs-Raine for providing financial support throughout my degree.

Last, but certainly not least I'd like to acknowledge past mentors, family, and friends:

To the University of Manitoba Co-op team, without who I wouldn't have sought out my initial position in the Triggs-Raine lab, thank you for all the interview preparation, feedback, suggestions through my undergraduate degree, and continued career mentorship through my graduate degree. It has truly helped to get me to where I am today.

To the Riverine Fish Ecology Lab and Dr. Eva Enders at the Department of Fisheries and Oceans Canada, thank you for opening my eyes to other career paths during my undergraduate degree, and teaching me how to be adaptable to different working environments.

To my parents Donna and Derek, and my big sister Sarah, thank you for supporting my dreams from day one, being my biggest cheerleaders, and teaching me that I can do whatever I set my mind to. Spending time with you all unwinding and most importantly laughing has kept me sane through tough exam periods and stressful times. You've taught me that no matter what it will all work out.

To my friends Meagan, Lara, and Cara; while you may not understand exactly what it is I do (and sometimes look at me like I've grown a second head), you've always been thrilled when explaining to others that I "work with mice". Thank you for the late-night coffee runs, long phone calls, even longer nights out and most importantly the joy you've brought into my life. To my "science" friends, Michelle, Bre and Morgan, thank you for commiserating with me about the difficulties of graduate school, life, and career directions; we'll all figure it out in the end.

Table of Contents

List of Figures

Appendix Figures

List of Tables

Appendix Tables

List of Abbreviations

4-MU-NANA	4-Methylumbelliferyl N-acetyl-a-D-neuraminic acid
4-MUGS	4-Methylumbelliferyl-7-(6-sulfo-2-acetamido2-deoxy-β-D-glucopyranoside
BBB	Blood brain barrier
BSA	Bovine serum albumin
CP	Citrate phosphate buffer
crRNA	CRISPR RNA
DAB	3,3′-diaminobenidine
dKO	Double knock-out; *Hexa*$^{-/-}$ *Neu3*$^{-/-}$
DMF	Dimethylformamide
dpc	Days post coitum
EMS	Endomembrane system
ERAD	Endoplasmic reticulum associated degradation
ERT	Enzyme replacement therapy
FB	Fecal boli
GalNAc	N-acetylglucosamine
GC	Glycine carbonate buffer
GlcNAc	N- acetyl glucosamine
GM2	GM2 ganglioside
GM2AP	GM2 activator protein
gRNA	Guide RNA
GT	Gene therapy
HexA	β-hexosaminidase A enzyme
HexB	β-hexosaminidase B enzyme
HexS	β-hexosaminidase S enzyme
hHexA	Human β-hexosaminidase A enzyme
hNeu3	Human neuraminidase 3

KI	Knock-in
KIKO	KIKO; *Hexa*$^{G269S/G269S}$ *Neu3*$^{-/-}$
KO	Knock-out
KSOM	Potassium simple optimized medium
LC	Liquid chromatography
LC-ESI-MS	Liquid Chromatography Electrospray Ionization Mass Spectrometry
LSD	Lysosomal storage disorder(s)
M6P	Mannose-6-phosphate
M6PR	M6P receptors
Man	Mannose
mHexA	Mouse β-hexosaminidase A enzyme
mNeu3	Mouse neuraminidase 3
MU	Methylumbelliferone/7-hydroxy-4-methylcoumarin
MUG	4-methylumbelliferyl N-acetyl-b-D-glucosamine
Neu3	Neuraminidase 3
Neu5Ac	N-acetyl neuraminic acid
NGT	N-acetylglucosamine thiazoline
PBS	Phosphate buffered saline
PC	Pharmacological chaperones
PYR	Pyrimethamine
RBT	Ricin toxin B-subunit
RER	Rough endoplasmic reticulum
S	Sample PCR product
S^+	S mixed with PCR product from WT DNA
SA buffer	Sodium acetate buffer
SD	Sandhoff disease
SRT	Substate reduction therapy
ssDNA	Single-stranded DNA donor
TBE	Tris/borate/EDTA buffer

TBS	Tris buffered saline
TSD	Tay-Sachs disease
ZANA	Zanamivir (4-Guanidino-2,4-dideoxy-2,3-dehydro-N-acetylneuraminic acid)

1 Introduction and Background

1.1 Lysosomal Storage Disorders and the Endomembrane System: An Overview

Lysosomal storage disorders (LSDs) are a group of congenital conditions characterized by deficiency of a lysosomal protein, resulting in pathological substrate accumulation inside the cell. The first known report of LSDs was a patient with Tay-Sachs disease (TSD) in 1881[1], with others like Gaucher[2] and Fabry disease[3] described by the end of the 1800s. More than 50 years later, the discovery of the lysosome would begin the area of research connecting these diseases. LSDs were first postulated in 1965 by Henri-Géry Hers and contain a broad range of disorders including mucopolysaccharidoses, lipidoses and other types of metabolic storage disorders[4]. As of the early 2000s, more than 50 different LSDs had been described; all are characterized by undegraded substrates accumulating in the lysosomes leading to progressive, multisystem organ dysfunction[5].

Lysosomes belong to the endomembrane system (EMS), a group of membrane bound organelles including the rough endoplasmic reticulum (RER), Golgi complex, and endosomes (Figure 1). The EMS is primarily responsible for folding and post-translational processing of proteins destined for the lysosome or for secretion. The EMS is also involved in trafficking cellular materials, digestion of exogenous materials from phagocytosis, and recycling of endogenous materials through cellular autophagy. Lysosomes are the terminal compartment of the EMS receiving these exogenous and endogenous materials from endosomes. Characterized by proton ATPase pumps on their membranes and a lack of mannose-6-phosphate (M6P) receptors, they are an acidic cellular compartment filled with the hydrolytic enzymes responsible for cellular digestion and autophagy[6].

mRNA coding for proteins destined for the endomembrane system are usually translated directly into the RER lumen. Once inside the RER, proteins are properly folded with the help of molecular chaperones. Lysosomal proteins undergo N-linked glycosylation, in which one or more high mannose oligosaccharides containing N-acetylglucosamine (GlcNAc) and mannose (Man) is attached, before being packaged into vesicles and moving to the *cis*-Golgi. At the Golgi, lysosomal proteins are modified with phosphorylation of Man on the oligosaccharide chain, creating an M6P tag. M6P receptors (M6PR) recognize this tag and transfer these proteins into the late endosome. M6PRs dissociate from their ligand in the late endosome, recycling back to the Golgi or travelling to the cell surface. Lysosomal proteins are packaged into the lysosomal lumen, and the acidic environment allows for the protein to become its final active form. Lysosomal proteins can also be recaptured at the cell surface by M6PR and retargeted to the late endosome[6,7].

Defects in processing at any point of this system can cause LSDs and typically result from mutations to genes encoding the enzymes, soluble activator proteins, integral proteins, and transporter proteins of the lysosome. Mutations effecting mRNA processing (splicing, capping, poly-adenylation) or frameshift mutations that result in nonsense mediated decay of transcripts commonly result in total deficiency[8]. Small in-frame insertions, deletions or point mutations result in extended protein-chaperone interaction and are retained in the RER. Although these proteins may be catalytically active, delayed folding or failed post translational modification do not pass the RERs quality control system and are removed by endoplasmic reticulum associated degradation (ERAD)[9]. This early removal of mRNA transcripts or nascent proteins results in low protein levels and severe phenotypes. Less severe phenotypes and later onset disease is typical

when small amounts of mutant protein can escape ERAD, making their way to the lysosome where the residual activity can act on the substrate as intended[6].

LSDs vary in onset, symptoms and clinical treatment depending on the severity of mutation and enzyme system affected. However, a genetic component, substrate accumulation, disability, organ dysfunction and premature death are common to all LSDs. Phenotypic variation in onset within the same disease is also common, with acute-early onset occurring with severe deficiency and chronic-late onset with residual enzyme activity. Early onset patients often present with hydrops fetalis, facial dysmorphism, skeletal dysplasia, developmental delay/regression, or hepatosplenomegaly. Late onset patients more often present with psychiatric illnesses, musculoskeletal symptoms, and progressive neurological symptoms such as ataxia and spasticity[10]. Neurological dysfunction is a dominating feature of the sphingolipidoses, LSDs in which sphingolipids are the accumulating substrate. Sphingolipid turnover in the central nervous system during development and maintenance is catabolized by a series of soluble enzymes and their activator proteins in the lysosome. Examples of sphingolipidoses include GM2 gangliosidoses, including TSD and Sandhoff disease (SD), along with GM1 gangliosidoses, Gaucher, and Fabry disease[5].

Overall incidence of individual LSDs is low, although collectively 1 in 5000 live births will have some form of LSD[11]. Some populations have disproportionately high incidence resulting from genetic isolation and founder effects. Ashkenazi Jewish populations are one such group, where the prevalence of Gaucher disease is 1:885 individuals compared to 1:57000 in other populations[12].

Significant advances have been made in the treatment of some LSDs since their discovery. Gaucher disease was the first to be successfully treated using enzyme replacement

therapy (ERT) by infusing purified enzyme to replace deficiencies[13]. Other treatments such as tissue transplants, substrate reduction, gene therapy, or use of molecular chaperones have also been used with variable success [13,14]. However, for many diseases like the GM2 gangliosidoses successful ERT or gene therapy has yet to be developed and thus only supportive care can be offered[15].

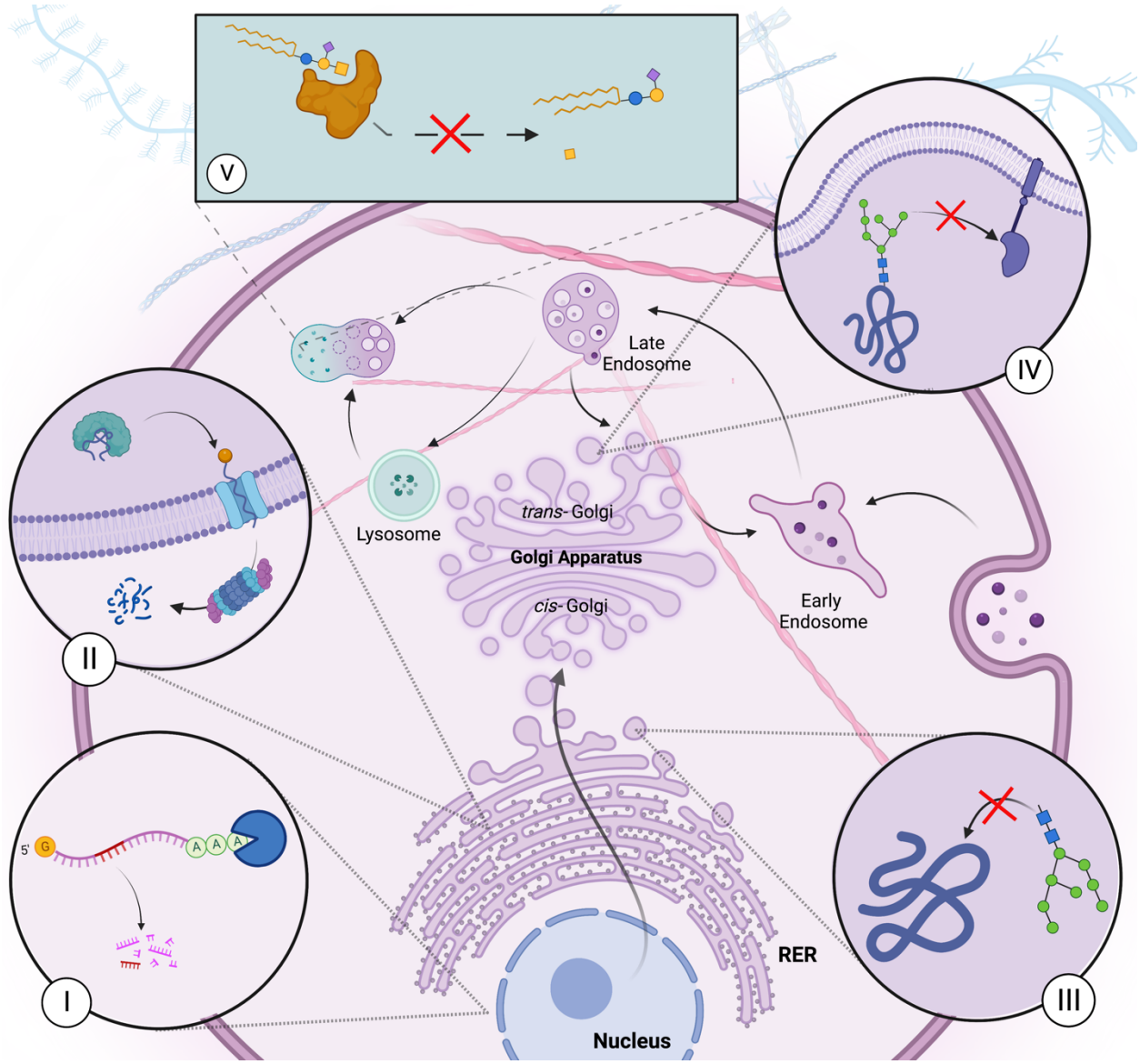

Figure 1. The Endomembrane System

The endomembrane system with defects commonly found in LSDs. I) Defects of mRNA processing (splicing, capping, or poly-adenylation) or nonsense mediated decay. II) ERAD; Mis-folded protein retained by chaperones, tagged with ubiquitin (orange), and transported to the cytoplasm for degradation by the proteasome. III) Defects in glycosylation at the ER block the transfer of lysosomal pre-protein out of the ER. Long term retention in the ER typically results in ERAD (see II). IV) Defects in glycosylation at the Golgi, particularly in creation of M6P tags, blocks MP6R interaction and proper targeting to the lysosome. V) Mutation to enzymes can decrease or delete enzyme activity on substrates at the lysosome. Pathway of intracellular trafficking of vesicles is indicated by arrows. Figure made with BioRender.

1.2 GM2 Gangliosidoses: Overview and History

GM2 gangliosidoses, TSD, SD and GM2 activator protein (GM2AP) deficiency are all rare LSDs characterized by accumulation of GM2 ganglioside (GM2) in the nervous system, resulting in a range of neurodegenerative disorders. These disorders result from mutations in the genes encoding the α- or β-subunits of the enzyme β-hexosaminidase, or more rarely GM2AP.

TSD was the first of these conditions to be described independently by ophthalmologist Warren Tay and neurologist Bernard Sachs in infants of Ashkenazi Jewish descent. Tay originally noticed the condition in a child he was treating and published his findings of macular degeneration in 1881 [1]. In 1887, Sachs described the pathology of the disease upon discovering it independently. Originally called familial amaurotic idiocy, Sachs concluded that the condition was passed through families. The neurodegenerative nature, familial transmission, and pathological findings of 'ballooned' neuronal cells filled with lipid at autopsy were the only information about this acute infantile disease at the time[16]. The mode of transmission, cellular mechanisms, genes, or accumulating substances involved would not be elucidated for many years.

Forty years later, tracking TSD cases within 80 families lead Slome to determine the disease was passed in an autosomal recessive manner in the 1930s[17]. Gangliosides, neuraminic acid containing sphingolipids, had been known to exist since the late 1920s[18] but further work by Klenk in the early 1940s provided their name, improved methods of extraction and helped to characterize their structure. Soon after his characterization of gangliosides, Klenk determined that the accumulating substance in TSD patients was a ganglioside [19]. Finally in 1962, Svennerholm isolated gangliosides from post-mortem brains of TSD patients and identified GM2

ganglioside as the accumulating substance[20]. By 1963, the structure of GM2 ganglioside was determined by Makita and Yamakawa, and later confirmed by Ledeen and Salsman [21,22].

In the late 1960s, after the discoveries of the lysosome by de Duve and proposal of LSDs by Hers[4], further investigation of the proteins responsible for ganglioside metabolism were made. In 1967, Gatt demonstrated that other sphingolipidoses such as Gaucher disease and Neimann-pick disease had defects in the stepwise degradation of gangliosides caused by acid hydrolase deficiency[23]. A year later, Robinson and Stirling isolated 2 β-hexosaminidase isoenzymes, named HexA and HexB from human tissue[24]. By the end of the 1960s, O'Brien and Okada displayed that the HexA isoenzyme was absent from the tissues of TSD patients. Using a labeled GM2 substrate, HexA deficiency was confirmed to limit catabolism of GM2 ganglioside and the molecular cause of TSD was elucidated[25].

Around this time, Sandhoff described TSD with visceral involvement, in which both HexA and HexB were deficient. This would later become known as Sandhoff disease or GM2 gangliosidoses O variant. An additional patient was also described with suspected TSD, but normal hexosaminidase activity. This would later become known as GM2AP deficiency, or GM2 gangliosidoses AB variant[26].

The new ability to detect HexA levels in tissues allowed diagnostic and preclinical carrier screening to become a reality. The first TSD prevention programs began in the early 1970s aiming to provide education, carrier screening and genetic counselling to the Jewish communities in Washington, D.C. and Baltimore, Maryland. Further programs initiated in various locations lead to >90% decrease in TSD incidence[27].

By 1973, the subunit structure of both HexA and HexB was revealed by Beutler and explained the difference between TSD and SD patients[28]. This, however, still did not account for

normal hexosaminidase activities in the AB variant. A decade of research from the mid 1970s to mid 1980s led by Conzelmann and Sandhoff determined that these patients had GM2AP deficiencies, and that the GM2AP-GM2 ganglioside complex was required for GM2 ganglioside catabolism[29].

By the end of the 1980s, localization, cloning, structure of the α and β subunit genes, along with their amino acid sequences were elucidated by Proia and O'Dowd, and the gene for GM2A was localized by Schroder and Burg [30–32]. These discoveries provided the basis for further analysis of individual mutations and their mode of causing disease, providing greater understanding of the GM2 degradation system and modes of treatment. The last 20 years have been focused on creation of animal models, research into the biochemical mechanism of the GM2 degradation system, as well as investigating efficacy of various treatments. Today, more than 150 different mutations have been described to cause GM2 gangliosidoses, but no treatments to prevent or reverse the disease have been discovered[15].

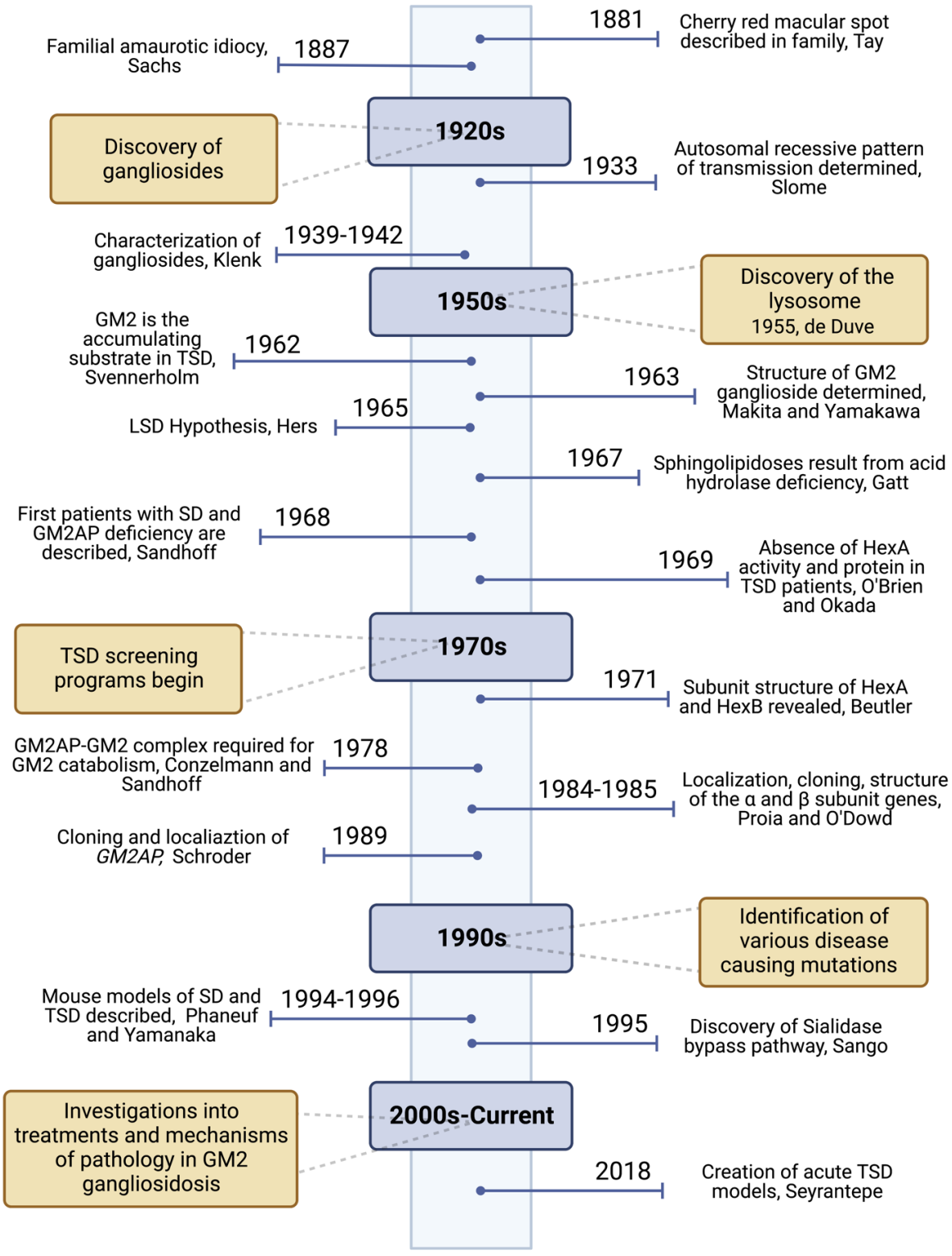

Figure 2. History and Important Discoveries in GM2 Gangliosidoses Research from 1880s to Present.

Figure made with Biorender

1.3 β -Hexosaminidase System and GM2 Ganglioside Degradation

The β-Hexosaminidase system consists of HexA, an αβ heterodimeric enzyme, along with two homo-dimeric enzymes HexB (ββ), and HexS (αα). The subunits for these isozymes are encoded on two evolutionarily related genes, *HEXA* the gene encoding the α-subunit and *HEXB*, the gene encoding the β-subunit, with 60% similarity between their primary amino acid sequences[33]. In their assembled forms, HexA and HexB are responsible for the degradation of GM2 ganglioside and globoside respectively. TSD is caused by loss-of-function mutations in *HEXA* and results in HexA deficiency, whereas SD is caused by mutations in *HEXB*, and results in HexA and HexB deficiency. Mutations in the GM2 activator protein gene, *GM2A,* lead to a condition with normal hexosaminidase activities but inability to extract GM2 from the lysosomal membrane, resulting in a third type of GM2 gangliosidoses with an identical phenotype to TSD[26].

HEXA, located on chromosome 15q24.2, spans a 35kb sequence, while *HEXB* spans a 40kb sequence located on chromosome 5q12 [34,35]. Both contain 14 exons and encode for proteins of similar sizes[30,36].*GM2A*, located on chromosome 5q31.2, contains 4 exons spread over a 16 kb sequence[32]. Notably, mRNA transcripts for *HEXA* or *HEXB* are not found in classical TSD or SD respectively, suggesting mutations that lead to nonsense mediated decay are common in these forms of disease[37]. *HEXA* may be alternatively spliced, while only one transcript of *HEXB* has been found[38,39].

Both *HEXA* and *HEXB* transcripts are translated into the RER lumen as pre-proproteins, which are then proteolytically cleaved to remove signal peptides, glycosylated with N-linked high mannose residues and folded[37]. Dimerization of β-subunits to form HexB also occurs here facilitated by binding of glycosyl residues to receptors within the RER and is essential for

transfer to the Golgi[40]. Dimerization of α and β subunits to form HexA is a slower process and occurs in a pre-lysosome compartment before being rapidly transferred to the lysosome[41].

The active site of the β-subunit in HexA and HexB can hydrolyze β-linked N-acetyl-D-hexosamines such as N-acetylglucosamine (GlcNAc) and GalNAc from oligosaccharides attached to a variety of neutral compounds[22]. However, the α-subunit of HexA is solely responsible for the hydrolysis of GalNac from GM2 ganglioside in the presence of GM2AP[42]. HexS, which is only detected in SD patients at low levels, acts on sulfated glycans such as chondroitin-6-sulfate trisaccharide[43]. Proper dimerization is essential for enzyme activity, and no evidence of activity in monomeric subunits has been shown[41].

GM2 ganglioside, the substrate of HexA, is an intermediate in the metabolism of higher brain glycosphingolipids such as GM1 ganglioside, and a component of nervous system cell membranes. Gangliosides found within membranes are important glycosphingolipids for signal transduction, cell to cell recognition, as well as complex neurological processes [44]. GM2 ganglioside contains a GalNAcβ(1-4)- [Neu5Ac (2-3)-]-Gal β (1-4)-Glc carbohydrate structure attached to ceramide[45]. In normal cells, GM2AP extracts GM2 from the lysosomal membrane allowing it to enter the aqueous environment of the lysosomal lumen where HexA resides[46]. The terminal GalNAc is guided to the active site of the HexA α -subunit, while positively charged amino acid residues around the α-subunit active site stabilize the negative charge from the adjacent N-acetyl neuraminic acid (Neu5Ac). While the active site of the β-subunit is negatively charged, repelling Neu5Ac residues, the β-subunit is essential to stabilize the interaction between GM2AP:GM2 and HexA. The quaternary complex, GM2AP:GM2 ganglioside with GalNAc positioned in the HexA α -subunit active site allows hydrolysis, releasing the GalNAc monosaccharide and GM3 ganglioside for further degradation[47] (Figure 3).

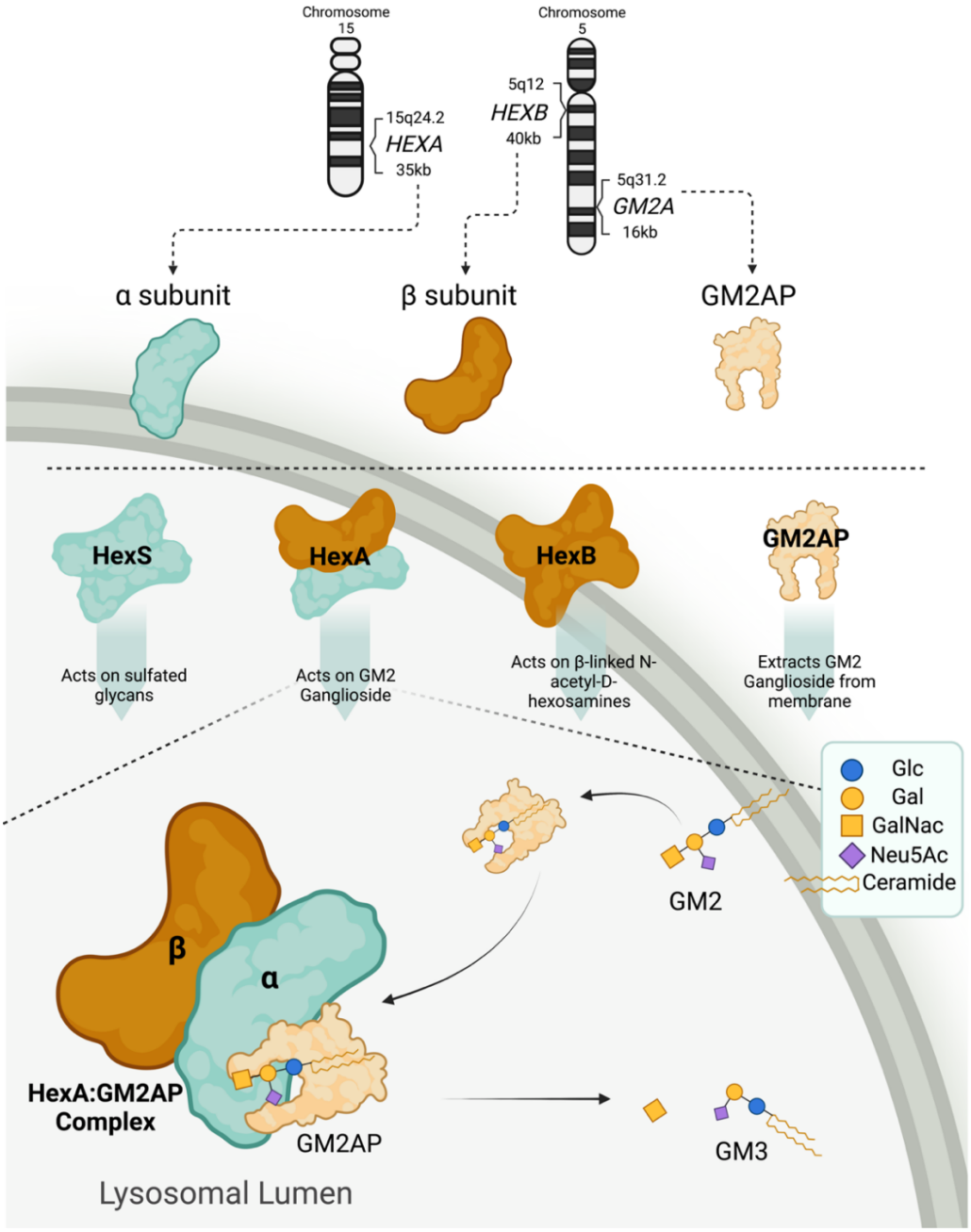

Figure 3. GM2 Degradation System.

Chromosome location, length of genes and proteins produced important for GM2 ganglioside degradation. HexS, HexA, and HexB enzymes with subunit conformations, along with GM2AP and their targeted substrates in humans are shown. GM2 degradation at the lysosome begins with GM2 extraction from the lysosomal membrane by GM2AP, which guides the terminal GalNAc of GM2 into the active site of the α subunit. Formation of this HexA:GM2AP complex is followed by hydrolysis of GM2 into GalNAc and GM3 ganglioside. Abbreviations: Glc; glucose, Gal; galactose, GalNac; N-Acetyl galactosamine, Neu5Ac: N-acetyl neuraminic acid. Figure made with Biorender.

1.4 GM2 Gangliosidoses Classification and Pathology

Due to the diversity of genetic mutations found in various genes, GM2 gangliosidoses vary widely in presentation, onset, and symptoms. Severity and onset of disease depend on the level of residual HexA activity, and symptoms become more severe as GM2 ganglioside accumulates[44].

GM2 gangliosidoses can be categorized based on onset, with 3 main subtypes: acute-infantile, subacute-juvenile or chronic-adult. Acute-infantile GM2 gangliosidosis is the most severe form of the disease, and includes TSD, SD, and GM2AP deficiency. Regardless of genetic cause, patients are initially normal at birth and disease progression is similar. Signs of illness appear within the first year of life and include the slowing or regression of developmental milestones, exaggerated startle response, muscle weakness and characteristic cherry-red macular spot. The maculae become opaque as GM2 ganglioside accumulates while the fovea, an area with fewer cellular layers, remains transparent to the red choroid below. This produces a red spot at the fovea with pale peri-foveal area in the macula[48].

By 18 months, rapid vision loss, difficulty swallowing, seizures and progressive macrocephaly are common. Patients with GM2AP deficiency are exceedingly rare, but all have acute-infantile disease identical to those with TSD[49,50]. In SD, there is additional visceral involvement and oligosaccharidiuria is found[48]. While presentation is the same, hexosaminidase activity varies between these diseases. In TSD, total hexosaminidase activity is normal due to the presence of active HexB, however HexA activity is absent. In SD total hexosaminidase activity is low due to the loss of both HexA and HexB, but 2-4% of normal activity is detected from active HexS[51,52]. With supportive care children can survive for 5-7 years however most succumb to their illness between 2-3 years[15].

Subacute-juvenile and chronic-adult GM2 gangliosidoses are the result of mutations to either *HEXA* or *HEXB* genes and are referred to as the B and O variants, respectively. Patients with these types have milder mutations, resulting in residual HexA activity between 1-5%[37,52,53]. Onset is determined by residual HexA activity, with juvenile-onset patients experiencing lower activity levels than adult-onset patients. The critical threshold for disease is estimated to be between 5-10% residual HexA activity, and individuals with activity above this level are asymptomatic[48,54].

Subacute-juvenile GM2 gangliosidoses is the least common of the GM2 gangliosidoses and is characterized by moderate disease progression. Onset is typically between 3-5 years of age and presents as slowing and eventual regression of developmental milestones. Cerebellar atrophy followed by cerebral atrophy is also characteristic upon brain imaging studies. By 10 years most patients experience progressive vision loss, dysphagia, abnormal gait or mobility issues, and seizures, before entering a vegetative state that becomes fatal by age 15-20[55,56].

Chronic-adult GM2 gangliosidoses present in late adolescence, usually within the second decade of life and have the most phenotypic variation between patients[15]. Patients initially present with lower muscle weakness due to loss of anterior horn motor neurons. Clumsiness and incoordination due to cerebellar atrophy and mild spasticity are also early signs[44,57]. Acute psychosis is more common in patients with *HEXA* mutations, while early sensory symptoms are more common in patients with *HEXB* mutations[58,59]. As the disease progresses, ambulation becomes difficult with inability to coordinate movements and muscle wasting in the lower extremities. Typically, lower muscle dysfunction is followed by progressive weakness to the upper extremities[60]. Due to this, adult forms of GM2 gangliosidoses are often misdiagnosed as spinal muscular atrophy or spinocerebellar ataxias[61]. Speech difficulties also emerge as a

prominent feature due to cerebellar dysarthria and spasmodic dysphonia, with characteristic 'breathy,' fast-paced speech and stuttering [62]. Patients with O variant have additional visceral accumulation of oligosaccharides causing visceromegaly. Most patients survive until the 3rd or 4th decade of life, with some having normal lifespans[15,48,49].

The neurodegeneration observed in GM2 gangliosidoses is due to multiple factors. First, accumulation of GM2 ganglioside disrupts cell functionality, particularly in the EMS leading to reduced cellular ability for autophagy and metabolism[63,64]. Secondly, abnormal lipid signaling, activation of intracellular pro-apoptotic and proinflammatory signaling trigger extracellular inflammatory responses between cells[65–68]. Proinflammatory microglia activation reduces microglial ability to sustain the neurons and oligodendrocytes, leading to their dysfunction and death[69]. Pathological findings include GM2 accumulation in membranous cytoplasmic bodies and lipofuscin deposits in neurons, microglia, and neuroglia, which take on a ballooned appearance as GM2 ganglioside accumulates[70,71]. Inability to degrade GM2 ganglioside also interferes with ability to form and prune synaptic junctions, as well as the ability to formation and maintain myelin[15,72].

Age and level of brain development at disease onset impacts the pathology of disease. During gestation and the first few years of life, substantial changes in lipid content and composition occur in the brain due to membrane rearrangement during axon elongation, myelination, and synapse formation. However, this rearrangement slows down as the brain matures and myelination is completed. Patients with some residual level of HexA may have sufficient activity to undergo normal early development and myelination until accumulation of GM2 ganglioside, along with other environmental and epigenetic factors contribute to disease onset [15].

	Acute-Infantile	Subacute-Juvenile	Chronic-Adult
Typical Onset	<1 year old	3-5 years old	20-30 years old
Progression	**Rapid Progression** *Early Findings* Developmental Arrest Exaggerated Startle Response Muscle Weakness Macular Cherry Red Spot *Late Stages* Vision Loss Difficulty Swallowing Seizures Progressive Macrocephaly Spastic Quadripelgia Visceral Accumulation	**Moderate Progression** *Early Findings* Slowing/Regression of Developmental Milestones Abnormal Gait Dysarthria/Language Difficulties Cerebellar Atrophy *Late Stages* Decerebrate Posture Psychosis Vision Loss Dysphagia Seizures Visceral Accumulation	**Slow Progression** *Early Findings* Lower Muscle Weakness Abnormal Gait Dysarthria/Language Difficulties Cerebellar Atrophy Dysautonomia Acute Psychosis *Late Stages* Muscle Wasting/Atrophy Ascending Muscle Weakness Worsening of Dysarthria Memory/Executive Function Impairment Decreased Balance Visceromegaly
Residual HexA Enzyme Activity	None; 2-4% detected from HexS; 100%	1-5%	5-10%
Lifespan	2 - 7 years	15 - 20 years	30 years - Normal
Disease Names	Tay Sachs Disease Sandhoff Disease GM2AP Deficiency/AB Variant	B Variant O Variant	B Variant O Variant

Figure 4. Summary of GM2 Gangliosidosis Characterization

Typical onset, disease progression, residual HexA activity, typical lifespan range and names of disease for each category of GM2 gangliosidoses. Red text indicates findings and features associated with mutations to *HEXA*. Blue text indicates findings and features associated with mutations to *HEXB*. Purple text indicates findings and features associated with mutations to *GM2A*. Adapted from Toro *et al,* and Sandhoff and Harzer[15,48]. Figure made with BioRender.

1.5 Genetic Epidemiology and Molecular Causes of the GM2 Gangliosidoses

Mutations causing GM2 gangliosidoses occur along the length of the *HEXA, HEXB* and *GM2A* genes. They can be categorized as partial gene deletions, splice variants, nonsense or missense mutations and can impact mRNA processing, preproprotein folding, processing and transport through the EMS, enzyme dimerization and stability, as well as ability to hydrolyze GM2 ganglioside at the α-subunit active site[37]. Mutations to *HEXA* occur most frequently, with 101 pathogenic variants known in multiple different ethnic groups around the world. 41 *HEXB* mutations have also been described in various groups, while *GM2AP* mutations are extremely rare with only 7 pathogenic mutations known[15,73]. In addition to the complexity of the genetic mutations, presence of various mutations in the same populations gives rise to compound heterozygous individuals, increasing the phenotypic diversity of GM2 gangliosidosis patients[74].

HEXA mutations occur in various populations but have higher carrier frequencies in Ashkenazi Jewish, Sephardic Jewish, French-Canadian, Cajun, and Japanese populations[75–78]. Carrier frequency varies in these populations and can be as high as 1 in 14, and 1 in 30 for Eastern French Canadians and Ashkenazi Jewish populations respectively, compared to 1:300 in the general population[53]. Mutations differ between populations but can also vary within populations; for example, several disease-causing mutations occur independently in the Ashkenazi Jewish population. A common deletion, 7.6kb, removes the 5' end and first exon of *HEXA,* making *HEXA* mRNA undetectable. This deletion causes 82% of all acute TSD in the French-Canadian population[77].

Nonsense mutations either resulting from point mutations or insertion/deletion frameshifts commonly produce premature stop codons. These mRNA are typically targeted for

nonsense-mediated decay. Therefore, mutations of these types are most often associated with acute presentations, and absent HexA activity. An insertion of TATC1278 in exon 11 results in a frameshift mutation, negligible mRNA levels and is responsible for acute-infantile TSD in 75% of Ashkenazi Jewish, 92% of Cajun and 20% of non-Jewish populations[76,78–80]. Eight other nonsense mutations have been described for *HEXA,* all of which result in acute-infantile TSD.

Mutations at and near 5'- and 3'-splice sites lead to alterations in splicing efficiency and accuracy, reducing the number of correct mRNA transcripts. More than half of these mutations cause acute-infantile TSD[37]. Other mutations, such as G508>A are the most common cause of chronic-adult GM2 gangliosidoses. The point mutation occurs at the end of exon 7, causing incorrect but in-frame splicing, producing a Gly269Ser (G269S) base change that decreases α-subunit stability. However, HexA with G269S is catabolically active against GM2 producing some residual activity that delays disease onset[57].

Missense mutations that change the primary protein sequence impact protein folding and function. While mRNA levels are normal in these patients, the amount of active mature enzyme is reduced. Retention and eventual removal of improperly folded protein by molecular chaperones in the ER even if the protein is catabolically active, results in low HexA at the lysosome and acute-infantile TSD. The less impactful a missense mutation is on proper folding, and therefore its trafficking into the lysosome, the less severe the phenotype. Examples include Tyr180His, which produces an active but particularly heat labile enzyme, and is associated with chronic-adult GM2 gangliosidoses[81].

Diagnostic screening using enzymatic assays can result in false positives due to pseudo-deficiency; gene mutations that result in α -subunit instability and appearance of enzyme levels below 5% critical threshold during diagnostic enzyme tests. However, these individuals remain

asymptomatic and further tests reveal >5% activity. Two different T>C mutations in exon 7 result in Arg247Trp and Arg249Trp are known to cause pseudo-deficiency. These α-subunit proteins fold well enough to avoid ERAD and can associate with β -subunits although the association is unstable, particularly under laboratory conditions[82].

The final type of mutations to *HEXA* cause the B1 variant GM2 gangliosidoses. Patients with B1 variant have normal transcript levels and active HexA and HexB when assaying with 4-methylumbelliferyl N-acetyl-b-D-glucosamine (MUG), a neutral synthetic β-hexosaminidase substrate. However, when using sulfated MUG (MUGS), a charged substrate specific to the alpha subunit, it was found to be inactive[83]. Changes to a specific amino acid in the active site, Arg178, responsible for proper orientation of GalNac on GM2 in the active site is the main cause of B1 variant cases. Arg178Cys and Arg178Leu result in acute phenotypes compared to Arg178His, which results in subacute phenotypes. Cys and Leu substitutions in this position diminish α -subunit dimerization, resulting in ER retention and ERAD, while those with His do not, accounting for the differences in phenotype[84,85].

HEXB mutations also cause GM2 gangliosidoses but have been less extensively studied. β -subunit deficiency usually results from mutations impacting mRNA transcription, protein translation, correct folding, post-translational modification, and dimerization. Certain populations have much higher carrier frequencies, up to 1 in 7 and 1 in 15 for communities such as the Maronite (Cyprus) and Metis (Saskatchewan, Canada) respectively[86,87]. Large gene deletions removing 16kb from the 5' end of *HEXB* account for 26% of all acute SD cases[88]. Three splice mutations in *HEXB* are known, and more commonly result in asymptomatic, chronic, and subacute GM2 gangliosidoses, as some percentage of correctly spliced mRNA is made. Preferential heterodimerization for creation of HexA results in slowed GM2 accumulation

if any, but deficiency of HexB may occur in these patients[89,90]. Nonsense mutations to *HEXB* have been described in compound heterozygous individuals resulting in acute-infantile SD in all cases[91]. Missense mutations in *HEXB* cause dysfunctional transport or dimerization, impeding movement out of the ER like other common *HEXA* missense mutations. Other missense mutations that have decreased impact to folding and dimerization, including Pro504Ser, Arg505Gln, and Ala543Thr result in chronic-adult GM2 gangliosidoses[92,93]. Interestingly, chronic-adult GM2 gangliosidoses patients with compound 16kb/Pro504Ser mutations have a higher hexosaminidase activity level, above the 10% threshold, when assayed using MUGS. However, activity to the natural GM2 ganglioside substrate was reduced. This mutation on the β -subunit instead impacts GM2 hydrolysis efficiency at the α -active site[94].

The newest class of GM2 gangliosidoses, GM2AP deficiency, also has the smallest number of known mutations. Most mutations to *GM2A* result in ER transport issues, with one known to be caused by a missense mutation resulting in absent mRNA[37,95]. The Cys138Arg substitution was the first to be found and is a transport mutation causing protein retention in the ER[96].

1.6 Treating GM2 Gangliosidoses: Possible Therapies

While the molecular, genetic, natural history and pathophysiology of GM2 gangliosidoses have been studied extensively and are well characterized, efforts to create treatments to reduce or reverse GM2 accumulation have failed. Successful therapies are available for many other LSDs based on enzyme replacement therapy (ERT), substrate reduction therapy (SRT), gene therapy (GT) and/or pharmacological chaperones (PCs) that stabilize mutant enzymes[97–99]. Several factors including HexA instability, the need for both α- and β-subunits to generate HexA, and the requirement therapies cross the blood brain barrier (BBB), have slowed progress toward treatment of these disorders. Therapeutic approaches focus on increasing enzyme activity either endogenously (GT, PC) or exogenously (ERT), or by reducing production of accumulating substrate (SRT).

The phenomenon of cross-correction, in which M6P tagged extracellular lysosomal proteins are recognized by M6PR and redirected into the lysosomes is the basis for ERT[100]. The first successful ERT was developed in the early 1970s for the treatment of Gaucher disease[101,102]. ERT using exogenous HexA is an attractive option for therapy with benefits expected if 10% activity levels are achieved, but delivery of HexA presents some challenges.

The first challenge in creating effective ERT for GM2 gangliosidis is HexA's instability, causing the heterodimeric enzyme to dissociate into its inactive monomers quickly. HexM, a candidate for ERT, has been developed to solve this issue. HexM is a stable homodimer enzyme made from an engineered subunit (μ) produced by Dr. Brian Mark (University of Manitoba) and Dr. Don Mahuran (Toronto Hospital for Sick Children, Emeritus). The μ-subunit combines the active site of the α-subunit with GM2AP binding regions and stability of the β-subunit. HexM therefore has two active sites to break down GM2 and has been effective *in vivo*[103].

The second challenge of using ERT is due to the BBB, which presents a significant issue as all therapeutics must cross this threshold to reach the central nervous system and be effective. Direct enzyme injection into the brain has been used to bypass the BBB in other LSDs where it is the only option, but the need for repeated injections along with risk of infection makes this a less attractive option than intravenous routes[104]. Methods to induce adsorptive-mediated endocytosis at the BBB, such as plant lectin ricin toxin B-subunit (RBT), could be used as a tag on the enzyme of interest to bypass these issues. This has been done previously in mice with GM1 gangliosidoses by fusing β-galactosidase and RBT[105,106].

Third, enzymes for ERT are produced by purifying secreted lysosomal proteins from mammalian cell secretions. However, phosphorylation of mannose for M6P is limited during production, diminishing uptake. A system to produce highly phosphorylated enzyme using co-transfected and over expressed GalNAc-1-phosphotransferase has been developed to produce highly phosphorylated enzyme for potential ERT[107]. Issues with enzyme diffusion through the brain, possible immune reactions and the need for repeated doses remain to be significant limitations to ERT[108].

Bone marrow transplants are another option for ERT that does not require repeated dosing. Monocytes from the graft tissue enter the host brain, producing and secreting active enzymes that can be taken up into the surrounding cells by cross correction[53]. Unfortunately, monocyte infiltration may be local, only allowing cross-correction in some brain areas. Although some improvement was shown in SD mouse models it was unsuccessful in treating human SD patients[69,109]. There has been some success in other LSD if grafting is done early enough in disease progression, and although this generally extends life it is not curative[110].

SRT approaches the issue of GM2 accumulation from the perspective of anabolism; reducing GM2 production should reduce its accumulation. While this does not reverse the disease, reduction of symptoms, increased lifespan, and potential for combination therapies are beneficial. Gaucher disease can be treated with eliglustat tartrate, an early step inhibitor of ganglioside synthesis, and could provide benefit to other sphingolipidoses[111,112]. However, eliglustat does not cross the BBB. Venglustat, another inhibitor of ganglioside synthesis with improved CNS penetration, is currently in clinical trials for chronic-adult GM2 gangliosidoses (NCT04221451)[15].

Pharmacological chaperone therapy utilizes small molecular chaperones to assist in the folding and/or stabilization of mutant proteins in the ER, allowing them to escape ERAD[113]. Many missense mutations causing chronic-adult GM2 gangliosidoses, display biochemically moderate activity but are present in low amounts at the lysosome due to ERAD. Pyrimethamine (PYR), and N-acetylglucosamine thiazoline (NGT) are small molecules that can be given orally and cross the BBB. PYR is a competitive inhibitor of HexA, binding to the active site of the αG269S-subunit and stabilizing it while in the ER. In other mutations with residual HexA activity such as splice variant αIVS8-7G>A, PYR and NGT were shown to increase HexA activity. PYR was also shown to stabilize the βArg505Gln, while NGT was shown to have better stabilization of the βPro504Ser mutation. PYR acts on monomers to stabilize them and assist in their trafficking through the ER, while NGT acts to stabilize the dimerization of HexA. Response to treatment with either chaperone is therefore mutation dependent[114]. Pharmacological chaperones usually act as inhibitors to their enzymes in a concentration dependent manner, such that dosage must be carefully monitored to minimize inhibitory impacts. Clinical trials with PYR

to treat adult GM2 gangliosidoses were undertaken in 2011, and while leukocyte HexA activity was increased, no clinical benefit was observed[115–117].

Gene therapy (GT) in which single genes are targeted and repaired or supplemented with wildtype gene copies is well suited to treating LSDs due to characteristic single gene mutations and simple regulatory systems. GT approaches have the possibility of providing curative, single dose treatment, which would be ideal. Cross-correction and low residual enzyme levels for correction also mean that transduction can be poor and still impact clinical outcomes[53].

A limiting factor to correction is the requirement for co-expression of both subunits in the same cell to produce large quantities of active HexA; typically, if only one subunit is overexpressed, the other becomes a limiting factor[118]. Multiple gene therapy approaches using recombinant AAV or lentiviral vectors have been successful in extending life and preventing disease in mouse, cat, and sheep models of GM2 gangliosidoses if both *HEXA* and *HEXB* were co-transduced[119–124]. Co-transduction was achieved either by co-injecting vectors with monocistronic *HEXA* and *HEXB,* or by using a bicistronic vector encoding both genes[122,125].

Interestingly, other methods using single gene therapy have also been successful. One study using a non-replicating herpes vector to administer *Hexa* gene therapy in mice with GM2 gangliosidoses (*Hexa*$^{-/-}$) was successful in reducing widespread GM2 storage in the brain[126]. However, this treatment was tested in a mild adult-chronic model of GM2 gangliosidoses and long-term studies were not reported. Single gene therapy with AAV9-*Hexb* was also successful in correction of disease in *Hexb*$^{-/-}$ mice. While long term correction was achieved, lung and liver tumors were observed and attributed to the high dosage of viral vector used in this study[127]. Alternatively, use of a single *HEXM* vector encoding the μ -subunit of the engineered HexM enzyme has been used to successfully reduce GM2 levels in SD disease mice [128,129]. Limitations

of treating GM2 gangliosidoses with gene therapy include the requirement for early intervention for best therapeutic response, creating challenges in the treatment of acute-infantile forms of GM2 gangliosidoses with this approach.

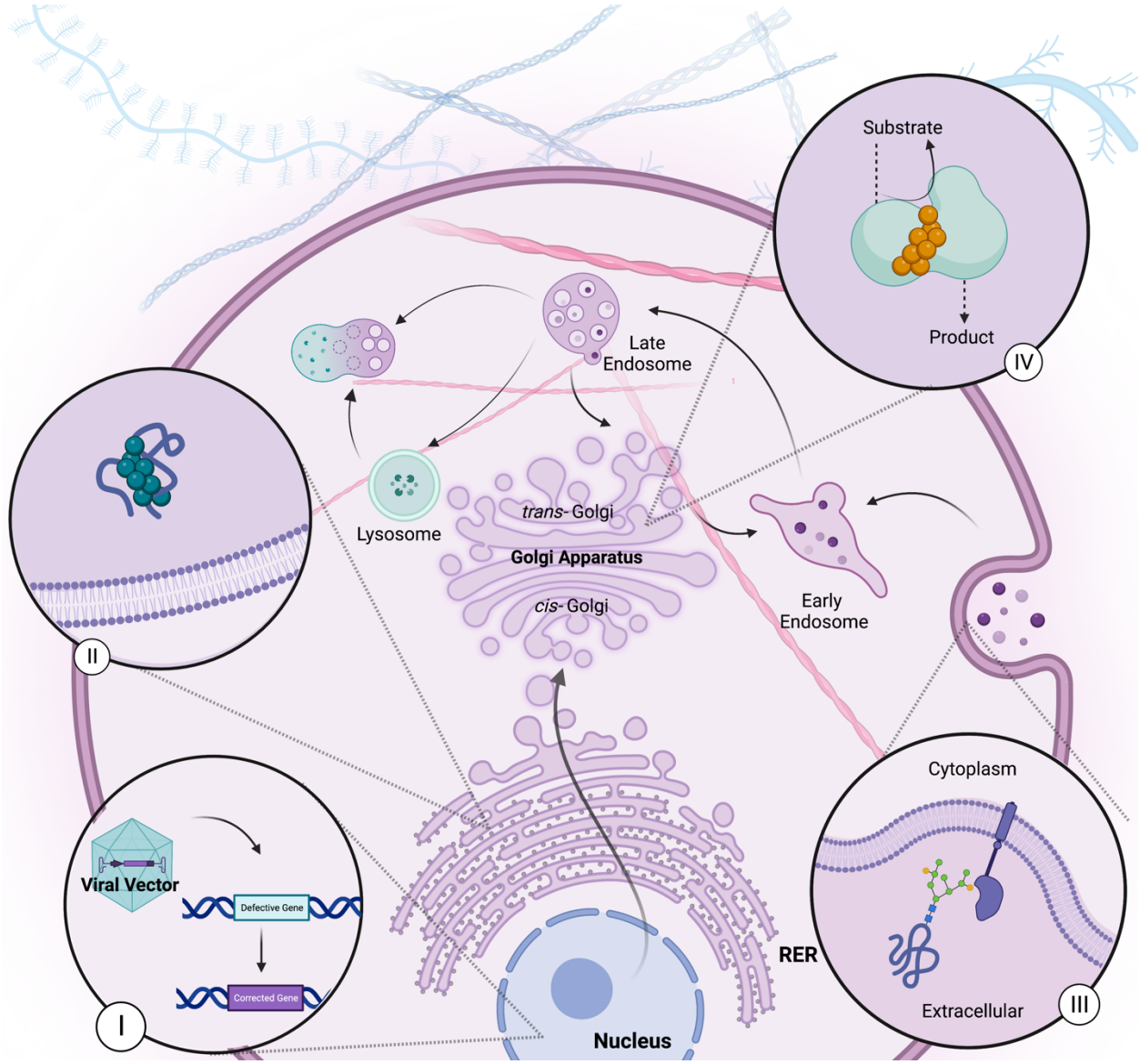

Figure 5. Current Treatment Targets within the Endomembrane System

I) Gene therapy with a viral vector carrying a corrected or modified gene. II) Pharmacological chaperones bind proteins in the ER, stabilizing folding and/or dimerization. III) ERT through cross-correction system where exogenous protein tagged with M6P is recaptured and targeted to the lysosome. IV) SRT acts in the Golgi by inhibiting biosynthetic enzymes that synthesize the accumulating product. Figure made in BioRender.

1.7 Animal Models for GM2 Gangliosidoses

Animal models have been indispensable in the research of human disease, both in determining pathophysiology and testing preclinical treatments. GM2 gangliosidoses have been known to exist naturally in many animals. Mice have been widely used in the basic sciences and pre-clinical testing of treatments for GM2 gangliosidoses, while larger animals such as felines and sheep have been used to test whether successful murine treatments will translate to larger more complex brains[130,131].

Modelling of SD with *Hexb*$^{-/-}$ in mice has been used to study potential GM2 gangliosidosis therapies since 1995. These mice display neurological phenotypes including motor impairment, tremors, gait disturbances, and seizures, as well as weight loss, and increased brain weight when compared to controls [132]. However, TSD models with *Hexa*$^{-/-}$ failed to produce a phenotype consistent with those found in acute TSD patients. These early TSD models displayed some of the disease markers of the human disease in specific brain areas but showed few signs of GM2 gangliosidosis until 1 to 1.5 years[133]. Compared with age matched *Hexb*$^{-/-}$ animals who have severe neurological phenotype and onset between 3-4 months, *Hexa*$^{-/-}$ animals appear normal. On histological analysis of GM2 accumulation, both *Hexb*$^{-/-}$ and *Hexa*$^{-/-}$ mice had accumulation through the brain, but accumulation was much less severe in *Hexa*$^{-/-}$ mice with only specific brain areas such as the hippocampus, and cerebral cortex showing more extensive accumulation[134].

Following onset of disease at one year *Hexa*$^{-/-}$ animals display typical disease progression with tremor, abnormal posture, and muscle weakness over the next year, a slowly progressing neurological phenotype typical of mild chronic-adult GM2 gangliosidoses [135]. Mouse models for

GM2AP deficiency have also been created and display an intermediate phenotype with motor and cerebellar pathology but normal lifespans[136].

An alternative pathway for GM2 degradation was discovered in mice that accounted for this discrepancy between SD, TSD and GM2AP deficiency models. Murine neuraminidase-3 (Neu3), is a membrane localized enzyme that will cleave the terminal Neu5Ac on GM2, creating GA2 ganglioside. GM2AP will then present GA2 to the β-subunit of HexA or HexB which hydrolyses it to GM3. The result is little GM2 accumulation even in the absence of HexA. Mice with acute/subacute GM2 gangliosidoses resulting from *Hexa* mutations have since been created by knocking out *Neu3* in addition to the *Hexa* gene. These models display typical human TSD findings such as neuronal cell ballooning, ataxia, and tremors [137]. In addition, neuroinflammation typical of TSD is also evidenced by astrocyte and microglial activation, proliferation and pro-inflammatory cytokine signaling[138].

Feline models exist only for acute-infantile SD and are caused by various *HEXB* mutations. Clinical signs begin between 4-7 weeks of age with head tremor, and ataxia progressing to seizures and death at 6 months[139]. One mutation with a 25bp inversion produces an inactive but antigenically intact protein which may be protective against immune response to exogenous enzyme or gene products[140]. A second known mutation causing a premature stop in exon 1 of *HEXB* results in a model that would be immunosensitive to foreign enzyme, providing a model to study the immune system response to ERT and GT [130]. An acute-infantile TSD model in Jacob Sheep has also been known to exist since 2010 and displays the clinical signs of TSD with reduced HexA activity. These sheep have a single bp mutation in exon 11 of *HEXA* resulting in Gly444Arg substitution[141].

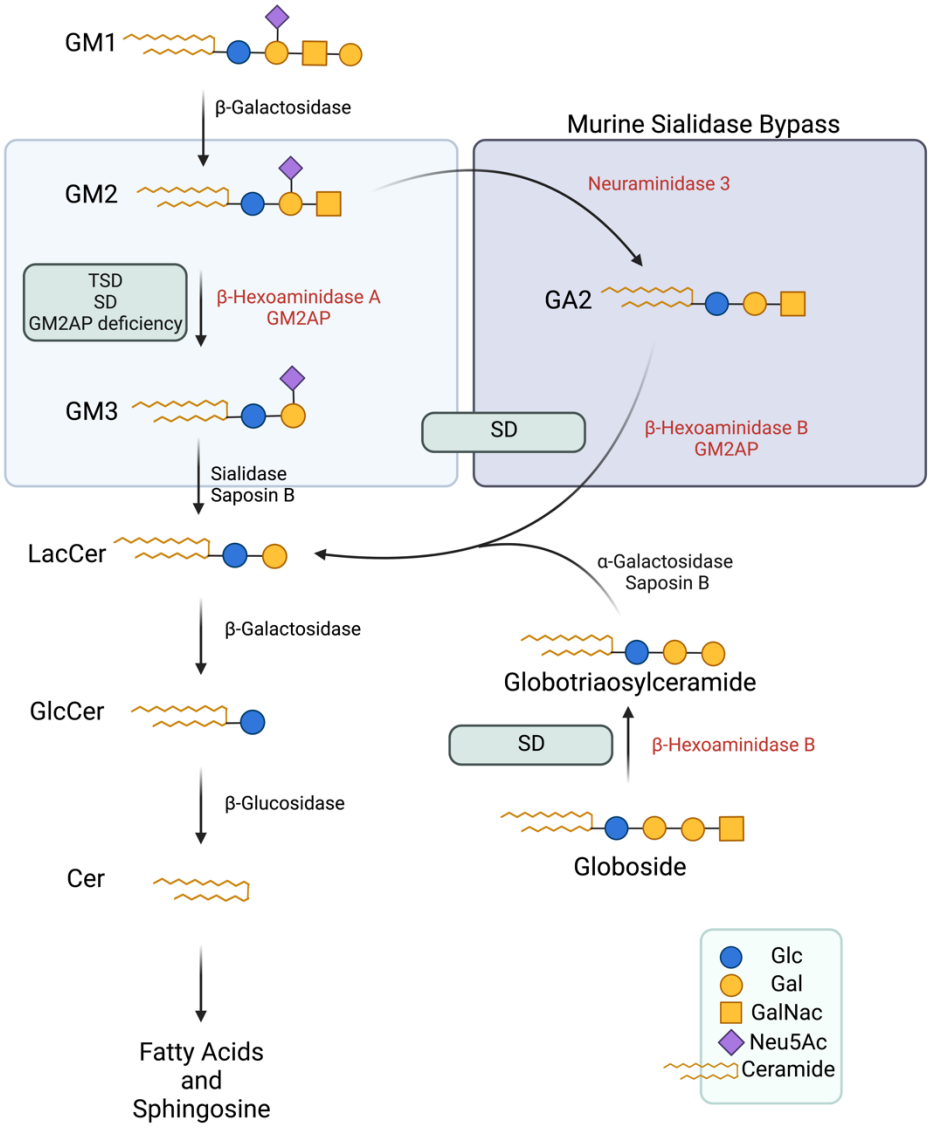

Figure 6. Stepwise Degradation of Gangliosides and Alternative Murine Sialidase Bypass Pathway

Stepwise degradation of gangliosides in humans. Enzymes important to GM2 gangliosidoses are indicated in red, resulting disease when enzymes are mutated are indicated in boxes. Murine sialidase pathway is indicated in dark blue box. Common pathway for GM2 degradation in humans and mice is indication in light blue box. Abbreviations: Glc; glucose, Gal; galactose, GalNac; N-Acetyl galactosamine, Neu5Ac: N-acetyl neuraminic acid, LacCer; lactosylceramide, GlcCer; glucosylceramide, Cer; Ceramide. Figure made with BioRender.

2 Hypothesis, Research Questions, Rationale and Experimental Design

2.1 Hypothesis and Research Questions:

Due to the residual activity of HexA G269S in humans with adult onset GM2 gangliosidosis, we hypothesize that mice with *Hexa* KI of the G269S mutation in combination with *Neu3* KO (*Hexa*$^{G269S/G269S}$*Neu3*$^{-/-}$ or KIKO) will have increased survival compared to those with both *Hexa* and *Neu3* KO (*Hexa*$^{-/-}$*Neu3*$^{-/-}$ or dKO), producing a late-onset GM2 gangliosidosis model in mice. We predict that signs of illness in KIKO mice, as well as other indicators of neurological and behavioural dysfunction will be less severe or have delayed onset compared to dKO mice.

1. Do *Hexa*$^{G269S/G269S}$*Neu3*$^{-/-}$ mice have increased survival or delayed onset, producing a late-onset GM2 gangliosidoses model?
2. Can we detect differences in the phenotype of *Hexa*$^{G269S/G269S}$*Neu3*$^{-/-}$ mice compared to *Hexa*$^{-/-}$*Neu3*$^{-/-}$*?*

2.2 Rationale

Currently no treatments for GM2 gangliosidosis exist and few have been tested in late-onset models. *HEXA* in humans has the highest number of known disease-causing mutations, and the recently discovered murine Neu3 bypass pathway now allows for the creation of GM2 gangliosidoses mouse models via combined *HexA* and *Neu3* mutation. Various theoretical treatments are only expected to work against specific mutations, and as such, the creation of animal models with mutations amendable to different therapeutic interventions could be useful for the development and research of clinical treatments. For example, pharmacological chaperone therapy such as pyrimethamine is only plausible for individuals whose mutations result in residual enzyme responsive to stabilization, such as G269S. Current models with *HexA* mutation either accumulate GM2 quickly (dKO) or only towards the very end of their life span

(*Hexa*$^{-/-}$). Producing models with intermediate phenotypes may allow for therapeutic interventions to take place at an earlier disease state before a critical accumulation of GM2 has occurred. GM2 accumulation at later stages maybe too advanced, and therapies may act to reduce this accumulation at a slow rate. This can limit our ability to detect significant reductions disease phenotype before animals must be euthanized. This would also allow us to increase the period of assessment and evaluate whether treatments continue to work long term, or if off target effects and possible attenuation of therapeutic agents by the immune system would limit their usefulness.

2.3 Experimental Design

To test this hypothesis, 11 dKO and 9 KIKO mice were monitored from 7 weeks until humane endpoint, determined by a 15% decrease in weight from maximum weight, seizure activity or severe mobility impairment. These experimental animals were age and sex matched to a litter mate, and when possible, these experimental pairs were housed and monitored together. Many different tests to detect differences between models were employed, including those to measure motor and neurological function, survival, GM2 ganglioside accumulation, as well as β-hexosaminidase-enzyme activities.

3 Materials and Methods

3.1 Generation of Mouse Models

All studies with mice were performed under protocol B2019-003 approved by the University of Manitoba Animal Care Committee and in a facility holding a certificate of Good Animal Practice from the Canadian Council on Animal Care.

3.1.1 Generation of *Hexa* KO, KI and *Neu3* KO mice using CRISPR/Cas9

Guided by previous studies[137], a TSD-like mouse model was created by combining *Hexa* and *Neu3* deficiency. In addition, a proposed late-onset GM2 gangliosidosis mouse model was created via site-directed knock-in (KI) of the G269S *Hexa* mutation combined with *Neu3* knock-out (KO).

Strategies to create the *Hexa* KI, *Hexa* KO and *Neu3* KO mouse lines were designed by members of the Triggs-Raine laboratory. The Custom Alt-R ® CRISPR-Cas9 guide RNA (gRNA) design tool at https://www.idtdna.com/pages was used for designing CRISPR RNAs (crRNA) to target the *Hexa* and *Neu3* genes. A 50 bp region in exon 7 of *Hexa* (NC_000075.7:59,443,992-59,474,974) including Gly269 was analyzed and a crRNA near to the Gly269 as well as single-stranded DNA donor (ssDNA in *Table 1*) was designed to introduce the NM_010421.5 c.805G>A p.G269S. The altered base in the donor (*capitalized, Table 1*) introduced the Gly to Ser substitution, created an ScrFI site, and simultaneously destroyed the CRISPR Pam site. A second base change of NM_010421.5 c.705C>A (*underlined, Table 1*) does not alter the coding sequence but destroys a second ScrF1 site to facilitate PCR-based screening.

A crRNA targeting exon 2 of *Neu3* (NC_000073.7:99,460,646-99,477,624) (*Table 1*) was identified and used without a single stranded donor DNA to create insertions/deletions. CRISPR materials and primers were purchased from Integrated DNA Technologies (IDT; Coralville, IA, USA).

The following work was implemented by the University of Manitoba transgenic service. *Hexa* and *Neu3* mutations were generated with the Alt-R® CRISPR-Cas9 System from IDT and following the approach of Qin et al[142]except that zygotes were generated by *in vitro* fertilization. Fertilized C57BL/6N oocytes were incubated for 2 hours in potassium simple optimized medium (KSOM) and then groups of 20-40 zygotes were electroporated in a 10 µL volume of Opti-MEM® (Thermo Fisher Scientific) containing 50 ng/µL Cas9 (Alt-R® S.p. Cas9 Nuclease V3), 200 ng/µL of the guide duplex prepared following the manufacturer's instructions, and for *Hexa*, 400 ng/µL of ss DNA donor). The electroporation was done using the BioRad Gene Pulser Xcell™ at 30V, 1s ON, 99s OFF, for 12 cycles. Embryos were cultured to the 2-cell stage and transferred to CD1 pseudo-pregnant mice (0.5 dpc).

Table 1. CRISPR components for creation of *Hexa* KI, *Hexa* KO and *Neu3* KO alleles

CRISPR component	5'- 3' sequence	Targeted gene
crRNA[a]	5'-actgcagctccattcttacc-3'	*Hexa*
ssDNA[b]	5'tgtgctggcagaatttgacactcctggccacactttgtc*a*tgggggccaAgtaag aa tggagctgcagttggaggcgtctgctaaaagaggggctccaggg-3'	*Hexa*
crRNA[c]	5'-tgcggggccatgttactgag-3'	*Neu3*

GenBank accession for reference sequences used:

a – NC_000075.7:59,443,992-59,474,974

b – NM_010421.5

c – NC_000073.7:99,460,646-99,477,624

Identification of founders with suitable *Hexa* and *Neu3* mutations was done by amplifying the region of interest and testing for the presence of small insertions or deletions using heteroduplex analysis. A 217 bp amplicon including the edited region of *Hexa* was generated using polymerase chain reaction (PCR) and the primers WPG1200 and WPG1201 (*Table 2*). The resulting PCR products were separated on an 8% polyacrylamide gel after restriction enzyme digestion with ScrF1 to test for the desired c.805G>A mutation or without ScrF1 digestion to screen for heteroduplexes. DNA heteroduplexes resulting from the mismatches between the mutant and wild type sequence result in slower migrating bands that are unique for each mutation. ScrF1 digestion resulted in 99, 49, 46, 16, and 8 bp fragments for the wild-type sequence and 99, 75, and 46 bp fragments for the mutant c.805G>A sequence. The CRISPR targeted *Neu3* exon 2 region was PCR-amplified using WPG1251 and WPG1252 (*Table 2*). The resulting 219 bp product was screened for insertions and deletions by heteroduplex analysis on 8% polyacrylamide gels. The gels were run at 100V for 45 minutes in 1X TBE (89 mM Tris Borate, 2mM EDTA, pH 8.3) buffer.

Two mutant alleles for each breeding line were chosen and bred to homozygosity. The *Neu3* KO line alleles were then both crossed with the *Hexa* KO and *Hexa* KI alleles to produce the TSD-like $Hexa^{-/-}$ $Neu3^{-/-}$ (dKO) and proposed late-onset GM2 gangliosidosis $HexA^{G269S/G269S}Neu3^{-/-}$ (KIKO) breeding lines.

Table 2 Primers used in screening and genotyping of *Neu3* and *Hexa* alleles

Primer Name	Sequence	Sense	Gene
WPG1200	5'- caaccctgtcactcacatctac -3'	Forward	*Hexa*
WPG1201	5'-caagagccaaggccaagata-3'	Reverse	
WPG1251	5'-ctactgatggaggccacattac-3'	Forward	*Neu3*
WPG1252	5'-ctcctcggtcaagtctttcac-3'	Reverse	

3.1.2 Genotyping

DNA was extracted from mouse ear clippings according to Müllenbach et al[143] and regions surrounding the *Hexa* and *Neu3* genes were PCR amplified using the primers listed in Table 2. Genotyping was conducted in the same manner as mutant screening using heteroduplex analysis for detection of *Neu3* and *Hexa* KO alleles, and ScrFI digest for detection of *Hexa* KI alleles. Homozygous KOs for either *Neu3* KO or *Hexa* KO were detected by running sample PCR products (S) with and without the addition of wild-type PCR product (S^+).

3.2 Model Characterization: Behavioural and Neurological Phenotype

Eleven dKO and 9 KIKO animals were paired to an age, sex matched control (either $Hexa^{-/+}$ $Neu3^{-/-}$ or $Hexa^{+/+}$ $Neu3^{-/-}$) for all monitoring and testing. These animals were housed together where possible, although 2 dKO and 3 KIKO male pairs were separated due to fighting. Long capped water bottles and placing food on cage floors was done to facilitate access for animals. These animals underwent routine monitoring and behavioural testing together before being euthanized once the dKO or KIKO animal reached a humane endpoint. The humane endpoint was determined when one or more of the following conditions were met: 1) 15% weight loss from maximum weight, 2) excessive shaking, or seizure activity, 3) isolating behaviour, and/or 4) inability to access food or water due to gait abnormalities causing immobility.

3.2.1 Routine Monitoring

Mice were monitored on a weekly basis starting at 7 -10 weeks of age for changes in indicators of normal physical, behavioural, or neurological function. The onset of disease, indicated by abnormal hindlimb extension reflex or visible tremors, resulted in an increase in

monitoring to three times per week. Indicators of changes in physical health including decreased body weight, fur ruffling, eye infection/irritation or skin wounds were recorded at each monitoring session. Animal behaviours, including decreased grooming, increased isolation and or abnormal escape responses were also noted. Scoring of abnormal hindlimb extension was used to monitor neurological disease progression, adapted from Miedel et al[144]. During this test, mice were suspended by the tail for 5 seconds and hindlimb extension reflex was scored according to Table 3. Righting reflex, another neurological measure, defined as the time for the animal to right itself after being placed in a supine position was also observed.

Table 3 Scoring of abnormal hindlimb flexion response on tail lift, adapted from Miedel et al[144].

Score	*Description*
0	No limb clasping; normal extension response.
1	One hindlimb exhibits incomplete extension and intermittent loss of mobility; toes exhibit a normal splay.
2	Both hindlimbs exhibit incomplete extension and intermittent loss of mobility; toes exhibit a normal splay
3	Both hindlimbs exhibit intermittent clasping/flexion, with curled toes and intermittent loss of mobility.
4	Both hindlimbs exhibit clasping/flexion, or are crossed, with curled toes and persistent immobility.

3.2.2 Open Field Test and Gait Analysis

Open field maze and gait analysis tests were performed on the same day at approximately 10, 14, 18 and 22 weeks of age. Animals were moved into the testing room and allowed to acclimate for at least 30 min prior to testing. Mice were placed in a 50 X 50 cm square open field arena (*Figure 7*) and recorded uninterrupted for 10 min using a Stoelting webcam and Bandicam video recording software (Version 4.6.5.1757). After 10 min mice were removed from the arena, and the number of fecal boli produced was recorded. Ethanol (10%) was used to clean the arena between tests. ANY-maze video tracking system software (Version 6.33) was used for video tracking and collection of data. Measures included distance travelled (m), maximum speed (m/s), average speed (m/s), time mobile(s), and time spent in the inner, outer, and corner zones (s) was recorded. Animals were allowed to rest for at least 30 min in their home cage before gait analysis was performed. Mice were restrained and non-toxic paint was applied to all feet using a paint brush. Distinct colours were used on the hind paws (blue) and fore paws (green) to help differentiate them at the analysis stage. Mice were then released into a paper-lined, 10 cm wide passage with a dark chamber at the end to encourage forward movement (*Figure 7*). Five or more consecutive strides with normal walking were acquired for each mouse. Forelimb and hindlimb stride and stance, as well as hindlimb sway distances were measured 3 times from this imprint and averaged for each mouse.

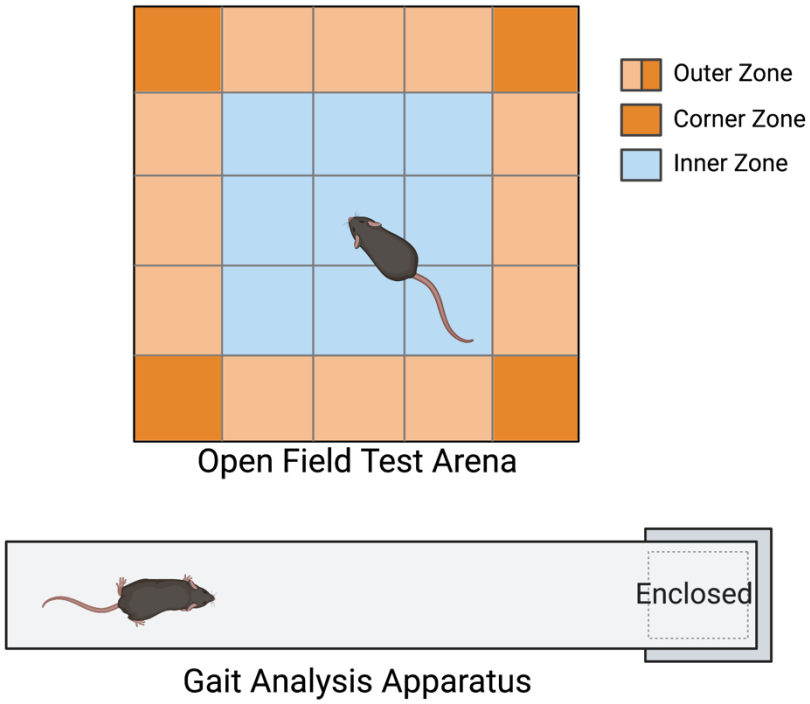

Figure 7. Apparatus for Open Field and Gait Analysis Tests

Apparatuses for open field (top) and gait analysis (bottom) tests. Zones defined in ANYmaze for open field tests are indicated by colours: blue for the inner/inside zone, orange for the outer/outside zone and dark orange for the corners. Arena measures 50x50cm. Gait analysis apparatus was used to keep the mice walking in a straight and forward direction. Walls and corridor were ~10cm, with enclosed dark area indicated at the end. Figure made with Biorender.

3.3 Euthanisia and Tissue Collection

Mice were euthanized via anesthetic overdose (40% isoflurane in poly-ethylene glycol) at humane endpoint. Whole blood was collected by cardiac puncture, allowed to coagulate at room temperature for 10 min, then centrifuged at 200 x *g* for 10 min to separate serum from cellular blood components. Serum was then stored at –80 °C for future enzyme activity assays. A subset of animals (KIKO n=4, dKO n=4) were perfused transcardially with 1X Dulbecco's PBS (PBS, phosphate buffered saline) at a flow rate of 5mL/min for 4 min for future matrix-assisted laser desorption/ionization mass spectrometry (MALDI).

Whole organs of interest for the study were removed and weighed. Brain hemisphere, liver and gastrocnemius samples were collected, and flash frozen on dry ice for later ganglioside extraction and enzyme assays. The other brain hemisphere, gastrocnemius, liver, lung, and heart were fixed in formalin for immunohistochemistry. Tibial lengths were measured after removal of the gastrocnemius with a ruler from knee joint to ankle joint. Tissues were fixed overnight, washed in PBS, and stored for up to 6 months in 70% ethanol at 4°C, before paraffin embedding.

3.4 Immunohistochemistry

Fixed tissues were processed using a 16 hr cycle (*Table 4*) on Shandon Citadel tissue processor (Model 1000, Thermo Sci.) and embedded in paraffin (Surgipath Paraplast X-tra, Leica). 5 µm sagittal sections from brain were taken, heat fixed for 30 min at 37°C. Slides were deparaffinized in two changes of xylene for 5 min each, before being rehydrated through a graded ethanol series. The graded ethanol series consisted of two changes of 100% ethanol for 5 min each, two changes of 95% ethanol for 3 min each, 70% ethanol for 3 min, 50% ethanol for 3 min and MilliQ distilled water for 3 min. Antigen retrieval was performed by immersing slides for 20 min in 10 mM sodium citrate (pH 6.0) preheated to 95°C, followed by slow cooling to room temperature. Sections were rinsed in two changes of MilliQ distilled water for 3 min each, and endogenous peroxidase was blocked with 3% H_2O_2 for 10 min. Slides were washed twice in Tris Buffered Saline (TBS) for 5 min each. Protein block was performed using a blocking solution of 3% bovine serum albumin (BSA) in TBS for 1 hour at room temperature. Endogenous biotin/avidin sites were blocked with Avidin/Biotin blocking kit according to the instructions of the supplier (Vector; VECTSP2001), using TBS as a washing solution between blocking steps. Sections were incubated overnight at 4°C with mouse monoclonal anti-GM2 IgM (1:1000, TCI, MK1-16) primary antibody diluted in blocking solution. Negative controls without primary antibody were incubated in only blocking solution on each slide.

Slides were rinsed three times in TBS for 5 min each. All sections including the negative control were treated with biotin-conjugated polyclonal goat anti-mouse IgM, µ chain specific (1:1000, Jackson Labs, 115-065-020) secondary antibody diluted in blocking solution for 1 hour at room temperature. Slides were washed three times with TBS for 5 min each before being treated with ABC complex kit (Vector Labs, PK4000) according to supplier instructions, made

with TBS. 3,3′-diaminobenidine (DAB) substrate was prepared using ImmPACT DAB EqV Peroxidase Substrate (Vector Labs, SK-4103). Sections were developed for 1min 15s before stopping the reaction with a 5 min MilliQ water rinse. Slides were counterstained with 0.5% methyl green in 0.1M sodium acetate buffer for 5 min and destained by rinsing in MilliQ distilled water. Further de-staining and dehydration was completed by quickly dipping the slides 10 times each in 95% ethanol, and 2 changes of 100% ethanol. Slides were cleared in two changes of xylene for 5 min each and mounted using Permount mounting medium (Fisher Scientific). Slides were imaged with Olympus VS200 slide scanner using 2x and 20x objectives, and images with scale bar were acquired using OlyVIA Software (Version 3.3, Build 24382). Various areas of the brain were examined, including deep nuclei and purkinje cell layer of the cerebellum, as well as nuclei of the medulla oblongata and pons. The thalamus, CA1 field of the hippocampus, hypothalamus, striatum, cerebral cortex, and superior colliculus were also examined.

Table 4. Processing times and solutions for paraffin embedded tissues.

Solution	Step	Time (hours:minutes)
70% Ethanol	1	1:00
95% Ethanol	2	1:30
	3	1:30
100% Ethanol	4	1:30
	5	1:30
	6	1:30
	7	1:30
Xylene	8	0:30
	9	1:00
	10	1:00
Paraffin	11	2:00
	12[a]	4:00

a. Under vacuum

3.5 Biochemical Studies

Frozen tissues from brain collected from dKO, KIKO mice and their controls were homogenized using a Sonic Dismembrator (Model 100, Fisher Scientific). 600 µl lysis buffer (PBS, pH 6.6 with mammalian proteinase inhibitor cocktail; 1:500, Sigma) was added to each sample before placing them on ice and sonicating for two 5s pulses at power 1, resting 30s between pulses. Tissue lysates were frozen at -80°C for future GM2 extraction and/or enzyme assays.

3.5.1 GM2 Ganglioside Extraction

Gangliosides were isolated using a protocol adapted from Walia *et al*[127]. 400 μL brain homogenate was spiked with 10μg of deuterated GM1 standard (N-omega-CD_3-Octadecanyl monosialoganglioside GM1(NH_4^+), cat. 2050, Matreya). Chloroform-methanol (2:1) was added to this and allowed to sit overnight at 4°C. Samples were centrifuged at 500 x *g* for 10 min at room temperature, and the supernatant collected. This crude lipid extract was then dried down under N_2 gas. Dried down lipids were resuspended in chloroform:methanol:PBS (1.5:1.5:1). Phases were partitioned by centrifuging at 500 x *g* for 5 min, removing the upper phase containing gangliosides. Phase partitioning was repeated twice more by adding methanol:PBS (1:1) to the lower phase. The upper phase was removed each time and combined. A hydrophobic column (Strata® C18-E (55 µm, 70 Å), 200 mg / 3 mL) was prepared by applying equal volumes of chloroform, methanol, and methanol:PBS (1:1) sequentially using positive pressure. The upper phase was then applied to the column and allowed to flow through by gravity. Gangliosides were eluted by gravity flow with equal volumes of methanol and then chloroform:methanol (1:1). Eluents were combined and dried down under N_2 gas. Tubes with dried lipid were filled with N_2 gas, before capping tightly and storing at –80°C.

3.5.2 GM2 Ganglioside Analysis with Liquid Chromatography Electrospray Ionization Mass Spectrometry (LC-ESI-MS)

Ganglioside extracts were sent to Dr. Shaun Whitehead (Western University, London, Ontario, Canada) for liquid chromatography electrospray ionization mass spectrometry (LC-ESI-MS). The following protocol for LC-ESI-MS was provided by Wendy Wang.

Dried lipid extracts were redissolved in 100 μL of methanol/chloroform (1:1) solvent and sonicated. 10 μL of lipid extract was loaded in each run. Samples were separated using a high-performance liquid chromatography (LC) with the Luna® 3 µm NH2 100 Å NH2 LC column (150 mm × 1 mm). LC conditions utilize two mobile phases for lipid separation. Mobile phase A is composed of 1 mM ammonium formate in acetonitrile/water (83:17), while mobile phase B is composed of 50 mM ammonium formate in 1: 1 acetonitrile/water (1:1). The initial gradient was held for 5 min at a solution mixture (A:B) of 100:0, converted linearly to A:B=25:75 for 5 min, then converted linearly to A:B=10:90 for 5 min and held there for 10 min. The flow rate was set to 0.15 mL/min and the temperature of the column was set to 40 °C.

ESI-MS was performed using the *Waters QToF Micro* instrument. Voltages were set as follows: Flight tube; 5630 V, MCP; 2700 V, source tube voltage; 3500 V and the sample cone; 40 V, all operated under negative ion mode. The source temperature was set to 100 °C and desolation temperature was set to 300 °C. Collision energy was set to 5 V and recorded mass ranges were (600 – 1800) m/z for MS only. The mass spectra were analyzed using the Skyline software.

3.5.3 Enzyme Assays

HexA and neuraminidase activities were determined from brain tissue collected from dKO, KIKO and control mice. Brain tissue sonicates were centrifuged at 17000 x *g* for 10 min and post-nuclear supernatant and pellet collected. The pellet was resuspended in 120 µL PBS.

Total protein concentration of each fraction was determined from a diluted sample (1:5) via Bradford assay using Bradford reagent (Biorad).

For HexA activity assays, the post-nuclear supernatant containing soluble proteins was used. 20 µg of protein was added with 0.1 M CP buffer (citrate phosphate buffer, pH 4.2, final concentration 0.65M), BSA (final concentration 0.5%), and 4 mM 4-MUGS (4-methylumbelliferyl-7-(6-sulfo-2-acetamido2-deoxy-ß-D-glucopyranoside) sodium salt, Toronto Research Chemicals; in CP buffer, final concentration 1mM) in a total reaction volume of 40 µL. A blank sample with all components above was made, replacing the sample protein with 2 µL lysis buffer used in sonication. Samples and blanks were prepared in triplicate and incubated at 37°C for 30 min before quenching the reaction with 960 µL GC buffer (0.17M glycine carbonate buffer, pH 10.2).

Neuraminidase activity assays were conducted on the pellet suspended in PBS using various concentrations of the NEU2/3 specific inhibitor Zanamivir (ZANA, 4-Guanidino-2,4-dideoxy-2,3-dehydro-N-acetylneuraminic acid, Sigma-Aldrich). ZANA stock solution was made in water (20mM) and further diluted in SA buffer (sodium acetate buffer, pH 4.4) for final reaction concentrations of 5, 10, 25, 50 and 200 µM. 150 µg, 225 µg and 300 µg of protein was used as replicates of each sample for every ZANA concentration or without inhibitor. Blank controls for each inhibitor concentration and without inhibitor was also conducted, replacing the volume of protein with lysis buffer used in sonication. 0.2 M SA buffer (final concentration 0.15M), and ZANA at each specified concentration were added to samples and incubated on ice for 15 mins. 6 µL of 2 mM 4MU-NANA (4-Methylumbelliferyl N-acetyl-a-D-neuraminic acid, Sigma-Aldrich) sodium salt suspended in dimethylformamide (DMF) and diluted in SA (final concentrations; 1% DMF, 200 µM 4-MU NANA) was added for a final reaction volume of 60

µL. Samples and blanks were incubated at 37°C for 1 hr before terminating the reaction with 940 µL GC buffer (0.17M, pH 10.2). Reaction tubes were spun at 17200 x *g* for 10 min to separate cellular pellet, and the supernatant containing the methylumbelliferone (MU) product was removed.

In both HexA and neuraminidase assays, 250 µL of the reaction solution was loaded into a black bottom 96-well plate along with MU standards (7-hydroxy-4-methylcoumarin) in GC buffer from 0 to 1000 nM. The MU cleavage product from 4-MUGS or 4-MU-NANA was detected using an excitation wavelength of 365 nm and an emission wavelength of 450 nm in a SpectraMax M2 plate reader.

3.6 Statistical Methods

Data were analyzed using Prism (GraphPad Prism Version 9.2). Outliers were identified and removed using the ROUT method (Q=1%). Mixed effects analysis using two-way ANOVA (Analysis of Variance) and Tukey's multiple comparisons, one-way ANOVA with Sidak's multiple comparison testing was used for statistical analysis with alpha 0.05. Kruskal-Wallis tests with Dunn's multiple comparison was conducted for testing average tail life scores, using an alpha of 0.1. Kaplan-Meier survival analysis using log-rank tests was used for survival analysis. The method of analysis is indicated for each figure, and statistical results are summarized in Tables A-E (*see* Appendix).

4 Results

4.1 Model generation

TSD-like mouse models were created by combining *Hexa* and *Neu3* deficiency. The proposed late-onset GM2 gangliosidosis mouse model was created via site-directed knock-in of the G269S *Hexa* mutation combined with *Neu3* KO. Various *Hexa* and *Neu3* KO mutations were combined to create a model expected to follow the natural history of a previously reported *HexaNeu3* dKO model[137].

Mutations in *Hexa* and *Neu3* genes were introduced into mice by the local transgenic service using CRISPR-Cas9. Zygotes derived by in vitro fertilization were treated with CRISPR-cas 9 and transferred into pseudo-pregnant mice when they reached the two-cell stage. The resulting offspring were analyzed for mutations to identify founders suitable for generating the *Hexa* KO, *Hexa* KI and Neu3 KO mice.

Mutations in each of these founders were sequenced, and two alleles for each breeding line (*Table 5*) were chosen and bred to homozygosity. The *Neu3* KO line alleles were then crossed with the *Hexa* KO and *Hexa* KI alleles to produce the TSD-like $Hexa^{-/-}Neu3^{-/-}$ dKO animals and proposed late-onset GM2 gangliosidoses $Hexa^{G269S/G269S}Neu3^{-/-}$ KIKO animals.

Table 5. Alleles with associated mutations for the *Neu3* KO, *Hexa* KO *and Hexa* KI breeding lines.

Breeding Line	*Mutation*	*Allele Name*
Neu3 KO	c.336ΔTGAGAGGTGC [a]	$Neu3^{em2btr}$
	c.336ΔTGinsA [a]	$Neu3^{em6btr}$
Hexa KI	c.805G>A [b]	$Hexa^{em2.2btr}$
	c.805G>A [b]	$Hexa^{em2.3btr}$
Hexa KO	c.790 Δttgtcct [b]	$Hexa^{em1.2btr}$
	c.792ΔGT [b]	$Hexa^{em1.3btr}$

[a] Reference Sequence: NC_000073.7: 99,460,646-99,477,624
[b] Reference Sequence: NC_000075.7: 59,443,992-59,474,974

DNA from offspring was PCR amplified with primers for the *Hexa* and *Neu3* genes to determine genotypes. Comparison of heteroduplex patterns between sample PCR product (S) and S mixed with PCR product from WT DNA (S^+) allowed for the genotyping of the various *Neu3* KO and *Hexa* KO alleles. Wildtype mice did not display heteroduplexes in either S or S^+, while heterozygous individuals displayed heteroduplexes in both. Homozygous KO individuals display heteroduplexes in S^+ only (*Figure 8 top, Table 6*).

Hexa KI alleles were detected with ScrFI digestion of sample PCR product. Appearance of a 73bp band indicated the presence of either KI mutant alleles, with the 49bp band disappearing in homozygous KI individuals (*Figure 8 bottom*, *Table 6*).

Table 6. Genotyping strategies and predicted appearance of bands on PAGE for the *Neu3 KO, Hexa KO and Hexa* KI alleles

Allele Name	**Genotyping Method**	**Sample**	**Genotype**		
			Wt	Het	KO
			Heteroduplex appearance (- or +)		
Neu3^{em2btr}	Heteroduplex	S [a]	-	+	-
Neu3^{em6btr}					
Hexa$^{em1.2btr}$		S^{+} [b]	-	+	+
Hexa$^{em1.3btr}$					
			Expected Bands (bp)		
Hexa$^{em2.2btr}$	ScrFI digestion	S [a] + ScrFI	99, 49, 45, 16, 8	99, 73, 49, 45, 16, 8	99, 73, 45
Hexa$^{em2.3btr}$					

[a] S – PCR product from sample (DNA extracted from mouse ear punch)
[b] S^{+} – PCR product from sample plus WT PCR product

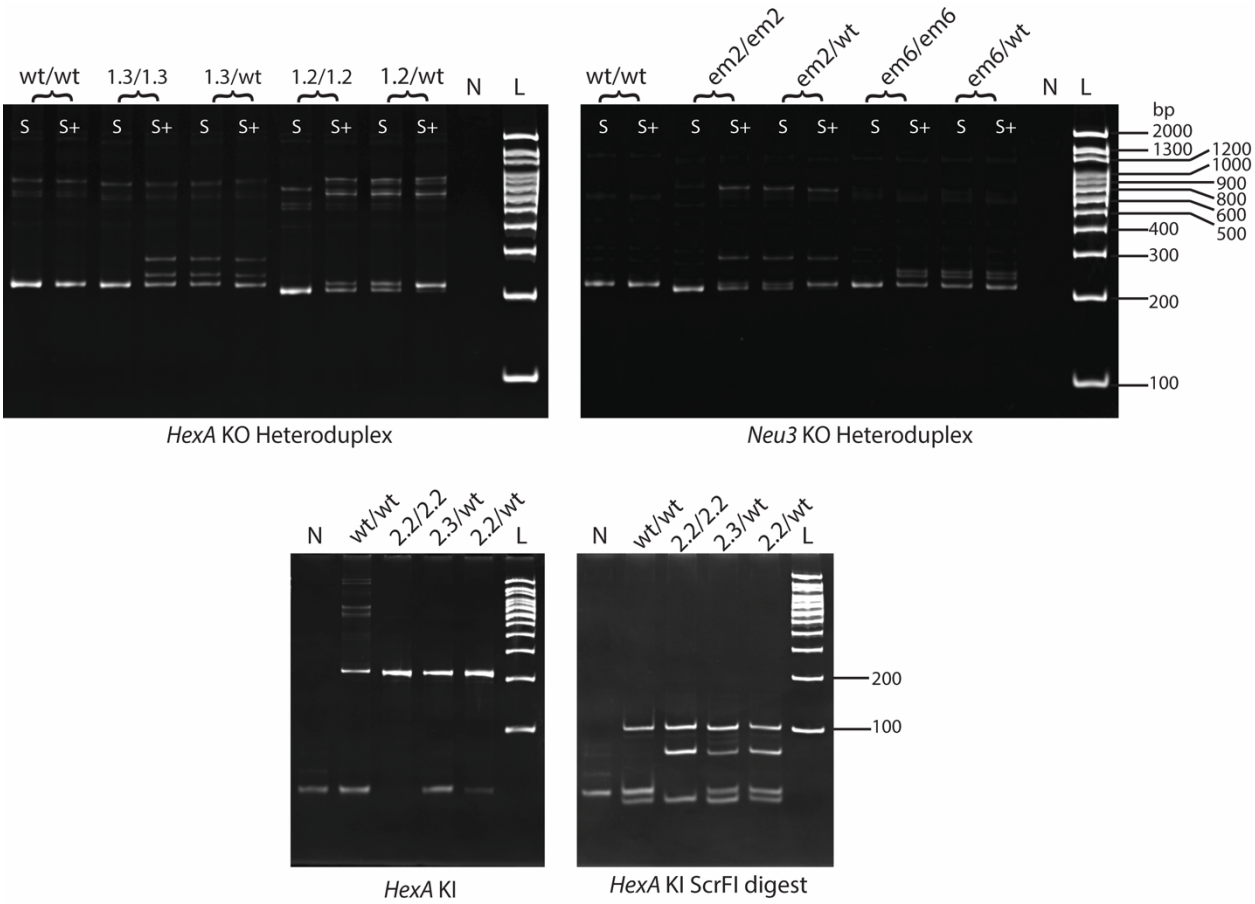

Figure 8: Heteroduplex analysis of *Neu3* KO, *Hexa* KO, and ScrFI digest of *Hexa* KI PCR products.

Polyacrylamide gel electrophoresis of *Neu3* KO (top right) and *Hexa* KO (top left) PCR products with heteroduplex analysis and ScrFI digest of *Hexa* KI (bottom) PCR products. For heteroduplex analysis, wildtype mice do not display heteroduplexes in either S or S^+, while heterozygous mice display heteroduplexes in both. KO mice display heteroduplexes in S^+ only. For ScrFI digest of *Hexa* KI PCR products, appearance of a 73 bp band indicates the G269S mutation. Wt/wt (99bp, 49bp, 45bp), 2.2./2.2 (99bp, 73bp, 45bp), 2.3/wt and 2.2/wt (99bp, 73bp, 49bp, 45bp). L: 100bp Ladder (ThermoFisher); N: Negative Control, S: PCR product of sample DNA, S^+: PCR product of sample DNA + WT DNA PCR product.

4.2 Disease Progression and Survival

dKO and KIKO animals were paired to an age, sex matched control (*Hexa*$^{+/-}$*Neu3*$^{-/-}$, *Hexa*$^{+/G269S}$*Neu3*$^{-/-}$ or *Hexa*$^{+/+}$*Neu3*$^{-/-}$) for all monitoring and testing. All dKO (n=11) or KIKO (n=9) mice consistently displayed a disease phenotype, while control animals (n=20) remained healthy. Both models displayed the first signs of illness at approximately 13 weeks, characterized by hindlimb flexion on tail lift or tremors. dKO and KIKO animals displayed ruffled fur, increased incidence of skin wounds (due to fighting or self-injury), and eye irritations. Ruffled fur along with fighting occurred after 14 weeks, while self-injury or eye irritations occurred after 20 weeks. No difference in onset of signs of illness was detected between models.

Mice were weighed weekly starting at 7-10 weeks until they reached a humane endpoint. dKO and KIKO animals gradually gained weight surpassing controls, which peaked at 16 weeks for dKOs (31.73 ± 5.81g) and at 18 weeks for KIKOs (29.01 ± 3.54g) before declining at ~1g/week until the humane end point (*Figure 9*).

Animals commonly reached humane end point due to weight loss or occasionally due to injury from fighting or self-mutilation. Kaplan–Meier survival analysis using Log-rank tests show a significant difference ($p<0.0001$) in the percent survival between dKO or KIKO from healthy controls (*Figure 10*). Humane endpoint for dKO and KIKO was on average 155±8 days and 154±7 days respectively (approximately 22 weeks). No difference between dKO and KIKO animal survival was detected.

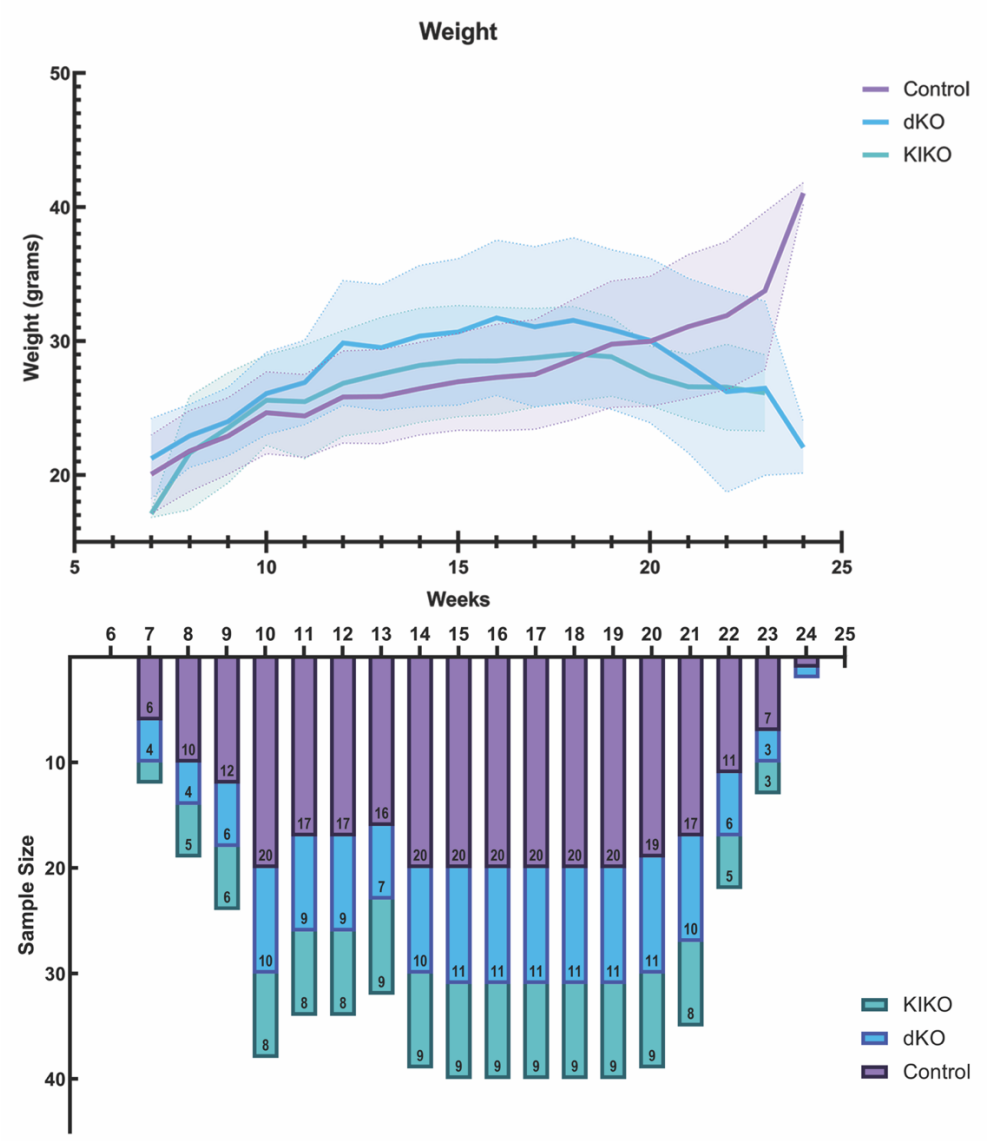

Figure 9. dKO and KIKO weight fluctuations over monitoring period compared to controls.

Mean weight in grams (top graph) of dKO (blue), KIKO (green) and Control (purple) animals from ages 7 to 24 weeks. Shaded areas indicate one standard deviation from mean. Sample size of animals monitored in each week is also shown (bottom graph).

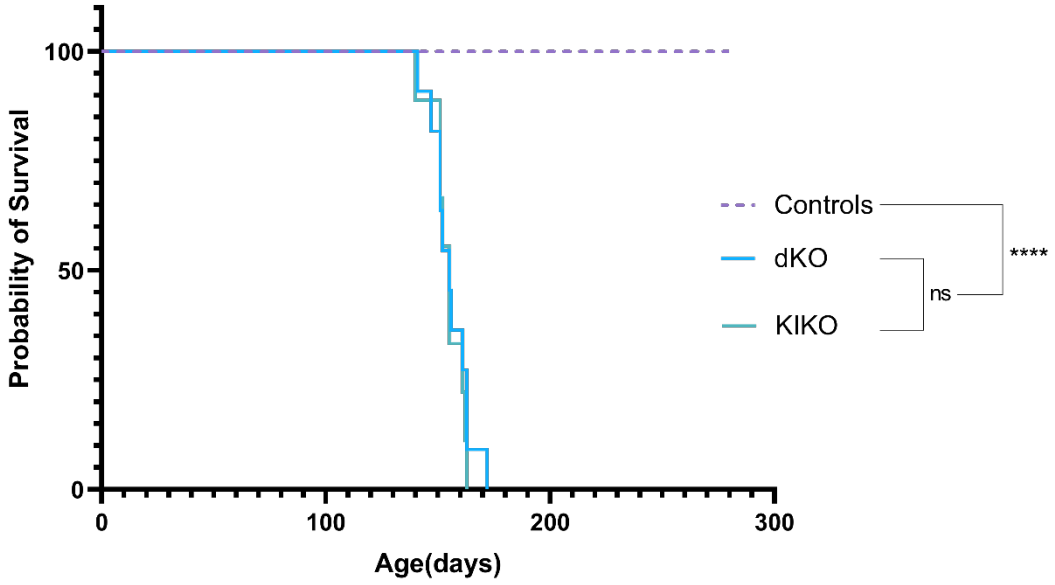

Figure 10. Kaplan–Meier survival analysis of dKO and KIKO models

Kaplan–Meier analysis for dKO (blue, n=11), KIKO (green, n=9), and Controls (purple dotted, n=35). Animals were monitored from 7 weeks after birth for humane endpoint, indicated by one or more of the following conditions: 1) 15% weight loss from maximum weight, 2) excessive shaking, or seizure activity, 3) isolating behaviour, and/or 4) inability to access food or water. The difference in survival probability between dKO or KIKO compared to controls was statistically significant $p<0.0001$ (****), however nonsignificant (ns) between dKO and KIKO groups.

4.3 Neurological and Behavioural Phenotype

Various neurological and behavioural testing including a tail lift test, open field test (OFT) and gait analysis was conducted to determine if any differences in phenotype between the models could be detected. Tail lift testing to score hindlimb flexion, along with other observations of neurological function and behaviour was conducted at routine monitoring between 1-3 times per week, however the data obtained at the ages of 10, 14, 18 and 22 weeks have been selected as representative for simplicity and comparison with open field testing and gait analysis results which was performed at similar intervals.

4.3.1 Routine Monitoring

During weekly routine monitoring, neurological and behavioural assessments were conducted. Signs of neurological dysfunction got progressively more severe as both dKO and KIKO mice aged, and included decreased avoidance towards handlers, decreased or absent rearing behaviour, and a slowing of righting reflex compared to controls. These observations were difficult to quantify but were consistent across various observers and animals. Hunched posture with elevated tail while walking were common observations in both dKO and KIKO mice as well.

Tail lift testing to induce the hindlimb extension reflex was completed at each monitoring session and scored according to Table 3 (*see* Materials and Methods). Repeated scoring over the monitoring period revealed a progressive reduction in extension reflex and eventual flexion response beginning at approximately 14 weeks in both models (*Figure 11*). Control animals occasionally had scores of 1 and was most often associated with over conditioning. Scores at 10, 14, 18 and 22 weeks were tested using Kruskal-Wallis's test with Dunn's multiple comparisons to compare dKO and KIKO with each other and the control group. By 18 weeks, both dKO and

KIKO scores are significantly increased from control animals, (*p=0.0229, p=0.0004* respectively) however no significant difference was detected when comparing the two models. Average scores for dKO, KIKOs and controls for every week can be found in Figure A (*see* Appendix).

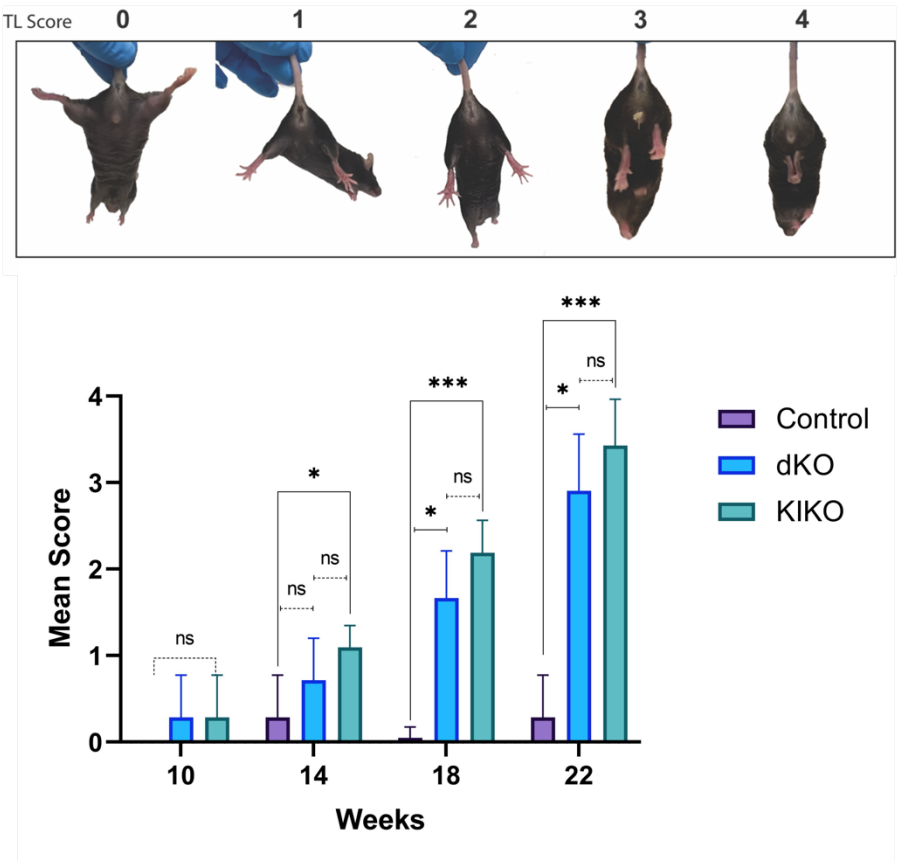

Figure 11. Tail lift testing for assesment of hindlimb extension reflex.

Kruskal-Wallis test with Dunn's multiple comparisons for mean tail lift testing score of dKO (blue, *n=7*), KIKO (green, *n=7*), and Controls (purple, *n=7*) at 10, 14, 18 and 22 weeks of age. Initially dKO and KIKO animals did not display significant hindlimb flexion (average score between 0 and 1) at 10 weeks compared to controls. By 18 weeks both dKO and KIKO scores increased significantly compared to controls without immobility or limb clasping. By 22 weeks, all dKO and KIKO animals display average scores above 2.5 with abnormal hindlimb flexion, while controls continued to have a normal extension response and average scores less than 1. TL score = tail lift score, according to Table 3 (*see* Materials and Methods). * ($p<0.05$), ***($p<0.001$), ns (non-significant).

4.3.2 Open Field Testing

Open field testing was used to measure changes to locomotion and behaviour throughout the monitoring period at 10, 14, 18 and 22 weeks of age. During the 10 minute testing, distance travelled, measures of speed, time mobile and time spent in various zones, and well as fecal boli produced were recorded.

4.3.2.a Mobility Measures

dKO and KIKO mice displayed differences in some mobility measures (*Figure 12*) when compared to controls, but remained stable for others. Distance travelled between all groups was relatively stable over weeks 10-18, until 22 weeks where all groups displayed the minimum average distance travelled within their respective groups. When tested using a two-way ANOVA with Tukey's multiple comparisons distance traveled between the dKO and KIKO groups was statistically significant at 22 weeks ($p<0.05$), but all other comparisons between groups were non-significant. Average speed (m/s) and maximum speed (m/s) when measured from the inside zone of the arena gradually declined in dKO and KIKO animals as they aged. Maximum speed was the most impacted measure of locomotion, with significant differences in dKO and KIKO compared to controls even at 10 weeks ($p<0.01$), indicating early mobility difficulties in both models. In both dKO and KIKO, maximum speed continued to decline steadily every 4 weeks until endpoint. Interestingly, KIKO mice showed the lowest maximum speed, average speed and distance travelled at 22 weeks, and was statistically significant when compared to dKOs ($p<0.05$), but not controls.

Controls were more likely to be immobile, while dKO or KIKO animals were often in constant motion. After removal of outliers, dKO and KIKO animals had similar mobility compared to controls (*see* Appendix, Figure D). dKO and KIKO mice were mobile for

approximately the same amount of time compared to controls at 22 weeks, however at a decreased speed. Thus, measures of average speed in the whole arena and distance travelled do not display significant differences when compared to control animals.

Balance and gait difficulties among the experimental animals were also observed during testing. Track plots illustrating the path animals took during the test showed a distinct wave pattern in dKO or KIKO animals' path from 18 weeks on due to gait and balance issues. These track plots also showed increased use of the inner zone compared to control animals by 22 weeks (*Figure 12, middle*). Additional track plots are shown in Figure B and C (*see pg. 82* Appendix).

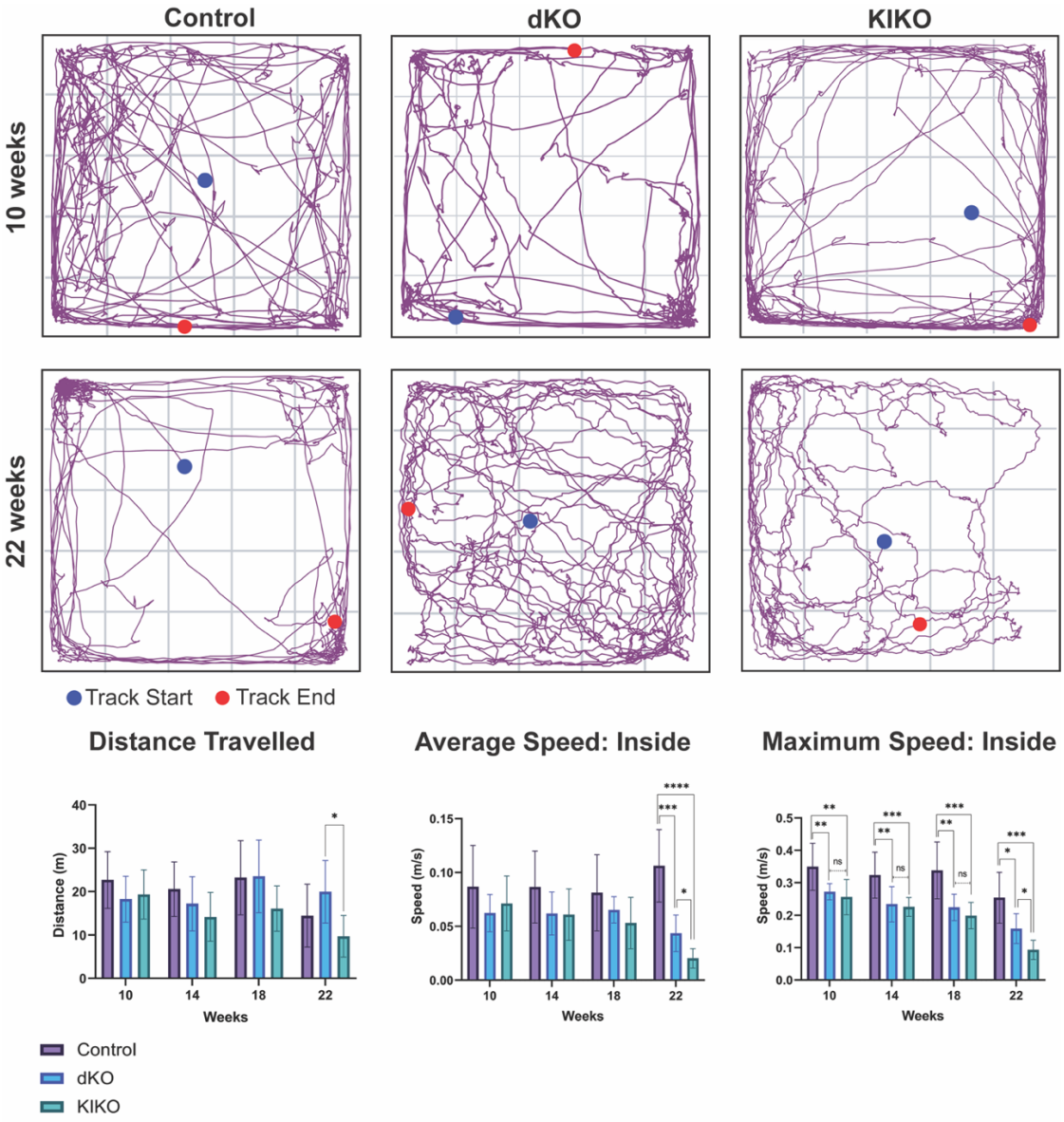

Figure 12. Mobility measures from open field testing

Representative track plots (top) for dKO, KIKO and respective control mice at 10 and 22 weeks from ANYmaze video tracking software. The beginning and end of the track is indicated by the blue and red circles respectively. Increased use of the inner zone, along with gait and balance disturbances were revealed. Distance traveled in meters (left bottom) by dKO (blue), KIKO (green) and controls (purple) at 10, 14, 18 and 22 weeks remained relatively stable.. Average speed (m/s) inside the inner zone (middle bottom) was relatively consistent within groups until 22 weeks. See Figure 13 for definition of zones. Decreases in max speed (m/s) for dKO and KIKO was progressive and significant when compared to controls at 10 weeks. Statistics were conducted using a two-way ANOVA with Tukey's multiple comparisons. * ($p<0.05$), ** ($p<0.01$), *** ($p<0.001$), **** ($p<0.0001$), ns (non-significant). N-values: 10 weeks, dKO (n=3); KIKO (n=8); Control (n=15). 14 weeks; dKO (n=8); KIKO (n=8); Control (n=16). 18 weeks, dKO (n=8); KIKO (n=6); Controls (n=15). 22 weeks, dKO (n=6); KIKO (n=5); Controls (n=10).

4.3.2.b Behavioural Measures

dKO and KIKO animals also showed changes to behavioural measures. These measures included the time animals spent in each zone and number of fecal boli produced during the test, which can indicate anxiety-related behaviour. A decrease in thigmotaxis, or tendency to travel along walls in the outer zone, was observed in dKO and KIKO at around 14 weeks, and continued to gradually diminish until 22 weeks. This was measured by ANYmaze software as time spent in the inner and outer zones (*Figure 13, top*). This supported track plot findings and confirmed that dKO and KIKO animals spend more time in the inner zone compared to controls from 14 weeks on. The largest difference in time spent in the inner zone was seen at 22 weeks, where dKOs spent the longest time of all groups in this zone and was statistically significantly ($p<0.001$) compared to age matched controls when using a two-way ANOVA with Tukey's multiple comparisons. Control animals also spent an increased amount of time in corners compared to dKO ($p<0.0001$) and KIKO ($p<0.001$) animals at 22 weeks (*Figure 13, bottom left*).

Conversely, fecal boli production by dKO and KIKO animals had a tendency to increased until 18 weeks before decreasing at 22 weeks. This increase however was not statistically significant. Fecal boli production by control animals remained consistent across weeks (*Figure 13, bottom right*).

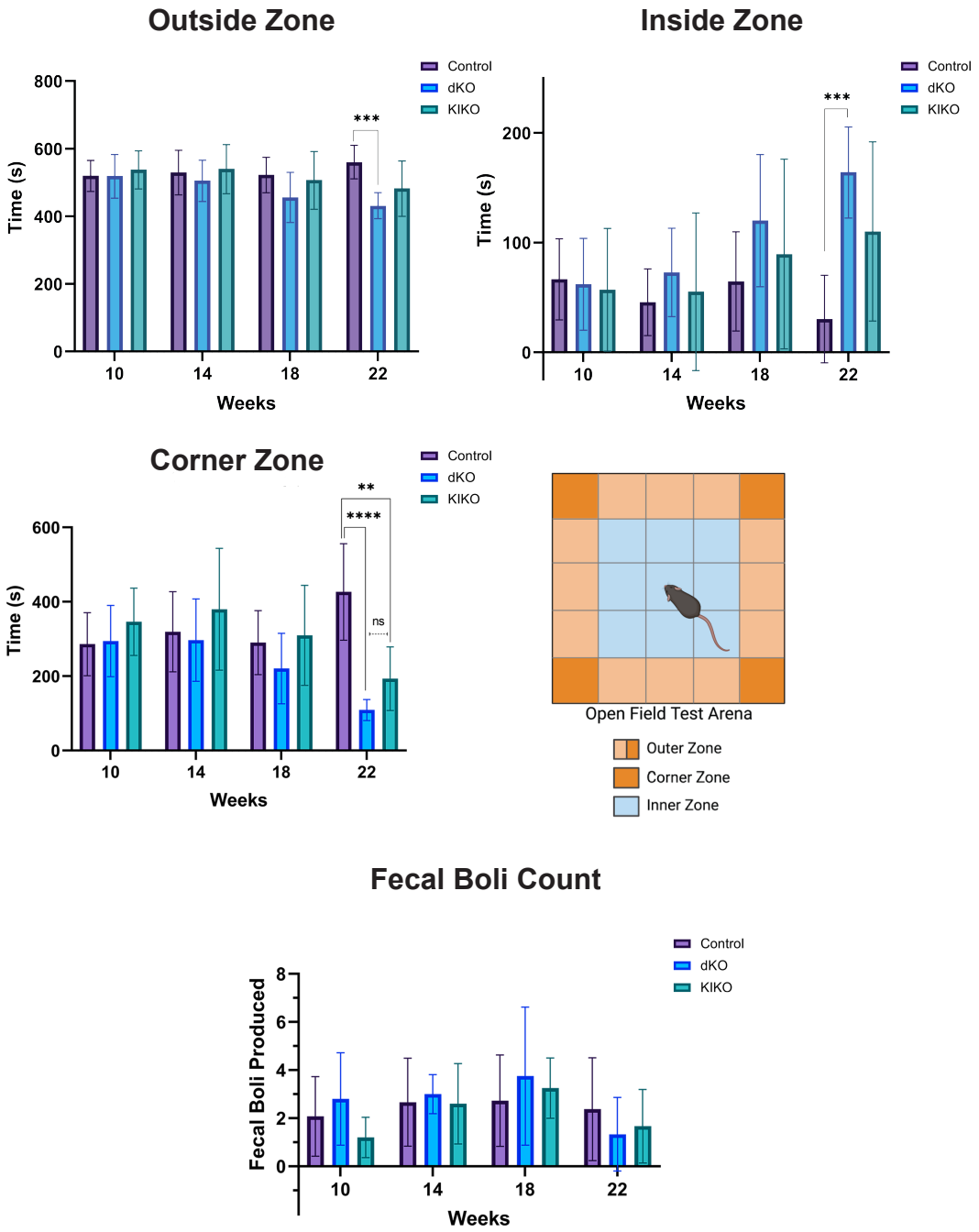

Figure 13. Behavioural measures from open field testing.

Time spent in the outer (top left), inner (top right) and corner (middle left) zones by Controls (purple), dKO (blue), and KIKO (green) at 10, 14, 18 and 22 weeks. dKO/KIKO display increased time in inner zone compared to the outer zone and corners. Fecal boli counts increased in dKO and KIKO groups up to 18 weeks before decreasing at 22 weeks. Statistics were done with a two-way ANOVA and Tukey's multiple comparisons. * ($p<0.05$), ** ($p<0.01$), *** ($p<0.001$), **** ($p<0.0001$), ns (non-significant). N-values: 10 weeks, dKO (n=3); KIKO (n=8); Control (n=18). 14 weeks; dKO (n=8); KIKO (n=8); Control (n=13). 18 weeks, dKO (n=8); KIKO (n=6); Controls (n=12). 22 weeks, dKO (n=6); KIKO (n=5); Controls (n=10).

4.3.3 Gait Analysis

Gait analysis was performed on the same day as open field testing at 10, 14, 18 and 22 weeks of age. dKO and KIKO animals appeared to have normal gait patterns compared to controls at 10 weeks, before becoming increasingly disorganized by 22 weeks (*Figure 14*). Additional gait prints from 14 and 18 weeks alongside those in Figure 14 can be found in Figure E (*see* Appendix).

Decreased coordination of fore and hindlimb paw placement was observed starting at 14 weeks and increased in severity until humane endpoint. Forelimb and hindlimb stride length and stance width, as well as hindlimb sway distance was measured 3 times from the center of each paw in consecutive steps (*Figure 14, top left*) and averaged for each animal, before being tested using two-way ANOVA and Tukey's multiple comparisons. At 10 weeks hindlimb stride lengths were similar to controls but began to decrease significantly for dKO animals at 14 weeks ($p<0.01$). KIKO animals had a similar pattern, with significant decreases in stride length at 14 weeks ($p<0.05$). Stride lengths continued to shorten over time, and by 22 weeks average hindlimb stride length had decreased by 45% and 41% for dKO and KIKO respectively when compared to controls (dKO, $p<0.05$; KIKO, $p<0.0001$). Forelimb stride (*Figure 15, top left*) followed a similar pattern with significant decreases in dKO ($p<0.05$) starting at 14 weeks and KIKO ($p<0.001$) starting at 18 weeks when compared to controls.

Hindlimb stance was significantly narrower in dKO and KIKO compared to controls at 14 weeks ($p<0.01$), before increasing at 18 weeks (*Figure 15, bottom right*). Decreases in hindlimb sway distance was also observed and significant when comparing dKO or KIKO to controls at 14 (dKO, $p<0.001$; KIKO, $p<0.01$) and 18 weeks (dKO, $p<0.0001$; KIKO, $p<0.05$) (*Figure 15, bottom left*). Consistent significant differences between dKO and KIKO models were not detected.

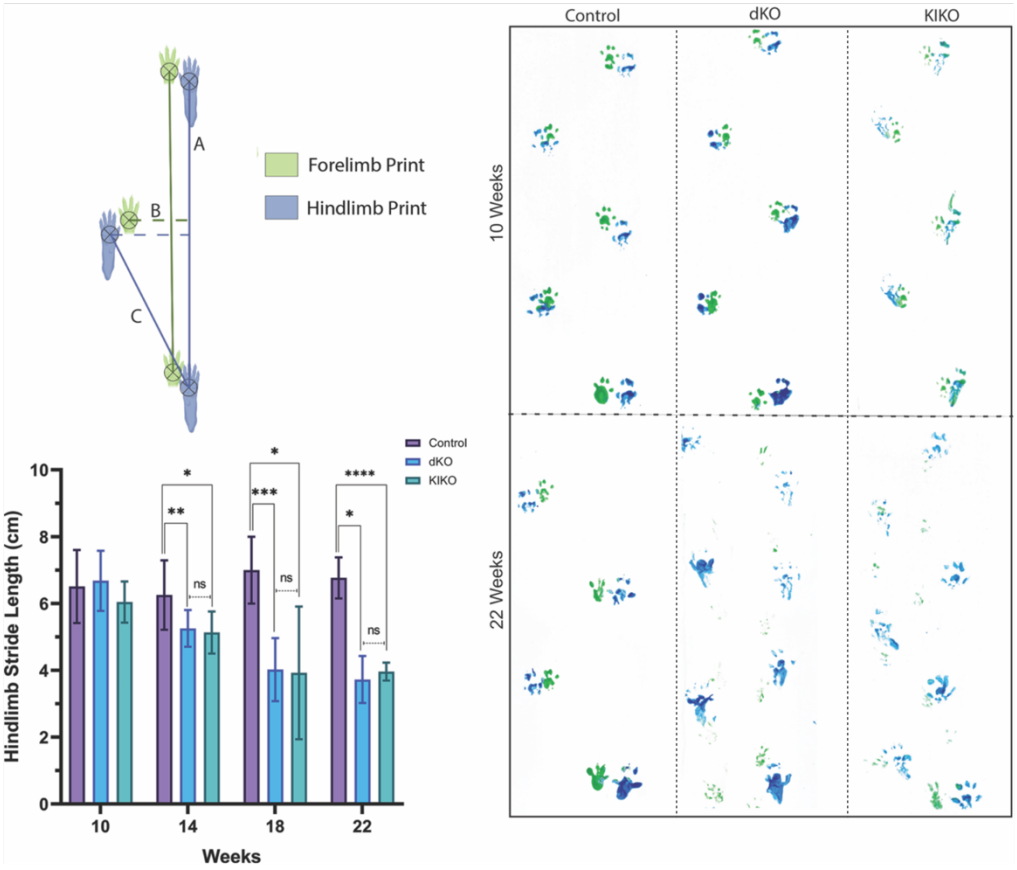

Figure 14. Gait analysis prints and hindlimb stride length

Representative footprints from gait analysis of dKO, KIKO and controls at 10 and 22 weeks. All animals have similar hindlimb stride length at 10 weeks with similar paw placement pattern. Gait becomes disorganized by 22 weeks in both models with significantly shortened hindlimb stride length (cm) from 14-22 weeks. Stride length, width and sway were measured according to top left figure (A: stride length, B: stance width; C: Hindlimb sway distance). Statistics were done with a two-way ANOVA and Tukey's multiple comparisons. * ($p<0.05$), ** ($p<0.01$), *** ($p<0.001$), **** ($p<0.0001$), ns (non-significant). N-values: 10 weeks: Control, n=13; dKO, n=5; KIKO, n=8. 14 weeks: Control, n=16; dKO, n=16; KIKO, n=7. 18 weeks: Control, n=10; dKO, n=5; KIKO, n=5. 22 weeks: Control, n=8; dKO, n=3; KIKO, n=5.

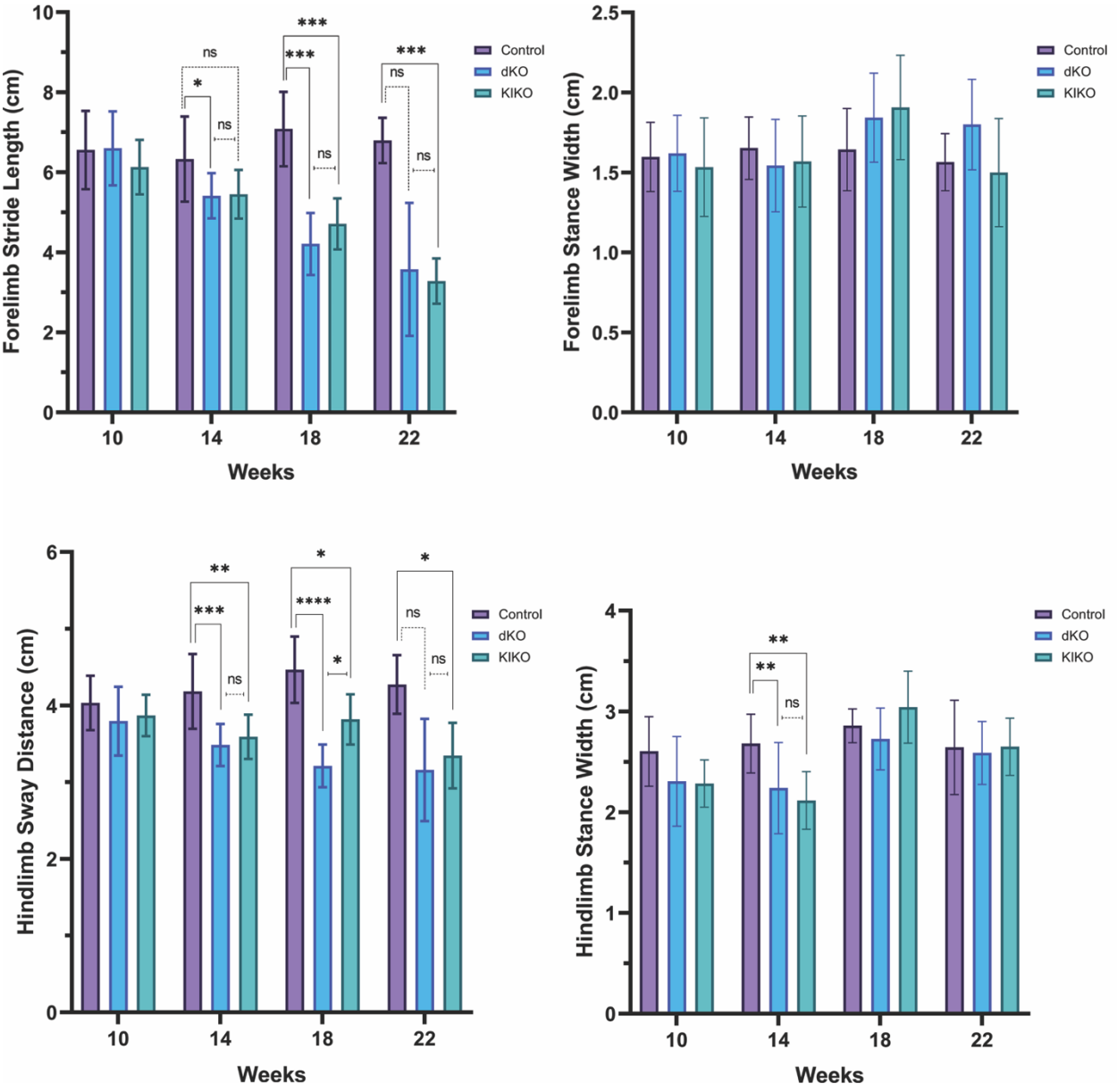

Figure 15. Additional gait analysis measures

Various gait measurements for dKO (blue), KIKO (green) and controls (purple) at 10, 14, 18 and 22 weeks. Stride, stance, and sway were measured according to Figure 14 (top left). Statistics were done with a two-way ANOVA and Tukey's multiple comparisons. * ($p<0.05$), ** ($p<0.01$), *** ($p<0.001$), **** ($p<0.0001$), ns (non-significant). N-values: 10 weeks: Control, n=13; dKO, n=5; KIKO, n=8. 14 weeks: Control, n=16; dKO, n=16; KIKO, n=7. 18 weeks: Control, n=10; dKO, n=5; KIKO, n=5. 22 weeks: Control, n=8; dKO, n=3; KIKO, n=5.

4.4 GM2 Detection in the Brain

Once dKO or KIKO animals reached humane endpoints they were euthanized with an age, sex matched control. Various methods to gather evidence of GM2 ganglioside accumulation in the brain were used including inspecting and weighing dissected brains, LC-ESI MS (data generated by collaborators in the Whitehead lab at Western University) and immunohistochemistry using anti-GM2 antibody.

4.4.1 Gross Anatomical Observations

Following euthanasia, brains were collected, photographed, and weighed. Brain images and weights from perfused animals were not included in this analysis. dKO and KIKO brains were consistently a pale-yellow colour (*Figure 16, bottom*) compared to controls following dissection. Brains from dKO and KIKO animals also appeared larger and had increased brain weight on average than controls. Within pairs, the dKO or KIKO animals had larger brain weights, and smallest body weights compared to controls (*Figure 16, top*). Attempts to normalize brain weights to tibia length was unsuccessful due to inability to accurately measure tibia lengths. While not statistically significant or normalized, these observations suggest large accumulations of GM2 in the brains of dKO and KIKO animals.

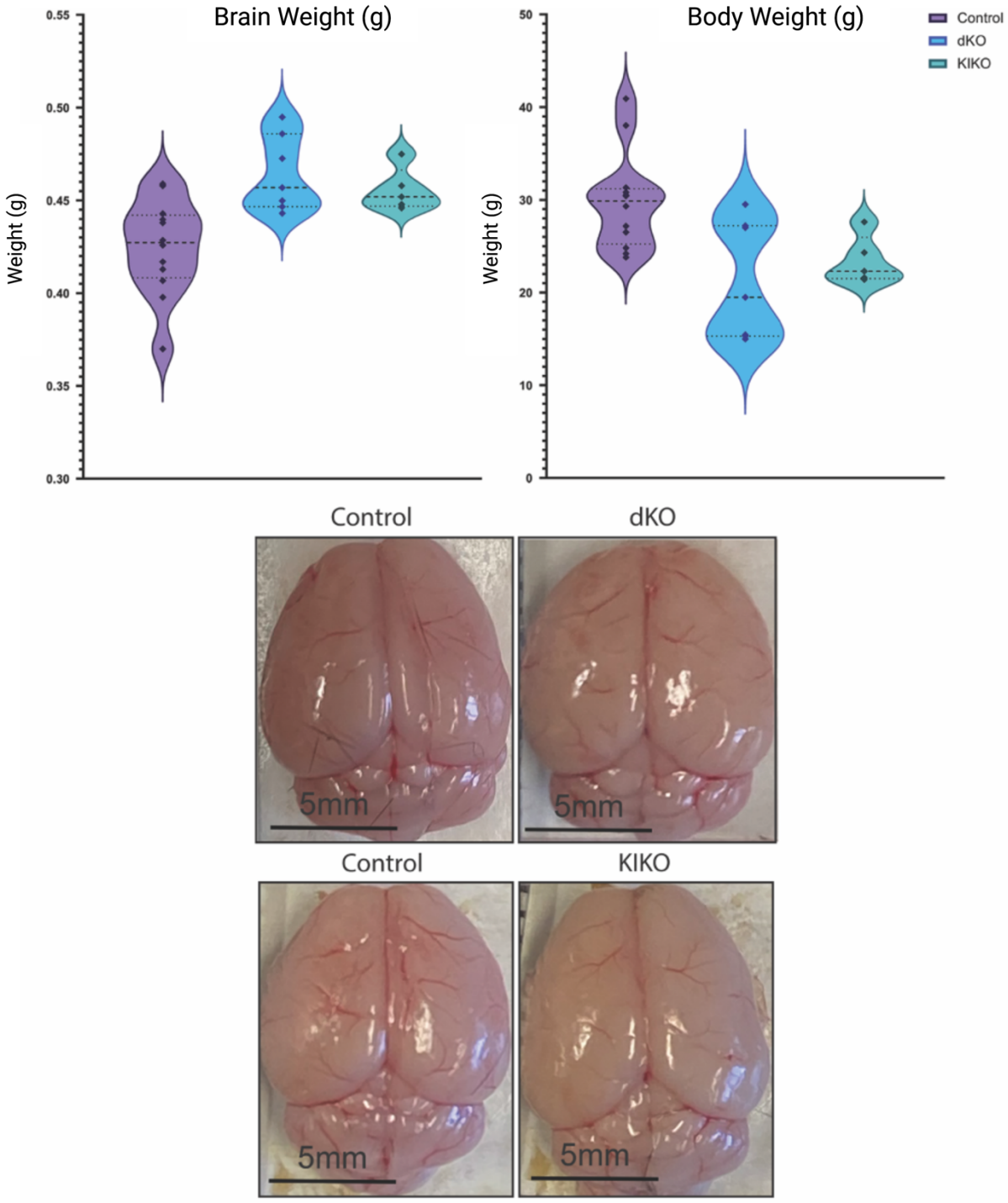

Figure 16. Gross anatomical brain images and weights of control and dKO or KIKO pairs.

Brain weight for dKO (n=7) or KIKO (n=5) animals (top left) was increased at humane endpoint compared to controls (n=12), while body weight (top right) was decreased. Dashed line on violin plots indicates mean, dotted lines indicate quartile, and diamonds inside are individual values for each sampled animal. Brains were imaged and weighed immediately after dissection.

4.4.2 Immunohistochemistry (IHC)

Brains were fixed in formalin, embedded in paraffin for immunohistochemistry and sagittal sections beginning at the midline moving laterally were taken from the brain. Matched slides for dKO or KIKO and control pairs were selected based on anatomical features including cerebellar nuclei, hippocampal formation and ventricle position using Allen Mouse Brain Atlas[145] (mouse.brain-map.org). Brains were immunostained using anti-GM2 antibody and counterstained with methyl green.

GM2 accumulation was observed in various brain regions of dKO and KIKO animals, causing cell shape changes and cytoplasmic swelling. Large granular accumulations were observed in the cell bodies of neurons in the pons, medulla oblongata and thalamus (*Figure 17*). Deep cerebellar nuclei and Purkinje cells of both dKO and KIKO animals also exhibited GM2 accumulation (*Figure 18)*. Some accumulation or cell vacuolization was also observed in the cerebral cortex, superior colliculus, hypothalamus, and striatum (Figure F, *see* appendix).

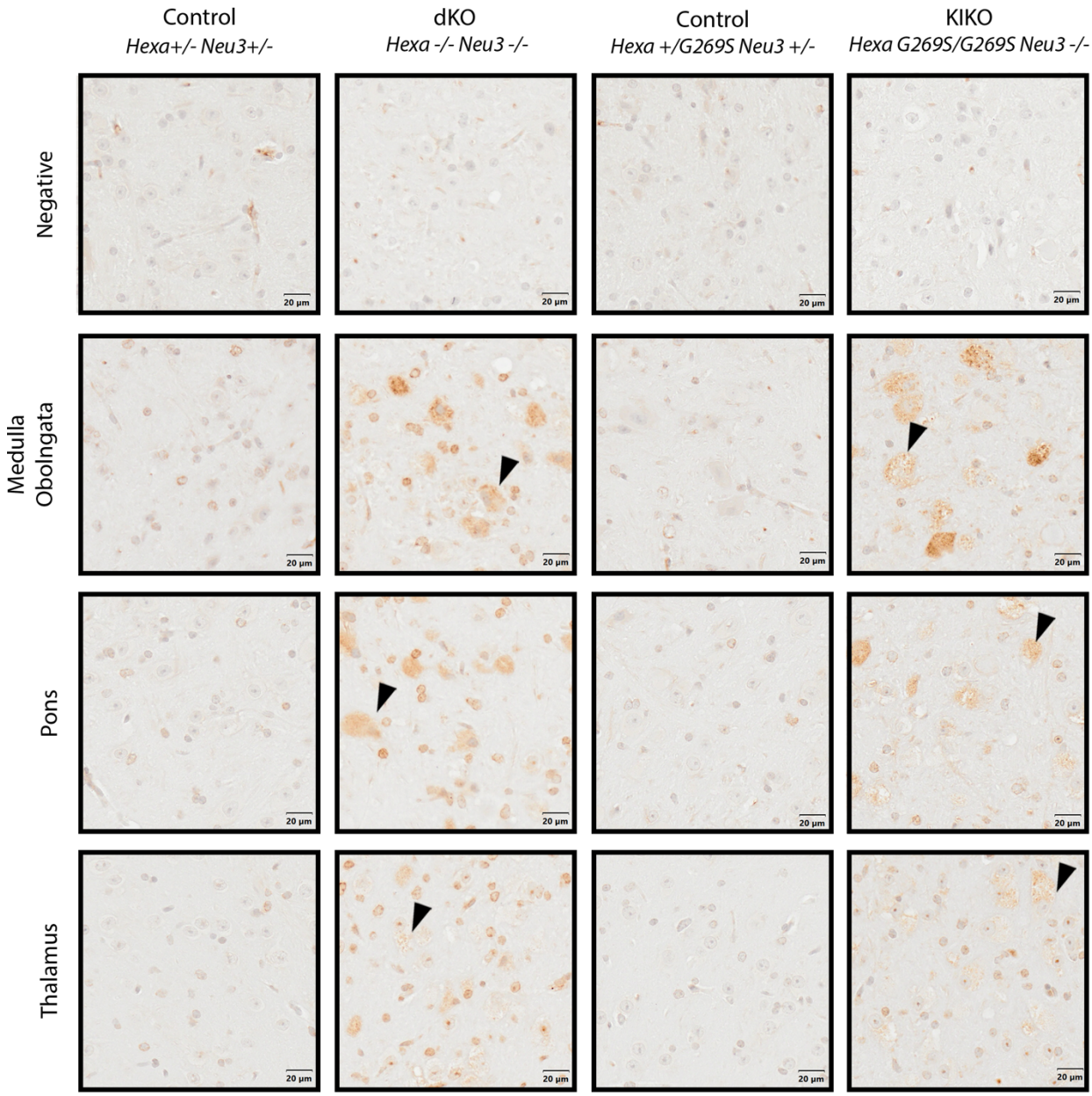

Figure 17. Immunohistological assessment of GM2 ganglioside accumulation.

Brains from dKO and KIKO animals with an age-sex matched control collected at humane endpoint between 22-23 weeks. Images are from 5-micron paraffin sections stained with anti-GM2 antibody counterstained with methyl green. Positively staining material inside cell bodies (black arrows) can be seen in multiple areas of dKO and KIKO animal brains. Negative controls (medulla oblongata shown) stained without anti-GM2 antibody did not contain these positively staining cells, although did show increased cytoplasmic areas, and vacuolization. Images were taken using a 20x objective on the Olympus VS200 scanning light microscope. Each scale bar represents 20μm.

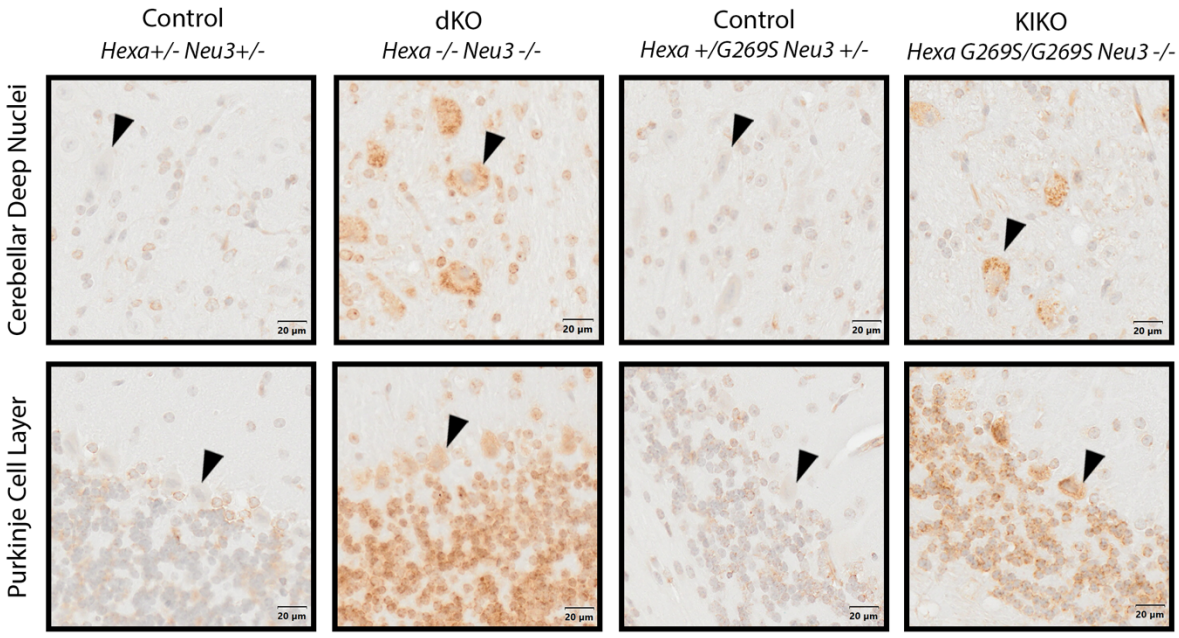

Figure 18. Immunohistological assessment of cerebellar deep nuclei and Purkinje cell layer for GM2 ganglioside accumulation.

Brains from dKO and KIKO with an age-sex matched control were collected at humane endpoint between 22-23 weeks. 5-micron paraffin sections immunostained with anti-GM2 antibody, and counterstained with methyl green were imaged using a 20x objective on the Olympus VS200 microscope. Purkinje cells and cell bodies in deep cerebellar nuclei (black arrows) with increased GM2 staining can be seen in dKO and KIKO animals.

4.4.3 LC-ESI-MS

LC-ESI-MS on the brains of an age and sex matched dKO/control pair was performed. Total percent of peak areas for GM1, GM2 and GM3 ganglioside were determined to examine the relative ganglioside levels. This revealed a 57% increase in relative GM2 content in the dKO animal compared to control. Relative levels of GM1 and GM3 ganglioside decreased by 37% and 20% respectively in dKO compared to the control. GM2 gangliosides with fatty acids of d16:1/18:0, d18:1/18:0, d20:1/18:0 and d20:1/20:0 were increased in the dKO animal as well. This further confirms GM2 ganglioside accumulation relative to other major gangliosides in the brains of dKO animals, however additional pairs will need to be analyzed.

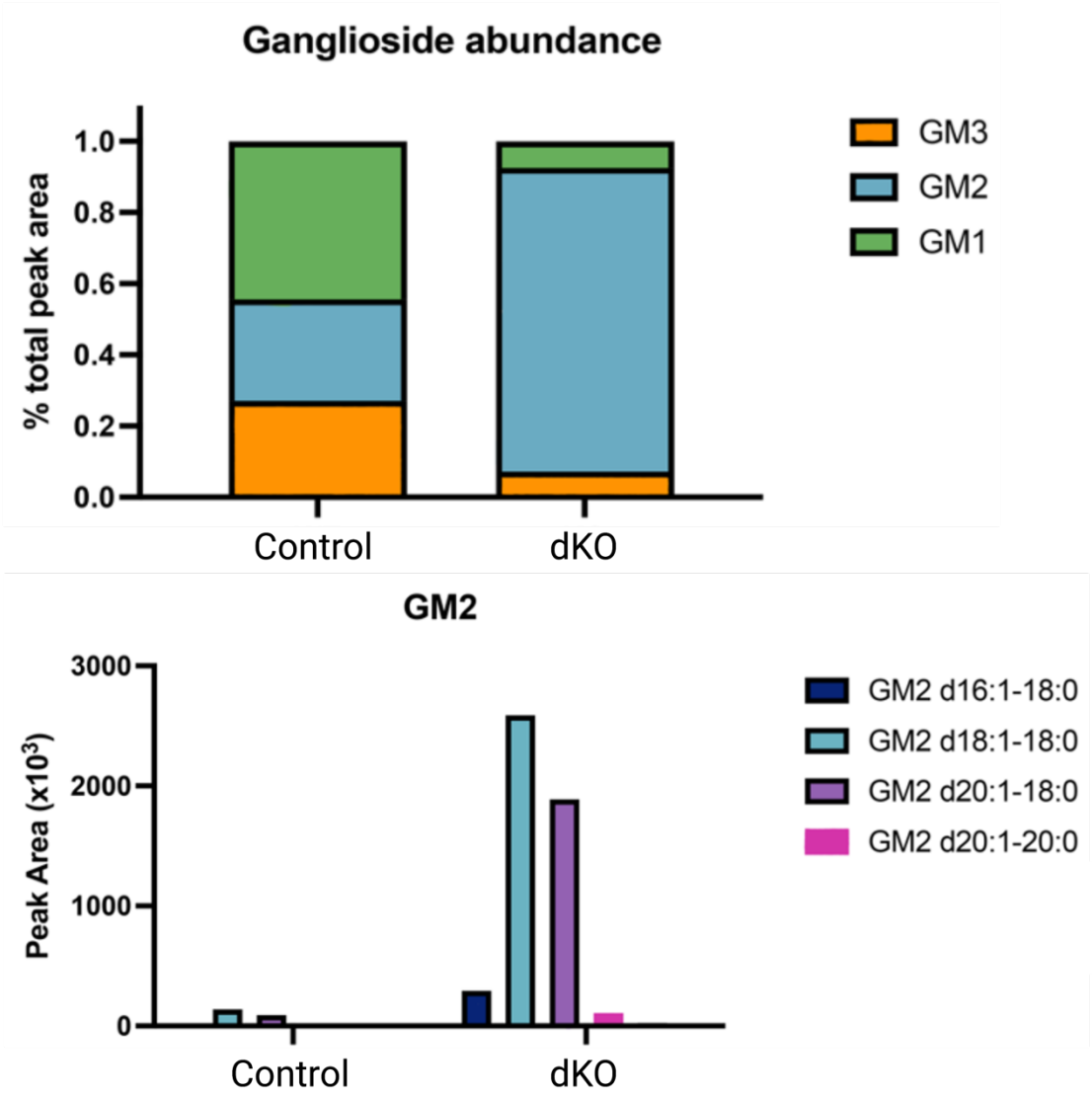

Figure 19. Ganglioside Changes in the Brains of a dKO animal vs Control

LC-ESI-MS results for gangliosides extracted from the brains of one dKO and control pair. Top: percent total area under the MS peaks for GM1, GM2 and GM3 ganglioside. Bottom: Peak areas for GM2 spectra with d16:1/18:0, d18:1/18:0, d20:1/18:0 and d20:1/20:0 fatty acid chains. Samples were separated using LC with Luna® 3 µm NH2 100 Å NH2 LC column (150 mm × 1 mm). ESI-MS was performed using the *Waters QToF Micro* instrument. Mass ranges were (600 – 1800) m/z for MS only. The mass spectra were analyzed using the Skyline software. Ganglioside extracts were conducted at University of Manitoba by Emily Barker (Triggs-Raine Lab). LC-ESI-MS data and figure was generated at Western University by Wendy Wang and fellow members of the Whitehead Lab.

4.5 β-Hexosaminidase Activity Assay

Total activity of β-hexosaminidase was measured using the fluorometric MU assay with 4-MUGS substrate. Both dKO and KIKO animals displayed significantly decreased production of MU, the MUGS cleavage product, and therefore enzyme activity (nM MU produced/μg protein/minute, $p<0.0001$) compared to controls, however, was non-significant when models were compared. All control animals contained at least one *Hexa* wt allele (*Figure 19*).

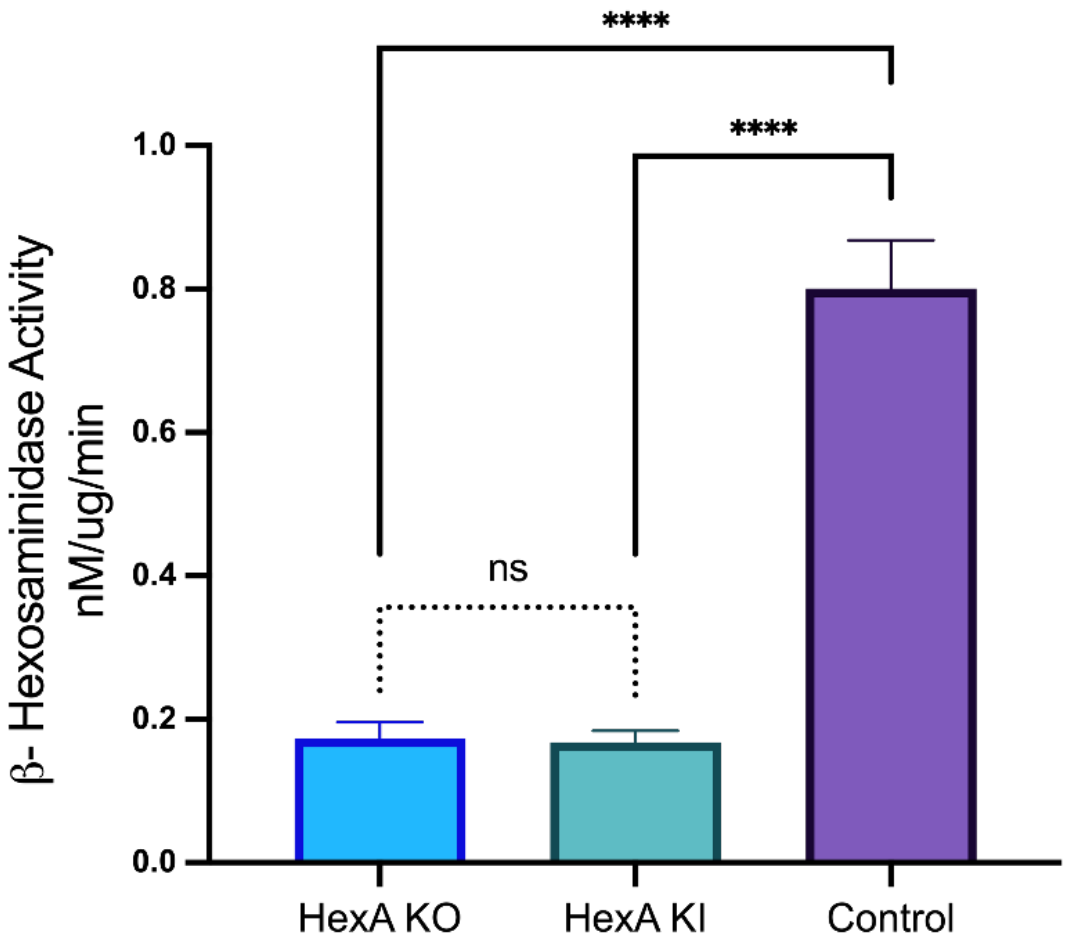

Figure 20. β-Hexosaminidase Activity Assay

β-Hexosaminidase activity (nM/μg/min) in *Hexa* KO (*Hexa*$^{1.2/1.2}$ or *Hexa*$^{1.3/1.3}$, n=6), *Hexa* KI (*Hexa*$^{2.2/2.2}$, n=5) compared to controls (*Hexa*$^{1.2/wt}$, *Hexa*$^{1.3/wt}$, *Hexa*$^{2.2/wt}$; n=10) from mouse brain tissue. Assay was conducted with 20 μg protein, 1mM MUGS in CP buffer (pH 4.2) for 30 minutes at 37℃. Reaction was quenched with GC buffer (pH 10.7), and raw fluorescent units were measured using SpectrMax M2 plate reader ($\lambda_{excitation}$: 365 nm; $\lambda_{emission}$: 450 nm). Standard curve (not shown) was generated with methylumbelliferone in GC buffer from 0 to 1000 nM for interpolation of sample values. In the brains of both models, HexA activity is significantly reduced ($p < 0.0001$, ****) compared to controls. However, differences between models are nonsignificant (ns). Statistics were generated using a one-way ANOVA with Sidak's multiple comparison testing.

4.6 Neuaminidase 3 Activity Assay

Relative activity of all neuraminidases was assayed using the production of fluorometric MU from 4-MU-NANA substrate and reported as nM of MU produced/μg protein/minute. Total neuraminidase activity in the presence of increasing concentrations of ZANA showed steady decline in *Neu3*$^{+/+}$ (WT) animals. *Neu3*$^{-/-}$ (Neu3 KO) animals displayed lower uninhibited neuraminidase activity than WT animals and did not show a similar trending decrease (*Figure 20)*.

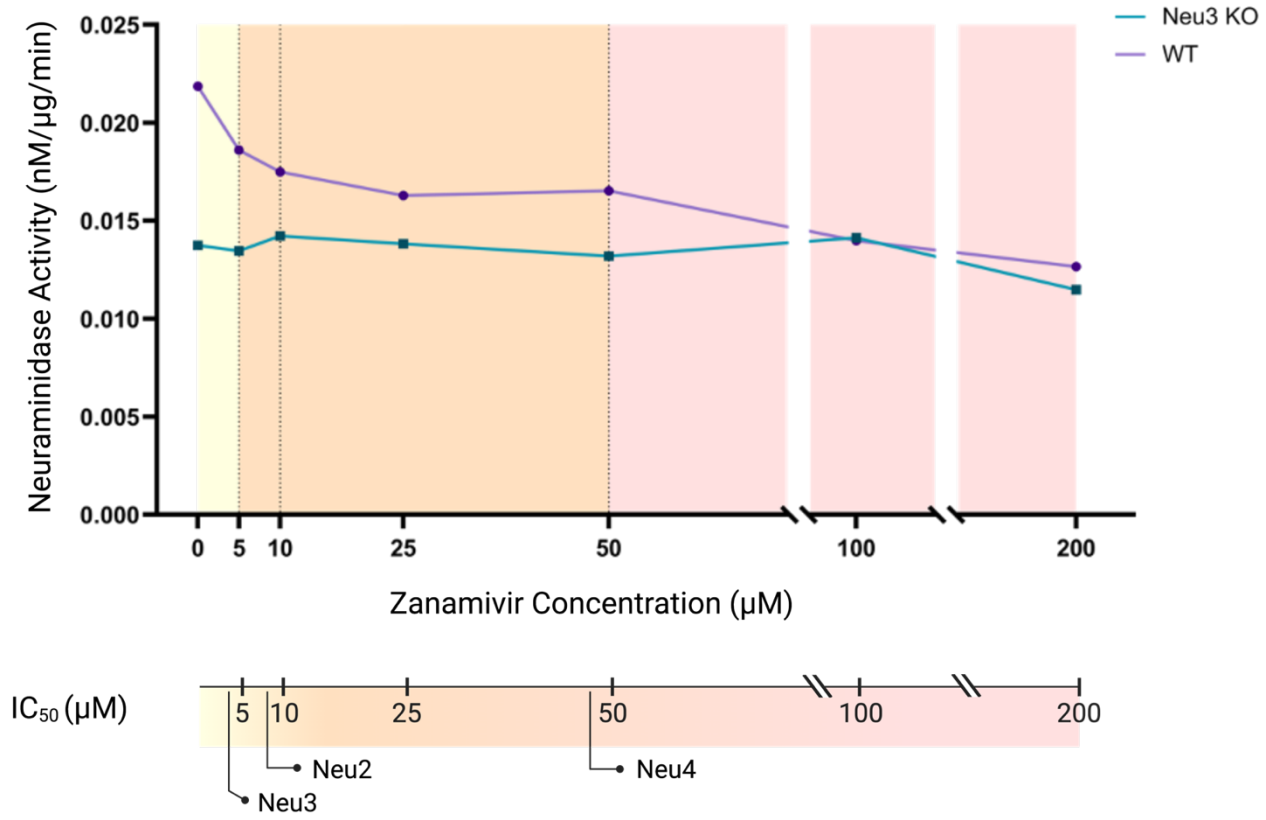

Figure 21. Neuraminidase Activity Assay

Top: Total neuraminidase activity (nM/μg/min) in *Neu3* KO (n=1) and WT (n=1) mouse brain tissue. Assay was conducted with 150, 225 and 300 μg protein, 200 μM 4-MU-NANA substrate in SA buffer (pH 4.4) for 1 hr at 37℃, at each concentration of Zanamivir (0, 5, 10, 25, 50, 100 and 200 μM). Reaction was quenched with GC buffer (pH 10.7), and raw fluorescent units were measured using SpectrMax M2 plate reader ($\lambda_{excitation}$: 365 nm; $\lambda_{emission}$: 450 nm). Standard curve (not shown) was generated with methylumbelliferone in GC buffer from 0 to 1000 nM for interpolation. Bottom: IC_{50} values are shown as μM Zanamivir against various human neuraminidases Neu3, Neu2 and Neu4 [146]. In *Neu3* KO animals, neuraminidase activity is lower compared to WT control and does not show decreased activity at the IC_{50} of ZANA against Neu3.

5 Discussion, Future Directions and Conclusion

5.1 Discussion

GM2 gangliosidoses including TSD, SD and GM2AP deficiency are rare LSDs in which accumulation of GM2 results in damage to the central nervous system. GM2 gangliosidoses vary in onset due to residual HexA activity and are characterized by changes to mobility and behaviour before often resulting in pre-mature death. Mice with deficiencies in *Neu3* and *Hexa* recapitulate juvenile GM2 gangliosidoses in humans and have shared features including GM2 accumulation and a progressive degeneration of the central nervous system, reappearance of reflexes from previous stages of development, as well as mobility and behavioural changes[137]. In this study, we attempted to create a mouse model for chronic-adult GM2 gangliosidoses using the most common adult-onset human mutation in *HEXA,* G269S, combined with *Neu3* deficiency for use in pre-clinical investigations of GM2 gangliosidoses treatments.

The dKO and KIKO models that we developed displayed signs of GM2 gangliosidoses comparable to those found in humans, however few significant differences were detected between the two models. Thus, the KIKO model does not appear to produce a late onset phenotype based on our investigations. Results of the neurological and behavioural testing, along with survival analysis suggested that *Hexa*^{G269S} KI did not produce any HexA, which would increase GM2 degradation in mice. Additionally, IHC findings did not reveal noticeable differences between the GM2 storage in KIKO and dKO brains. Enzyme assays testing HexA activity confirmed this with HexA activity in the KIKO mice comparable to dKO mice.

Both dKO and KIKO models displayed premature death at ~22 weeks with disease onset at ~13 weeks. This is consistent with a previously reported dKO model (*Hexa*$^{-/-}$*Neu3*$^{-/-}$*)* that survived up to 22 weeks[137], and *Hexb*$^{-/-}$ models of SD which survive up to 26 weeks[132,134]. While

dKO animals were previously reported to be sterile, instances of dKO females and males producing offspring were observed.

Progression of disease in all these models recapitulates GM2 gangliosidoses in humans with initially normal development compared to littermates, followed by progressive neurodegeneration and behavioural changes. dKO and KIKO models exhibit premature death and earlier onset compared to the *Hexa*$^{-/-}$ model which is on the mild end of the adult-onset forms of GM2 gangliosidoses, has disease onset at ~ 1 year and death at 2 years[135].

Slow movement, loss of reflexes and rearing behaviours, tremors, loss of gait coordination and balance with similar progression and onset were observed in both models, suggesting severe neurological dysfunction. Widespread accumulation of GM2 throughout the CNS is the probable cause of this dysfunction, which was seen with equal severity in both models. Accumulation of GM2 in areas involved in motor coordination and sensory signal relay such as the cerebellum, thalamus and brainstem were also seen in both models, and may be responsible for the neurological deficits.

The hindlimb extension reflex where adult mice extend all four paws when lowered towards a surface by the tail, was diminished in these models. This progressive decrease in hindlimb extension reflex and increase in flexion resulted in hindlimb clasping towards humane endpoint. This reflex can be initiated by visual stimuli and tactile sensations in the vibrissae (whiskers) or paws. In mice less than 2 weeks old, limb clasping is slowly converted to extension once the eyes are open, however tactile stimuli to the vibrissae is sufficient to cause hindlimb extension throughout the postnatal period[147]. In dKO or KIKO mice, normal extension reflex is observed until about 14 weeks, before progressively becoming weaker and finally regressing to limb clasping. Loss of reflexes or regression to a previous developmental stage is a sign of a

severe neurological disorder, and in GM2 gangliosidoses across multiple onsets, exaggerated reflexes and reappearance of Babinski reflex is common[61,97].

Loss of the hindlimb extension reflex has been associated with models such as spinocerebellar atrophy[148] and dystonia musculorum deformans[149], where cerebellar degeneration or denervation is a prominent feature. Cerebellar nuclei in both models were one of the most prominent areas of accumulation of GM2 in the brain, suggesting damage to this area may be partially responsible for the abnormal reflexes. Additionally, specific nuclei in the pons and medulla that are responsible for relaying somatic sensory information from the hindlimbs to the brain[150] also exhibit a high degree of GM2 accumulation in these models.

Behavioural changes were observed in both models including decreased avoidance and a significant decrease in thigmotaxis suggesting lowered anxiety[151]. This contradicts previous findings of thigmotaxis which were increased in dKO mice[137]. Caution must be used when drawing conclusions about animal emotionality using the open field test particularly when using models where mobility is impaired[152]. To ensure ambulatory ability of the animal being tested was not a confounding variable, distance travelled between mice should be similar. Indeed, changes to distance travelled was not significant for both models when compared to controls at all timepoints suggesting that while coordination and speed are impacted general mobility is not. Thigmotaxis is also reliant on tactile sensations such as whisker contact with the walls of the maze. Damage to these, or the communication between the sensory neurons and the higher processing centers, can result in decreased thigmotaxis[153]. Light conditions during testing are a key factor, and different lighting conditions can impact testing scores[154]. While lighting during OFT was controlled between experiments, the possibility of visual impairments in these models may confound this. The previously reported dKO animals[137] did exhibit GM2 accumulation in

the retina, suggesting visual problems. Thus, while decreased thigmotaxis may indicate decreased anxiety, other factors including loss of visual and tactile sensations may explain these decreases.

Fecal boli (FB) production tended to increase in dKO and KIKO animals during open field testing up to 18 weeks, before decreasing at 22 weeks. Any increases in FB production from dKO and KIKO animals compared to controls were not significant. FB is another indication of anxiety in rodents[153], though it's use as a measure of emotionality has previously been criticized due to several factors impacting defecation[153]. For example, reduced food consumption in these models, as evidenced by rapid weight loss after 18 weeks, could contribute to the drop in FB production at 22 weeks regardless of emotional state [152]. Nerve conduction to and within the gastrointestinal system could also be damaged by GM2 accumulation, impacting defecation. Severe autonomic dysfunction of the GI tract was previously reported in a case of adult-onset SD in humans and was attributed to accumulation of GM2 in the mesenteric ganglion cells[155]. Thus, while this increased defecation may not indicate significant changes to anxiety-related behaviours, it may provide an indication of the trends in feeding behaviours and gastrointestinal function in these models.

Most animals were euthanized at humane endpoint due to weight loss, even though food and water were readily available on the floor of cages and general mobility was preserved until endpoint. Brain areas involved in satiation such as the hypothalamus did show some GM2 accumulation in both models and may account for loss of weight. Further as animals age and neurological dysfunction worsens, difficulties swallowing, or dysphagia may result in weight losses[135]. KIKO animals began to lose weight after 18 weeks compared to 16 weeks for dKO, suggesting that these animals may have a later onset dysphagia. This however did not appear to

lengthen lifespan. Poor volition has also been determined as the cause of weight loss for patients with juvenile forms of SD[156], and this may also play a role in weight loss of mice.

While both models have features of GM2 gangliosidoses, failure of the KIKO model with the G269S mutation to recapitulate adult onset GM2 gangliosidoses draws attention to the limitations of these models and could be due to multiple reasons.

One reason could be differences in protein structure between human HexA (hHexA) and mouse HexA (mHexA) when the G269S mutation is introduced. Human *HEXA* and mouse *Hexa* cDNA share 82% similarity with each other, with conservation of many residues that cause TSD in humans when mutated. However, *Hexa* does have one amino acid that is deleted and an additional predicted N-glycosylation site, though it is unknown whether this site is used[157]. While Gly269 is conserved in mHexA, there are other residues (conserved and non-conserved) that may interact with Ser269 differently in mouse vs human HexA. Human studies of the G269S mutation show that the interaction of Ser269 C^{β} with C^{β} of another conserved residue Glu220 is unfavourable. This displaces the carbon backbone and a key residue in the active site, leading to reduced activity. This shift also results in a misfolded and unstable α-subunit protein product that is retained in the ER and degraded through the ERAD system, resulting in between 4-8% residual activity in human cells[47]. It is possible that G269S in mHexA results in a greater impact to protein folding than in hHexA, causing a greater degree of ERAD to mHexA than is seen in humans.

Alternatively, it is possible that G269S results in an unstable HexA enzyme in mice. This has been shown in certain human mutations that result in pseudo-deficiency, in which some α-subunit proteins fold well enough to avoid ERAD and associate unstably with β -subunits, particularly under laboratory conditions[82]. This results in retained hHexA activity in cells, but

low to undetectable levels on laboratory testing. Interestingly, overexpression of mutant human αG269S subunits with normal β-subunits in COS cells results in a heat liable HexA which is unstable at 37℃[158]. Further destabilization in mice could result in either diminished α-subunits due to ERAD or could produce a highly unstable enzyme with low activity in the lysosome and/or in laboratory testing.

Another reason differences were not observed between dKO and KIKO models could be due to the required removal of *Neu3*. While human NEU3 (hNEU3) does not have specificity toward gangliosides with internally linked Neu5Ac residues such as GM1 and GM2, mouse NEU3 (mNEU3) does [159,160]. Indeed, removal of *Neu3* and *Hexa* caused a more severe phenotype, increased GM2 accumulation and models acute GM2 gangliosidoses compared to *Hexa* KO alone. However, it is difficult to determine relative impact each gene deletion has on phenotype in this multi-gene system, and it is unknown how much *Neu3* removal contributes to severity of the model. If *Neu3* contributes to severity more than *Hexa* it may limit phenotypic variation in models with different *Hexa* alleles. Some evidence for this was observed after we began breeding $Hexa^{+/-}Neu3^{-/-}$ animals together consistently, in which numerous $Neu3^{-/-}$ $Hexa^{-/-}$ or $Hex^{+/-}$ animals died suddenly before 9 weeks old. If phenotypic differences do exist between KIKO and dKO models, the severity of *Neu3* KO and its contribution to phenotype may overshadow any differences due to *hexa* between models. In addition, methods used in this study may not be sensitive enough to detect subtle differences, especially if differences were confounded by severe phenotype attributed to *Neu3* KO.

Neu3 KO has obvious impacts the phenotype of these models by facilitating accumulation of GM2, however it also has off-target effects to other systems not typical of human GM2 gangliosidoses. These may limit the similarity of the dKO and KIKO model to human TSD or

contribute to phenotypes that mask differences between models. For example, while humans and mice with *HEXA/Hexa* mutations do not accumulate GM2 in their visceral organs[134], previous dKO models with *Hexa* and *Neu3* mutations showed moderate accumulation in the liver and kidney. This indicated a disease model that is more similar to SD models with *Hexb*$^{-/-}$ in terms of GM2 accumulation than TSD models with *Hexa*$^{-/-}$. It also indicated importance of NEU3 activity in ganglioside metabolism outside of the CNS. Further, mNEU3 is specific to other gangliosides that contain terminal α2,3- Neu5Ac residues such as GD1a and GM3 [159,161]. As such, other substrates accumulate in these models, including GA2, lactosylceramide and GM3[137]. Thus, additional accumulation of these substrates inside and outside the CNS may also contribute to the phenotype of these models.

In addition to changes in substrate accumulation, modulation of ganglioside metabolism may also alter signalling events and contribute to phenotype. In both species, NEU3 is localized at the membrane surface in sphingolipid rich lipid rafts and contributes to modulation of ganglioside content *in situ* [159,161]. Gangliosides and other sphingolipids are known signaling molecules, and changes to levels mediate intra-, extra- and inter-cellular signaling cascades. Silencing of *Neu3* has been shown to induce myoblast apoptosis due to increasing levels of GM3 and down-regulation of epidermal growth factor receptor[162]. In addition to modulating signalling through ganglioside metabolism, NEU3 has been shown to interact directly with signalling molecules such as phosphatidic acid. Further, cellular motility and clathrin-mediated endocytosis also involve NEU3.[163]

While other models of GM2 gangliosidoses such as Jacob sheep are better models for human GM2 gangliosidoses, difficulties in using these models for scientific study limit their utility for testing pre-clinical treatments. Despite limitations of translation to humans, creation of

mouse models that recapitulate the human disease still provide a useful tool to test preclinical treatments and to continue learning more about the pathophysiology behind GM2 accumulation.

5.2 Future Directions

Currently there are no curative treatments for any of the GM2 gangliosidoses. Development of model animals to test new therapies are essential to discovering treatments for GM2 gangliosidosis. Characterization of these models is also essential for evaluating how treatment affects the natural disease progression.

Further work on the dKO and KIKO model including comparisons of neuroinflammation, and investigations of visceral organ involvement are required to complete model characterization. Previously reported models combining *Neu3* and *Hexa* deficiency accumulate GM2 as well as GA2 ganglioside in the CNS and viscera[137]. These animals also exhibited increases in proinflammatory markers, decreases in anti-inflammatory markers, along with activation of microglia, astrocytes, and infiltration of peripheral blood mononuclear cells [138]. Inflammatory markers such as TNFα, IL1β, and TGFβ1 are chronically expressed in *Hexb*$^{-/-}$ mice, and in humans with GM2 gangliosidosis[65,138]. Molecular profiling of gene expression in humans with GM2 gangliosidoses also revealed activation of microglia, astrocytes, and macrophages[67]. This has been demonstrated in many animal models of GM2 gangliosidosis and is the likely mechanism behind pathology and neuronal cell death[65]. Further evidence for this is seen in models which combine *Hexb*$^{-/-}$ and either *Tnf*$\alpha^{-/-}$ or *Mip1*$\alpha^{-/-}$, genes for pro-inflammatory proteins. These models have improved neurological function, delayed of neuronal cell loss, and increased lifespan compared to mice with only *Hexb*$^{-/-}$ [66,164]. Further, suppression of natural killer and CD8+ T cells in *Hexb*$^{-/-}$ through deletion of anti-inflammatory *Il15* resulted in decreased lifespan compared to *Hexb* KO alone [165]. Infiltration of peripheral blood mononuclear cells into the brain has also been seen in models of SD, and inhibition of this process increases survival[166].

Further investigation of neuroinflammation in our models is necessary to assess whether this important aspect of GM2 gangliosidosis was modeled, and if any differences between the models exist. Additionally, these investigations identify new targets for therapy and can contribute to development of new treatments.

Studies to understand why the G269S mutation does not produce a late onset model in mice may reveal key differences between mHexA and hHexA. Crystallographic structures for hHexA and structural modeling of various known human mutations exist[47], however similar investigations into mHexA have not been undertaken. Understanding the structure of mHexA may provide information about important non-conserved residues and their interaction. This could inform future research about mutations that are likely to retain some residual activity.

Further investigation to determine how G269S results in enzyme deficiency in mice, whether through decreases in activity via unstable dimerization, retention by the ER and subsequent removal via ERAD or a combination would be useful to determine why residual activity was not observed in mice. In addition, investigations into how the G269S mutation in mice impacts the hydrolysis of MUGS, the synthetic substrate used in laboratory testing, compared to a natural GM2 substrate may be required to determine if residual activity exists in vivo but is not detectable with current assays.

Investigations into the contribution of *Neu3* on the severity of phenotype would also be useful to assess whether late onset models could be produced in the presence of *Neu3* KO. If *Neu3* KO contributes to the phenotype of these animals to a great extent, a less severe *Neu3* KI mutation may be required in addition to *HexA* KI to delay disease onset.

Other *HEXA* mutations found in patients with chronic-adult GM2 gangliosidoses, or those responsible for pseudo-deficiency combined with *Neu3* KO or less severe *Neu3* KI mutations

could be an option for future models. Mutations that result in pseudo-deficiency such as R247W and R249W in humans have activities above the 10% threshold and patients are asymptomatic[37]. These mutations may provide residual activities in mice that are sufficient to slow disease onset, but insufficient to avoid disease altogether, resulting in increased survivability and a late-onset phenotype compared to dKO animals. Mutations that result in chronic-adult GM2 gangliosidoses such as IVS8-7G>A could also be used. This mutation reduces the number of properly spliced mRNA transcripts, reducing overall α-subunits available for dimerization. Interestingly, this mutation has been shown to respond to PYR in cell lines and could produce a chronic-adult GM2 gangliosidoses model that is responsive to PC treatment[114]. Additionally, other chaperones such as NGT may be used on our current model if further investigations with PYR do not delay disease onset.

In the future, these models will be used to test PC therapy with and without HexM ERT, along with a HexM gene therapy with AAV vector. HexM has previously been used in gene therapy studies on *Hexb*$^{-/-}$ mice, and we expect similar rescue of phenotype in these animals[129,167].

5.3 Conclusion

GM2 gangliosidoses are a group of rare LSDs with a wide phenotypic spectrum characterized by lysosomal accumulation of GM2 ganglioside in the nervous system. Despite almost 150 years of research since the discovery of TSD, curative treatment for any form of GM2 gangliosidoses are not available. Production of mouse models that recapitulate the human disease to test a variety of pre-clinical treatments such as ERT, PC and GT may be useful in the development of treatment approaches.

In this study we attempted to create a late-onset GM2 gangliosidosis model amendable to multiple therapies using the *HEXA* G269S mutation. Previously reported dKO juvenile GM2 gangliosidosis models were created for comparison, however KIKO animals did not display any significant differences in disease onset, behaviour, neurological phenotype, survival or GM2 accumulation based on our investigations. Thus, both dKO and KIKO models appear to produce a juvenile-subacute model for GM2 gangliosidoses. Future investigations on the effect of G269S in mice, the impact of the *Neu3* deletion to the severity of these models and investigations into whether treatment with PYR will improve survival in KIKO will be important to understand how these systems differ between mice and humans and inform future pre-clinical treatment research in these models.

6 Appendix

6.1 Supplemental Tables

Appendix Table A. Summary of Mixed Effects Model Analysis: Two-way ANOVA with Tukey's Multiple Comparisons by Figure.

Figure	Group		n-value	SD	*p*-value		
					Control vs dKO	Control vs KIKO	dKO vs KIKO
Figure 9. Weight (grams)	7 wks	Control	6	2.95	0.9110	0.6827	0.5195
		dKO	4	2.99			
		KIKO	2	0.283			
	8 wks	Control	10	3.03	0.9006	0.9975	0.8992
		dKO	4	2.36			
		KIKO	5	4.23			
	9 wks	Control	12	2.86	0.8747	0.9580	0.9812
		dKO	6	2.56			
		KIKO	6	4.11			
	10 wks	Control	20	3.07	0.6776	0.8691	0.9683
		dKO	10	3.08			
		KIKO	8	3.38			
	11 wks	Control	17	3.09	0.3473	0.8363	0.7776
		dKO	9	3.15			
		KIKO	8	4.25			
	12 wks	Control	17	3.45	0.0643	0.8472	0.7776
		dKO	9	4.66			
		KIKO	8	3.94			
	13 wks	Control	16	3.52	0.1557	0.6239	0.6439
		dKO	7	4.71			
		KIKO	9	4.24			
	14 wks	Control	20	3.46	0.0535	0.5832	0.5185
		dKO	10	5.27			
		KIKO	9	4.26			
	15 wks	Control	20	3.63	0.0619	0.6566	0.5083
		dKO	11	5.47			
		KIKO	9	4.16			
	16 wks	Control	20	3.97	* 0.0192	0.7615	0.2326
		dKO	11	5.81			
		KIKO	9	4.00			
	17 wks	Control	20	4.11	0.0781	0.7611	0.4656
		dKO	11	5.98			
		KIKO	9	3.69			
	18 wks	Control	20	4.49	0.1735	0.9694	0.4049
		dKO	11	6.16			
		KIKO	9	3.55			
	19 wks	Control	20	4.71	0.7824	0.8515	0.5520
		dKO	11	5.94			
		KIKO	9	2.95			
	20 wks	Control	19	4.86	0.9992	0.3130	0.3715
		dKO	11	6.13			
		KIKO	9	2.24			
	21 wks	Control	17	5.38	0.2144	0.0440	0.7276
		dKO	10	6.52			
		KIKO	8	2.42			
	22 wks	Control	11	5.54	* 0.0287	0.0602	0.9919
		dKO	6	7.50			
		KIKO	5	3.22			

Figure	Group		n-value	SD	*p*-value		
					Control vs dKO	Control vs KIKO	dKO vs KIKO
Figure 9. Weight (grams)	23 wks	Control	7	5.87	* 0.0422	* 0.0312	0.9948
		dKO	3	6.51			
		KIKO	3	2.84			
	24 wks	Control	1	0.78	** 0.0062		
		dKO	1	1.91			
		KIKO	0				
Figure 12. Mobility measures from open field testing (Distance (meters))	10 wks	Control	15	6.515	0.3242	0.4948	0.9472
		dKO	6	5.281			
		KIKO	8	5.651			
	14 wks	Control	16	6.263	0.4877	0.0782	0.6407
		dKO	8	6.231			
		KIKO	8	5.623			
	18 wks	Control	15	8.540	0.9940	0.0779	0.1073
		dKO	8	8.369			
		KIKO	6	5.190			
	22 wks	Control	10	7.234	0.2578	0.4030	* 0.0354
		dKO	6	7.196			
		KIKO	5	4.819			
Figure 12. Mobility measures from open field testing (Average Speed Inside)	10 wks	Control	15	0.038	0.1256	0.4936	0.7063
		dKO	6	0.017			
		KIKO	8	0.025			
	14 wks	Control	16	0.033	0.0861	0.1052	0.9954
		dKO	8	0.020			
		KIKO	8	0.024			
	18 wks	Control	15	0.035	0.2799	0.1242	0.5176
		dKO	8	0.012			
		KIKO	6	0.024			
	22 wks	Control	10	0.033	*** 0.0006	**** <0.0001	* 0.0468
		dKO	6	0.017			
		KIKO	5	0.009			
Figure 12. Mobility measures from open field testing (Max Speed)	10 wks	Control	15	0.073	** 0.0052	** 0.0071	0.7411
		dKO	6	0.025			
		KIKO	8	0.054			
	14 wks	Control	16	0.071	** 0.0080	*** 0.0003	0.9285
		dKO	8	0.054			
		KIKO	8	0.029			
	18 wks	Control	15	0.088	** 0.0010	*** 0.0003	0.4975
		dKO	8	0.041			
		KIKO	6	0.040			
	22 wks	Control	10	0.078	* 0.0220	*** 0.0002	* 0.0478
		dKO	6	0.046			
		KIKO	5	0.030			
Figure 13. Behavioural measures from open field testing. Fecal Boli	10 wks	Control	15	1.407	0.2631	0.3744	0.0644
		dKO	7	1.773			
		KIKO	8	1.126			
	14 wks	Control	17	1.921	0.5187	0.8083	0.2899
		dKO	10	1.197			
		KIKO	8	1.753			
	18 wks	Control	15	1.882	0.9956	0.9967	0.9899
		dKO	8	2.828			
		KIKO	6	1.751			
	22 wks	Control	10	2.011	0.2053	0.6754	0.7495
		dKO	6	1.095			
		KIKO	5	1.517			

Figure	Group		n-value	SD	*p*-value		
					Control vs dKO	Control vs KIKO	dKO vs KIKO
Figure 13. Behavioural measures from open field testing. Inside time	10 wks	Control	15	37.01	0.9674	0.9015	0.9785
		dKO		41.91			
		KIKO	8	55.94			
	14 wks	Control	16	30.43	0.2562	0.9307	0.8231
		dKO	8	40.34			
		KIKO	8	71.93			
	18 wks	Control	15	45.21	0.0987	0.7885	0.7447
		dKO	8	60.21			
		KIKO	6	86.32			
	22 wks	Control	10	39.94	0.0002	*** 0.1922	0.4296
		dKO	6	41.52			
		KIKO	5	81.68			
Figure 13. Behavioural measures from open field testing. Outside time	10 wks	Control	15	46.17	0.9995	0.7345	0.8300
		dKO	7	64.54			
		KIKO	8	56.73			
	14 wks	Control	16	66.29	0.6562	0.9406	0.5761
		dKO	8	60.86			
		KIKO	8	72.99			
	18 wks	Control	15	52.71	0.1058	0.9129	0.4971
		dKO	8	73.54			
		KIKO	6	85.36			
	22 wks	Control	10	49.94	*** 0.0002	0.2108	0.4634
		dKO	6	37.85			
		KIKO	5	81.98			
Figure 13. Behavioural measures from open field testing. Conrners time	10 wks	Control	15	84.67	0.9784	0.3002	0.5484
		dKO	6	95.52			
		KIKO	8	90.69			
	14 wks	Control	16	107.6	0.8862	0.6234	0.4826
		dKO	8	110.9			
		KIKO	8	163.8			
	18 wks	Control	15	85.98	0.2314	0.9409	0.3885
		dKO	8	94.84			
		KIKO	6	134.5			
	22 wks	Control	10	129.9	**** <0.0001	** 0.0037	0.1861
		dKO	6	28.26			
		KIKO	5	85.37			
Figure 14. Gait analysis prints Hindlimb stride length	10 wks	Control	13	1.094	0.9399	0.4395	0.4000
		dKO	5	0.901			
		KIKO	8	0.614			
	14 wks	Control	16	1.039	** 0.0069	* 0.0135	0.8969
		dKO	16	0.550			
		KIKO	7	0.631			
	18 wks	Control	10	1.000	*** 0.001	* 0.0249	0.9936
		dKO	5	0.943			
		KIKO	6	1.983			
	22 wks	Control	8	0.615	* 0.0115	**** <0.0001	0.8498
		dKO	3	0.703			
		KIKO	5	0.270			
Figure 15. Additional gait analysis measures Hindlimb stance width	10 wks	Control	13	0.345	0.4228	0.0526	0.9946
		dKO	5	0.444			
		KIKO	8	0.234			
	14 wks	Control	16	0.291	** 0.0083	** 0.0027	0.7127
		dKO	16	0.453			
		KIKO	7	0.286			
	18 wks	Control	10	0.167	0.6652	0.5552	0.3400
		dKO	5	0.307			

Figure	Group		n-value	SD	*p*-value		
					Control vs dKO	Control vs KIKO	dKO vs KIKO
		KIKO	5	0.357			
	22 wks	Control	8	0.467			
		dKO	3	0.313	0.9728	0.9995	0.9591
		KIKO	5	0.284			
Figure 15. Additional gait analysis measures Forelimb stride length	10 wks	Control	13	0.977			
		dKO	5	0.925	0.9957	0.4792	0.6098
		KIKO	8	0.679			
	14 wks	Control	16	1.065			
		dKO	16	0.564	* 0.0155	0.0548	0.9887
		KIKO	7	0.609			
	18 wks	Control	10	0.930			
		dKO	5	0.775	*** 0.0003	*** 0.0003	0.5335
		KIKO	5	0.638			
	22 wks	Control	8	0.564			
		dKO	3	1.316	0.0657	*** 0.0001	0.9979
		KIKO	4	0.565			
Figure 15. Additional gait analysis measures Forelimb Stance Width	10 wks	Control	12	0.216			
		dKO	5	0.238	0.9814	0.8688	0.8392
		KIKO	8	0.308			
	14 wks	Control	16	0.195			
		dKO	16	0.289	0.4399	0.7688	0.9793
		KIKO	7	0.285			
	18 wks	Control	10	0.256			
		dKO	5	0.278	0.4134	0.3195	0.9421
		KIKO	5	0.327			
	22 wks	Control	8	0.178			
		dKO	3	0.231	0.5578	0.9474	0.6265
		KIKO	3	0.338			
Figure 15. Additional gait analysis measures Hindlimb Sway Distance	10 wks	Control	13	0.355			
		dKO	5	0.448	0.5700	0.4755	0.9408
		KIKO	8	0.269			
	14 wks	Control	16	0.488			
		dKO	16	0.274	*** 0.0001	** 0.0051	0.6951
		KIKO	7	0.288			
	18 wks	Control	10	0.432			
		dKO	5	0.278	**** <0.0001	* 0.0251	* 0.0334
		KIKO	5	0.328			
	22 wks	Control	8	0.382			
		dKO	3	0.667	0.1624	* 0.0105	0.9054
		KIKO	5	0.427			
Figure D. Additional OFT measures Average Speed	10 wks	Control	15	0.011			
		dKO	7	0.009	0.2226	0.4203	0.9119
		KIKO	8	0.009			
	14 wks	Control	16	0.010			
		dKO	8	0.010	0.4514	0.0568	0.5793
		KIKO	8	0.009			
	18 wks	Control	15	0.014			
		dKO	8	0.014	0.9971	0.0842	0.1435
		KIKO	6	0.027			
	22 wks	Control	10	0.024			
		dKO	6	0.033	0.3396	0.3318	0.0512
		KIKO	5	0.016			

Figure	Group		n-value	SD	*p*-value		
					Control vs dKO	Control vs KIKO	dKO vs KIKO
Figure D. Additional OFT measures Max Speed	10 wks	Control	15	0.066	0.8889	* 0.0273	0.6100
		dKO	7	0.102			
		KIKO	8	0.044			
	14 wks	Control	16	0.058	**** <0.0001	**** <0.0001	0.9565
		dKO	8	0.045			
		KIKO	8	0.035			
	18 wks	Control	15	0.063	**** <0.0001	**** <0.0001	0.2261
		dKO	8	0.042			
		KIKO	6	0.043			
	22 wks	Control	10	0.053	0.2339	0.1522	0.7918
		dKO	6	0.141			
		KIKO	5	0.161			
Figure D. Additional OFT measures Freezing Episodes	10 wks	Control	15	25.42	0.2449	0.5687	0.0673
		dKO	7	3.445			
		KIKO	8	22.70			
	14 wks	Control	16	37.63	0.2498	0.8904	0.4828
		dKO	8	22.16			
		KIKO	8	25.51			
	18 wks	Control	15	23.43	0.4513	0.7594	0.7728
		dKO	8	22.84			
		KIKO	6	13.15			
	22 wks	Control	10	24.05	** 0.0010	0.5357	* 0.0305
		dKO	6	11.08			
		KIKO	5	17.04			
Figure D. Additional OFT measures Time Freezing	10 wks	Control	15	127.7	0.7906	0.7550	0.3175
		dKO	7	61.07			
		KIKO	8	89.37			
	14 wks	Control	16	169.5	0.1537	0.9996	0.1760
		dKO	8	81.83			
		KIKO	8	127.4			
	18 wks	Control	15	74.01	0.9262	0.5521	0.4861
		dKO	8	85.37			
		KIKO	6	50.41			
	22 wks	Control	10	156.4	* 0.0346	0.5962	0.2014
		dKO	6	41.93			
		KIKO	5	99.51			
Figure D. Additional OFT measures Outside Zone; Distance Travelled	10 wks	Control	15	4.813	0.3537	0.6627	0.9256
		dKO	7	3.917			
		KIKO	8	4.989			
	14 wks	Control	16	4.476	0.0753	* 0.0276	0.7930
		dKO	8	3.775			
		KIKO	8	4.208			
	18 wks	Control	15	6.419	0.4649	0.0985	0.4855
		dKO	8	4.731			
		KIKO	6	4.969			
	22 wks	Control	10	5.397	0.9326	0.1824	0.1753
		dKO	6	5.725			
		KIKO	5	4.241			
Figure D. Additional OFT measures Inside Zone; Distance Travelled	10 wks	Control	15	2.293	0.1432	0.5344	0.9838
		dKO	7	1.581			
		KIKO	8	3.342			
	14 wks	Control	16	2.286	0.7837	0.7075	0.4722
		dKO	8	2.770			
		KIKO	8	2.979			
	18 wks	Control	15	2.678	0.1444	0.6126	0.0604
		dKO	8	3.845			
		KIKO	6	2.414			
	22 wks	Control	10	2.349	** 0.0033	0.9907	** 0.0072
		dKO	6	1.907			
		KIKO	5	1.635			

Figure	Group		n-value	SD	*p*-value		
					Control vs dKO	Control vs KIKO	dKO vs KIKO
Figure D. Additional OFT measures Inside Zone; Entries	10 wks	Control	15	11.92	0.2797	0.4482	0.9946
		dKO	7	7.111			
		KIKO	8	13.24			
	14 wks	Control	16	10.68	0.6763	0.6205	0.3266
		dKO	8	10.87			
		KIKO	8	14.08			
	18 wks	Control	15	14.68	0.2320	0.6008	0.0972
		dKO	8	19.71			
		KIKO	6	14.16			
	22 wks	Control	10	10.04	** 0.0036	0.2990	0.0662
		dKO	6	10.71			
		KIKO	5	8.927			
Figure D. Additional OFT measures Time Mobile	10 wks	Control	15	11.09	0.1045	0.0924	0.8996
		dKO	7	35.10			
		KIKO	8	28.77			
	14 wks	Control	16	17.56	0.6262	* 0.0211	0.2442
		dKO	8	33.74			
		KIKO	8	27.90			
	18 wks	Control	15	16.30	0.8084	* 0.0204	0.1831
		dKO	8	31.39			
		KIKO	6	19.06			
	22 wks	Control	10	19.80	0.6518	0.8574	0.4905
		dKO	6	18.71			
		KIKO	5	23.60			

Appendix Table B. Kaplan–Meier Survival Analysis Test Summary

Figure	Statistical Test	Group	n-value	Log-rank test		
				Chi-Square	df	p-value
Figure 10. Survival	Log-Rank test	Control	35	64.07	2	Control vs dKO or KIKO, $p<0.0001$ dKO vs KIKO, ns
		dKO	11			
		KIKO	9			

Appendix Table C. Summary Statistics for Figure 16

Figure	Group		n-value	Mean	SD	*p*-value (One-way ANOVA, Tukeys Multiple Comparisons)		
						Control vs dKO	Control vs KIKO	dKO vs KIKO
Figure 16. Gross anatomical brain images and weights of control and dKO or KIKO pairs.	Various ages (149-171 days)	Control	12	0.425	0.026	** 0.0032	* 0.0397	0.7888
		dKO	7	0.464	0.020			
		KIKO	5	0.456	0.012			

Appendix Table D. Statistical Information for One-way ANOVA with Sidak's Multiple

Figure	Group		N1-value	N2-value	Mean Difference	SE of difference	t	DF	*p*-value
Figure 19. β-Hexosaminidase Assay	Various ages (149-171 days)	dKO vs Contol	10	6	0.00506	0.03013	0.1681	18	0.9977
		KIKO vs Control	10	5	-0.6328	0.02725	23.22	18	**** <0.0001
		dKO vs KIKO	6	5	-0.6278	0.02560	24.43	18	**** <0.0001

Appendix Table E. Statistical Information for Kruskal-Wallis's test with Dunn's Multiple Comparisons

Figure	Weeks	Kruskal-Wallis Statistic (P value)	Comparison	Mean Rank 1	Mean Rank 2	Mean Rank Difference	Z	N1	N2	*p*-value
Figure 11	10	2.353 (0.4842)	Control vs dKO	9	12	-3.00	1.328	7	7	0.5521
			Control vs KIKO	9	12	-3.00	1.328	7	7	0.5521
			dKO vs KIKO	12	12	0	0	7	7	>0.9999
	14	8.296 (0.138)	Control vs dKO	6.857	11.14	-4.286	1.515	7	7	0.3891
			Control vs KIKO	6.857	15	-8.143	2.879	7	7	* 0.0120
			dKO vs KIKO	11.14	15	-3.857	1.364	7	7	0.5180
	18	15.32 (<0.0001)	Control vs dKO	4	12.64	-8.643	2.668	7	7	* 0.0229
			Control vs KIKO	4	16.36	-12.36	3.815	7	7	*** 0.0004
			dKO vs KIKO	12.64	16.36	-3.714	1.147	7	7	0.7546
	22	14.90 (<0.0001)	Control vs dKO	4	12.93	-8.929	2.752	7	7	* 0.0178
			Control vs KIKO	4	16.07	-12.07	3.720	7	7	*** 0.0006
			dKO vs KIKO	12.93	16.07	-3.143	0.9686	7	7	0.9982

6.2 Supplemental Figures

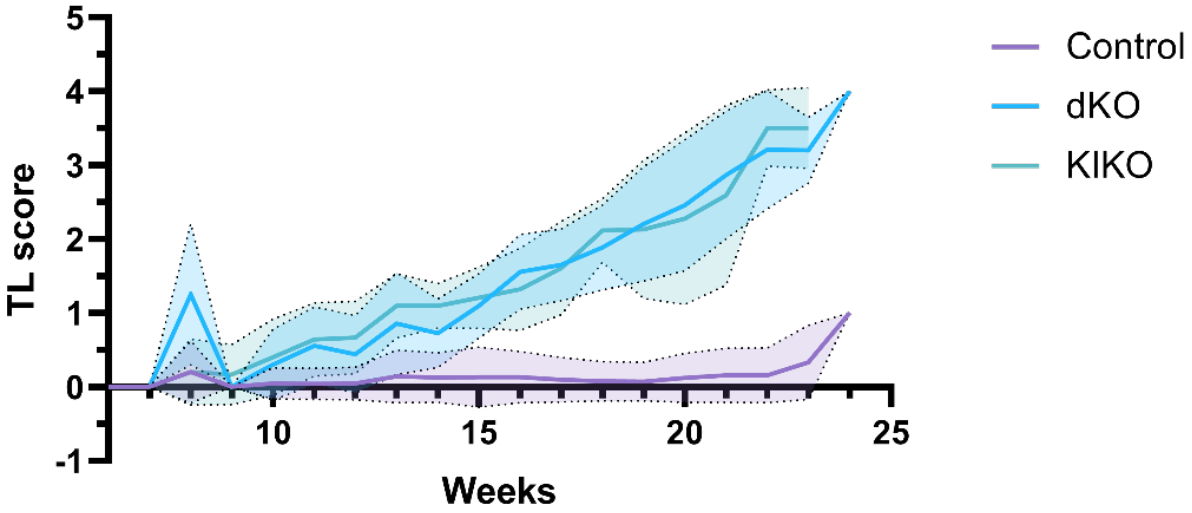

Appendix Figure A. Average tail lift testing score of dKO, KIKO, and Controls from 7 to 24 weeks of age.

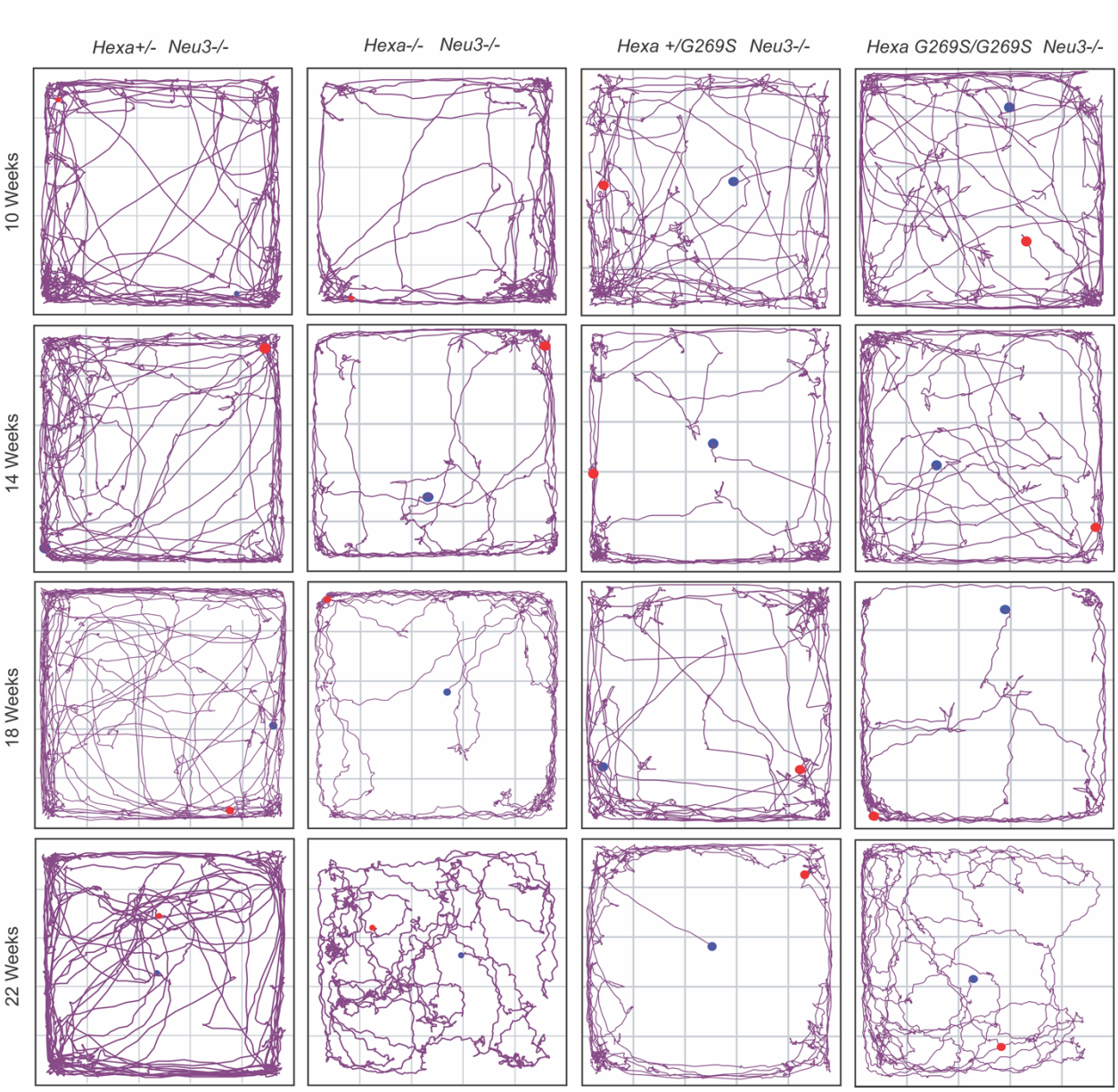

Appendix Figure B. Additional Track Plots from Open Field Testing

Track plots from dKO (*Hexa*$^{-/-}$ *Neu3*$^{-/-}$), KIKO (*Hexa*$^{G269S/G269S}$ *Neu3*$^{-/-}$) and control (*Hexa*$^{+/-}$ *Neu3*$^{-/-}$ or *Hexa*$^{+/G269S}$*Neu3*$^{-/-}$) male mice from 10, 14, 18 and 22 weeks generated by ANYmaze tracking software. Both dKO and KIKO exhibit similar track plots compared to controls at 10 weeks, however had increased use of inner zone and characteristic wavey path by 22 weeks.

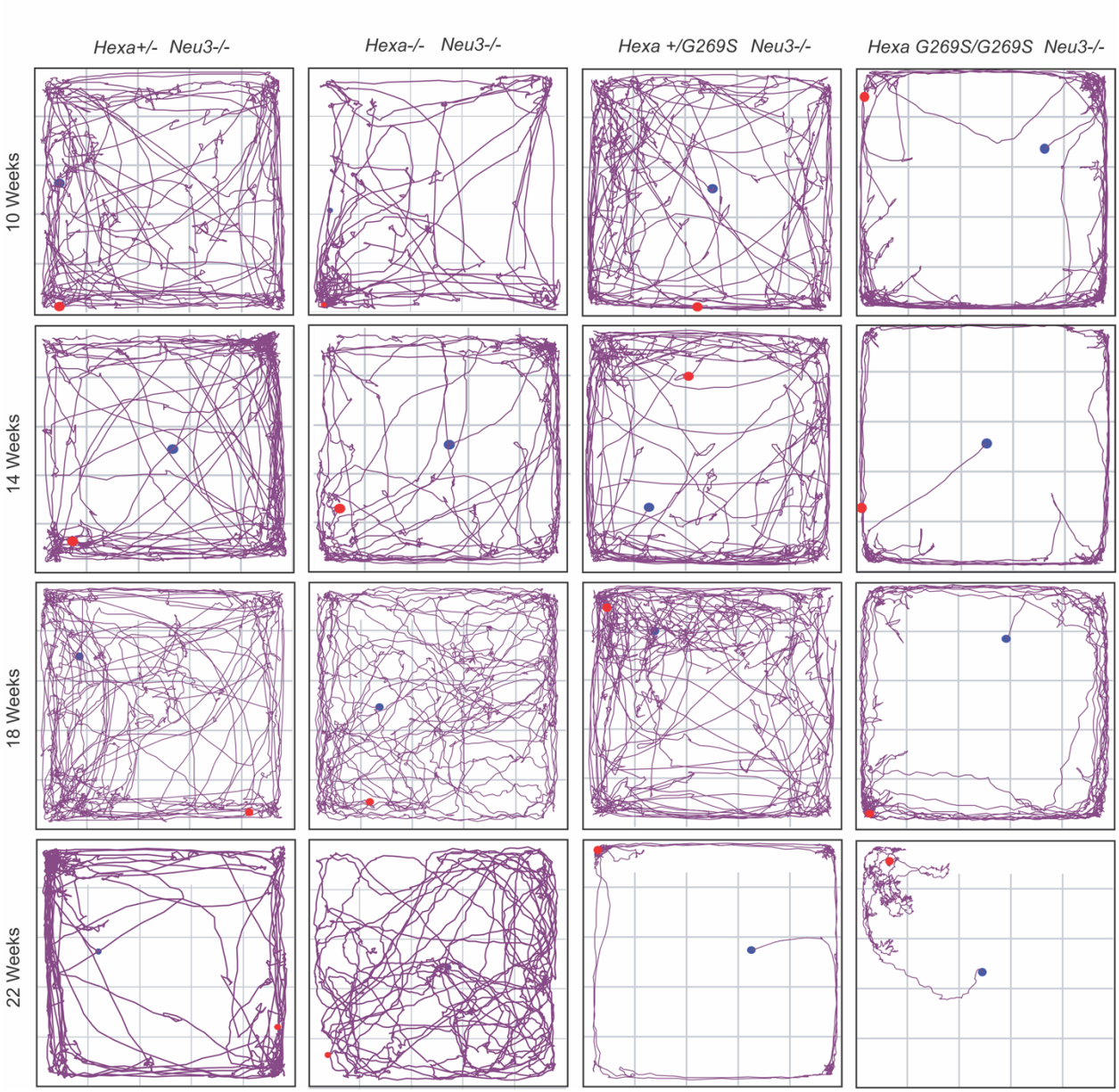

Appendix Figure C. Additional Track Plots from Open Field Testing

Track plots from dKO (*Hexa*$^{-/-}$ *Neu3*$^{-/-}$), KIKO (*Hexa*$^{G269S/G269S}$ *Neu3*$^{-/-}$) and control (*Hexa*$^{+/-}$ *Neu3*$^{-/-}$ or *Hexa*$^{+/G269S}$*Neu3*$^{-/-}$) female mice from 10, 14, 18 and 22 weeks generated by ANYmaze tracking software. Both dKO and KIKO exhibit similar track plots compared to controls at 10 weeks, however had increased use of inner zone for dKO, and characteristic wavey path in both dKO and KIKO by 22 weeks.

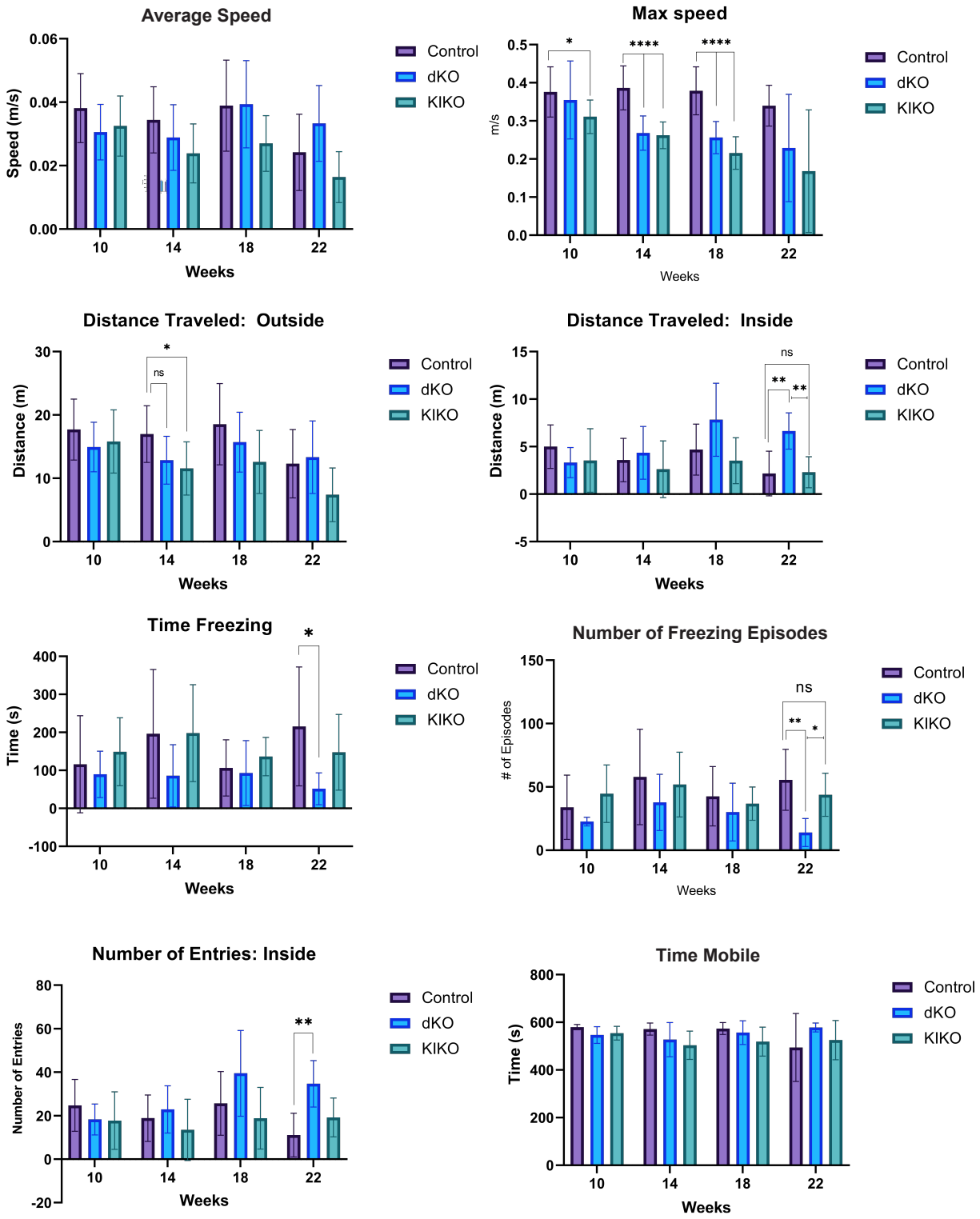

Appendix Figure D. Additional Open Field Test Measures

Average Speed, Max Speed, Distance Travelled Outside, Distance Travelled Inside, Time Spent Freezing, Number of Freezing Episodes, Number of Entries Inside, Time mobile from 10, 14 ,18 and 22 weeks.


Control
dKO
KIKO
10 Weeks
14 Weeks


Control
dKO
KIKO
18 Weeks
22 Weeks

Appendix Figure E. Additional Footprints from Gait Analysis

Representative footprints from gait analysis of dKO, KIKO and controls at 10, 14, 18 and 22 weeks. All animals have approximately the same hindlimb stride length at 10 weeks with similar paw placement pattern. Placement of fore and hind paws becomes uncoordinated starting at 14 weeks, leading to disorganized gait by 22 weeks in both models with significantly shortened hindlimb stride length (cm) from 14-22 weeks.

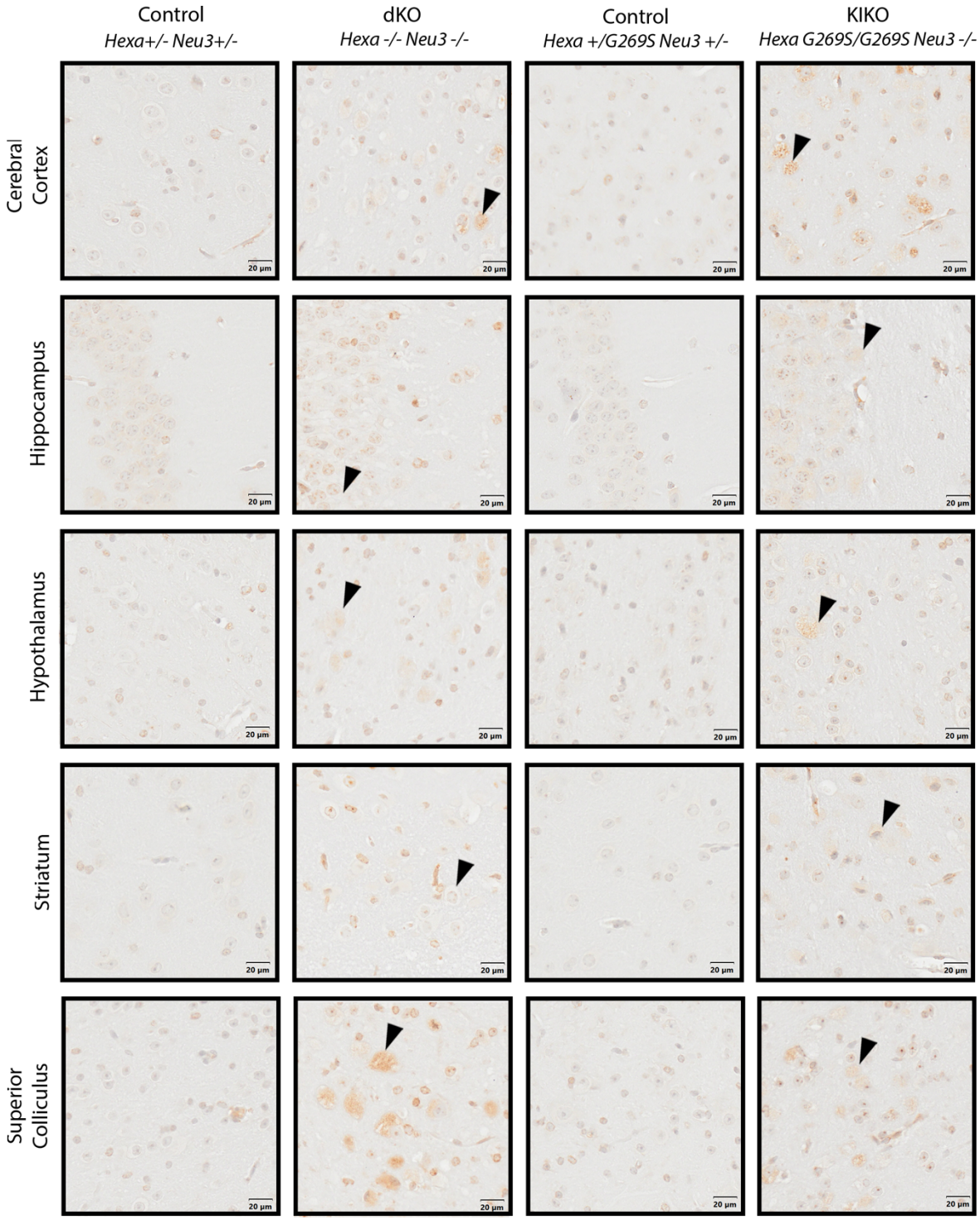

Appendix Figure F. IHC Assessment of GM2 Accumulation

Brains from dKO and KIKO with an age-sex matched control collected at humane endpoint between 22-23 weeks. Images are from 5-micron paraffin sections stained with anti-GM2 antibody, and counterstained with methyl green. Black arrows indicate cells with accumulation of GM2 or

vacuolization. Images were taken using a 20x objective on the Olympus VS200. Each scale bar represents 20μm.

References

1. Tay, W. Symmetrical Changes in the Region of the Yellow Spot in Each Eye of an Infant. *Trans Ophthalmol Soc U K* 155–57 (1881).
2. Gaucher, P. C. E. De l'epithelioma primitif de la rate, hypertrophie idiopathique de la rate sans leucemie. (Paris, 1882).
3. Brady, R. O. Fabry Disease. in *Lysosomal Storage Disorders* (eds. Barranger, J. A. & Cabrera-Salazar, M. A.) 307 (Springer, 2007).
4. De Duve, C. From lysosomes to storage diseases and back: A personal reminiscence. in *Lysosomal Storage Disorders* (eds. Barranger, J. & Cabrera-Salazar, M.) 1–5 (Springer, 2007). doi:10.1007/978-0-387-70909-3_1.
5. Platt, F. M. Sphingolipid Lysosomal Storage Disorders. *Nature* **510**, 68–75 (2014).
6. Brooks, D. & Parkinson-Lawrence, E. Lysosomal biogenesis and disease. in *Lysosomal Storage Disorders* (eds. Barranger, J. A. & Cabrera-Salazar, M. A.) 7–36 (Springer, 2007). doi:10.1007/978-0-387-70909-3_2.
7. Mehta, A. & Winchester, B. Lysosomal Storage Diseases : Historic Landmarks and Scientific Principles. in *Lysosomal Storage Disorders: A Practical Guide* (eds. Mehta, A. & Winchester, B.) 3–8 (Wiley-Blackwell, 2022).
8. Myerowitz, R. & Costigan, F. C. The major defect in Ashkenazi Jews with Tay-Sachs disease is an insertion in the gene for the α-chain of β-hexosaminidase. *Journal of Biological Chemistry* **263**, 18587–18589 (1988).
9. McCracken, A. A. & Brodsky, J. L. Evolving questions and paradigm shifts in endoplasmic-reticulum-associated degradation (ERAD). *BioEssays* **25**, 868–877 (2003).
10. Edmond Wraith, J. & Beck, M. Clinical Aspects and Clinical Diagnosis. in *Lysosomal Storage Disorders: A Practical Guide* (eds. Mehta, A. & Winchester, B.) 13–19 (John Wiley & Sons, Ltd, 2012). doi:10.1002/9781118514672.ch2.
11. Micsenyi, M. C. & Walkley, S. U. The Lysosomal System: Pathology. in *Lysosomal Storage Disorders: A Practical Guide* (eds. Mehta, A. & Winchester, B.) 19–29 (John Wiley & Sons, Ltd, 2022). doi:10.1002/9781118514672.ch1.
12. Hopwood, J. J. Genetics of Lysosomal Storage Disorders and Counselling. *Lysosomal Storage Disorders: A Practical Guide* 29–36 (2012) doi:10.1002/9781118514672.ch4.
13. Brady, R. O. The concept of treatment in lysosomal storage diseases. in *Lysosomal Storage Disorders* (eds. Barranger, J. A. & Cabrera-Salazar, M.) 37–43 (Springer, 2007). doi:10.1007/978-0-387-70909-3_3.
14. Brady, R. O. Therapy for the sphingolipidoses. *Arch Neurol* **55**, 1055–1056 (1998).
15. Toro, C., Zainab, M. & Tifft, C. J. The GM2 gangliosidoses: Unlocking the mysteries of pathogenesis and treatment. *Neurosci Lett* **764**, (2021).
16. Sachs, B. On Arrested Cerebral Development with Special Reference to Cortical Pathology. *J Nerv Ment Dis* 541–553 (1887).
17. Slome, D. The genetic basis of amaurotic family idiocy. *J Genet* **27**, 363–372 (1933).
18. Landsteiner, K. & Levene, P. A. On the heterogenetic hapten. *Proc. Soc. Exp. Biol. Med* 343–344 (1926).
19. Klenk, E. Beitr¨age zur Chemie der Lipoidosen. Niemann-Picksche Krankheit und amaurotische Idiotie. *Hoppe-Seyler's Physiol. Chem.* 128–143 (1939).

20. Svennerholm, L. Identification of the accumulated ganglioside. in *Advances in Genetics* (eds. Desnick, R. J. & Kaback, M. M.) vol. Tay Sachs 33–41 (Academic Press Inc., 2001).
21. L. Makita, A. & Yamakawa, T. The glycolipids of the brain ofTay-Sachs disease. The chemical structures of a globoside and main ganglioside. *Jpn. J. Exp. Med.* 361–368 (1963).
22. Ledeen, R. & Salsman, K. Structure of the Tay-Sachs ganglioside. *Biochemistry* **4**, 2225 (1965).
23. Frohwein, Y. Z. & Gatt, S. Isolation of beta-n-acetylhexosaminidase, beta-n-acetylglycosaminidase and beta-n-acetylgalactosaminidase from Calf Brain. *Biochemistry* **6**, 2775–2782 (1967).
24. Robinson, D. & Stirling, J. L. Hexosaminidase Isoenzymes. in *Advances in Genetics* (eds. Desnick, R. J. & Kaback, M. M.) vol. 44 43–49 (Academic Press Inc., 2001).
25. Okada, S. & O'Brien, J. S. Discovery of β-hexosaminidase a deficiency in Tay-Sachs disease. in *Advances in Genetics* (eds. Desnick, R. J. & Kaback, M. M.) vol. 44 61–66 (Academic Press Inc., 2001).
26. Sandhoff, K. The GM2-Gangliosidoses and the Elucidation of the Beta-Hexosaminidase System. in *Tay-Sachs Disease: Advances in Genetics* (eds. Desnick, R. J. & Kaback, M. M.) vol. 44 67–87 (Academic Press Inc., 2001).
27. Kaback, M. M. & Desnick, R. J. Tay-Sachs disease: From clinical description to molecular defect. in *Advances in Genetics* (eds. Kaback, M. M. & Desnick, R. J.) vol. 44 1–9 (Academic Press Inc., 2001).
28. Beutler, E., Yoshida, A., Kuhl, W. & Lee, J. E. S. The subunits of human hexosaminidase A. *Biochemical Journal* **159**, 541–543 (1976).
29. Conzelmann, E., Burg, J., Stephan, G. & Sandhoff, K. Complexing of glycolipids and their transfer between membranes by the activator protein for degradation of lysosomal ganglioside GM2. *Eur. J. Biochem* **123**, 455 – 464 (1982).
30. Proia, R. L. & Soravia, E. O. Organization of the gene encoding the human β-hexosaminidase α-chain. *J. Biol. Chem.* **12**, 5677–5681 (1987).
31. Schröder, M. *et al.* Isolation of a cDNA encoding the human GM2 activator protein. *FEBS Lett* **251**, 197–200 (1989).
32. Burg, J., Conzelmann, E., Sandhoff, K., Soloman, E. & Swallow, D. M. Mapping of the gene coding for the human GM2 activator protein to chromosome 5. *Ann Hum Genet* **49**, 41–45 (1985).
33. Myerowitz, R., Piekarz, R., Neufeld, E. F., Shows, T. B. & Suzuki, K. Human beta-hexosaminidase alpha chain: coding sequence and homology with the beta chain. *Proc Natl Acad Sci U S A* **82**, 7830–7834 (1985).
34. Takeda, K. *et al.* Fine Assignment of beta-Hexosaminidase on 15q23-q24 by High Resolution In Situ Hybridization. *Tohoku Journal of Experimental Medicine* **160**, 203–211 (1990).
35. George, D. L. & Francke, U. Evidence for localization of the gene for hexosaminidase B to the cen-q13 region of human chromosome 5 using mouse-human hybrid cells. *Somat. Cell Genet.* **22**, 408–41 (1978).
36. Neote, K. *et al.* Characterization of the human HEXB gene encoding lysosomal β-hexosaminidase. *Genomics* **3**, 279–286 (1988).
37. Mahuran, D. J. Biochemical consequences of mutations causing the GM2 gangliosidoses. *Biochim Biophys Acta Mol Basis Dis* **1455**, 105–138 (1999).

38. Korneluk, R. G. *et al.* Isolation of cDNA Clones Coding for the alpha Subunit of Human Beta-Hexosaminidase. *J Biol Chem* **261**, 8407–8413 (1986).
39. O'Dowd, B. F. *et al.* Isolation of cDNA clones coding for the β subunit of human β-hexosaminidase. *Proc Natl Acad Sci U S A* **82**, 1184–1188 (1985).
40. Sonderfeld-Fresko, S. & Proia, R. L. Synthesis and assembly of a catalytically active lysosomal enzyme, β-hexosaminidase B, in a cell-free system. *Journal of Biological Chemistry* **263**, 13463–13469 (1988).
41. Proia, R. L., d'Azzo, A. & Neufeld, E. F. Association of alpha- and beta-subunits during the biosynthesis of beta-hexosaminidase in cultured human fibroblasts. *Journal of Biological Chemistry* **259**, 3350–3354 (1984).
42. Kytzia, H. J. & Sandhoff, K. Evidence for two different active sites on human β-hexosaminidase A: Interaction of GM2 activator protein with β-hexosaminidase A. *Journal of Biological Chemistry* **260**, 7568–7572 (1985).
43. Hepbildikler, S. T., Sandhoff, R., Kölzer, M., Proia, R. L. & Sandhoff, K. Physiological substrates for human lysosomal β-hexosaminidase S. *Journal of Biological Chemistry* **277**, 2562–2572 (2002).
44. Gravel, R. A., Kaback, M. M. & Proia, R. L. The GM2 Gangliosidoses. in *The Online Metabolic and Molecular Bases of Inherited Disease* (eds. Valle, D. L., Antonarakis, S., Ballabio, A., Beaudet, A. L. & Mitchell, G. A.) 1–85 (McGraw Hill, 2019). doi:10.1036/ommbid.184.
45. Yu, R. K., Tsai, Y., Ariga, T. & Yanagisawa, M. Structures , Biosynthesis , and Functions of Gangliosides-an Overview. *Journal and Oleo Science* **544**, 537–544 (2011).
46. Meier, E. M., Schwarzmann, G., Furst, W. & Sandhoff, K. The human GM2 activator protein. A substrate specific cofactor of β-hexosaminidase A. *Journal of Biological Chemistry* **266**, 1879–1887 (1991).
47. Lemieux, M. J. *et al.* Crystallographic Structure of Human β-Hexosaminidase A: Interpretation of Tay-Sachs Mutations and Loss of GM2 Ganglioside Hydrolysis. *J Mol Biol* **359**, 913–929 (2006).
48. Sandhoff, K. & Harzer, K. Gangliosides and Gangliosidoses: Principles of Molecular and Metabolic Pathogenesis. *The Journal of Neuroscience* **33**, 10195–10208 (2013).
49. Charria-Ortiz, G. A. The GM2 Gangliosidoses. in *Lysosomal Storage Disorders* (eds. Barranger, J. A. & Cabrera-Salazar, M.) 229–244 (Springer, 2007).
50. Jarnes Utz, J. R. *et al.* Infantile gangliosidoses: Mapping a timeline of clinical changes. *Mol Genet Metab* **121**, 170–179 (2017).
51. Sandhoff, K., Harzer, K., Wässle, W. & Jatzkewitz, H. Enzyme Alterations and Lipid Storage in Three Variants of Tay-Sachs Disease. *J Neurochem* **18**, 2469–2489 (1971).
52. O'Dowd, B. F. *et al.* Molecular heterogeneity in the infantile and juvenile forms of Sandhoff disease (O-variant G(M2) gangliosidosis). *Journal of Biological Chemistry* **261**, 12680–12685 (1986).
53. Cachon-Gonzalez, M. B., Zaccariotto, E. & Cox, T. M. Genetics and Therapies for GM2 Gangliosidosis. *Curr Gene Ther* **18**, 68–89 (2018).
54. Navon, R. & Gangliosidosis, I. A. G. M. Late-Onset G M2 Gangliosidosis and Other Hexosaminidase. in *Advances in Genetics* (eds. Desnick, R. J. & Kaback, M. M.) vol. 44 185–197 (Academic Press Inc., 2001).

55. Maegawa, G. H. B. *et al.* The natural history of juvenile or subacute GM2 gangliosidosis: 21 New cases and literature review of 134 previously reported. *Pediatrics* **118**, e1550–e1562 (2006).
56. Brett, E. M. *et al.* Late onset GM2-gangliosidosis: Clinical, pathological, and biochemical studies on 8 patients. *Arch Dis Child* **48**, 775–785 (1973).
57. Paw, B. H., Kaback, M. M. & Neufeld, E. F. Molecular basis of adult-onset and chronic GM2 gangliosidoses in patients of Ashkenazi Jewish origin: substitution of serine for glycine at position 269 of the α-subunit of β-hexosaminidase. *Proc Natl Acad Sci U S A* **86**, 2413–2417 (1989).
58. Stendel, C. *et al.* Paranoid delusion as lead symptom in two siblings with late-onset Tay–Sachs disease and a novel mutation in the HEXA gene. *J Neurol* **262**, 1072–1073 (2015).
59. Grunseich, C. *et al.* Peripheral neuropathy in a family with Sandhoff disease and SH3TC2 deficiency. *J Neurol* **262**, 1066–1068 (2015).
60. Jahnová, H. *et al.* Amyotrophy, cerebellar impairment and psychiatric disease are the main symptoms in a cohort of 14 Czech patients with the late-onset form of Tay–Sachs disease. *J Neurol* **266**, 1953–1959 (2019).
61. Jamrozik, Z. *et al.* Late onset GM2 gangliosidosis mimicking spinal muscular atrophy. *Gene* **527**, 679–682 (2013).
62. MacQueen, G. M., Rosebush, P. I. & Mazurek, M. F. Neuropsychiatric aspects of the adult variant of Tay-Sachs disease. *Journal of Neuropsychiatry and Clinical Neurosciences* **10**, 10–19 (1998).
63. Colussi, D. J. & Jacobson, M. A. Patient-Derived Phenotypic High-Throughput Assay to Identify Small Molecules Restoring Lysosomal Function in Tay–Sachs Disease. *SLAS Discovery* **24**, 295–303 (2019).
64. Puri, V. *et al.* Cholesterol modulates membrane traffic along the endocytic pathway in sphingolipid-storage diseases. *Nat Cell Biol* **1**, 386–388 (1999).
65. Jeyakumar, M. *et al.* Central nervous system inflammation is a hallmark of pathogenesis in mouse models of GM1 and GM2 gangliosidosis. *Brain* **126**, 974–987 (2003).
66. Wu, Y. P. & Proia, R. L. Deletion of macrophage-inflammatory protein 1α retards neurodegeneration in Sandhoff disease mice. *Proc Natl Acad Sci U S A* **101**, 8425–8430 (2004).
67. Myerowitz, R. *et al.* Molecular pathophysiology in Tay-Sachs and Sandhoff diseases as revealed by gene expression profiling. *Hum Mol Genet* **11**, 1343–1350 (2002).
68. Virgolini, M. J., Feliziani, C., Cambiasso, M. J., Lopez, P. H. & Bollo, M. Neurite atrophy and apoptosis mediated by PERK signaling after accumulation of GM2-ganglioside. *Biochim Biophys Acta Mol Cell Res* **1866**, 225–239 (2019).
69. Wada, R., Tifft, C. J. & Proia, R. L. *Microglial activation precedes acute neurodegeneration in Sandhoff disease and is suppressed by bone marrow transplantation*. *Proceedings of the National Academy of Sciences of the United States of America* vol. 97 10954–10959 (2000).
70. Shirabe, T., Hirokawa, M. & Asaki, H. An Autopsy Case of Tay-Sachs Disease–With Special Reference to Axonal Swellings of the Central Nervous System and Freeze-Fracture Replication Studies of the Membranous Cytoplasmic Bodies. *Psychiatry Clin Neurosci* **34**, 515–523 (1980).
71. Kornfeld, M. Neuropathology of chronic GM2 gangliosidosis due to hexosaminidase A deficiency. *Clin Neuropathol* **27**, 302–308 (2008).

72. Haberland, A., Brunngraber, E., Witting, L. & Brown, B. The White Matter in GM2 Gangliosidosis. *Acta Neuropathol* **24**, 43–55 (1973).
73. Henrie, A. *et al.* ClinVar Miner: Demonstrating Utility of a Web-Based Tool for Viewing and Filtering ClinVar Data. *Hum Mutat* **39**, 1051–1060 (2019).
74. O'Brien, J. S., Tennant, L., Veath, M. L., Scott, C. R. & Bucknall, W. E. Characterization of unusual hexosaminidase A (HEX A) deficient human mutants. *Am J Hum Genet* **30**, 602–608 (1978).
75. Tanaka, A., Sakuraba, H., Isshiki, G. & Suzuki, K. The Major Mutation Among Japanese Patients with Infantile Tay-Sachs Disease: A G-to-T Transversion at the Acceptor Site of Intron 5 of the β-Hexosaminidase α-Gene. *Biochem Biophys Res Commun* **192**, 539–546 (1993).
76. Triggs-Raine, B., Mahuran, D. J. & Gravel, R. A. Naturally occurring mutations in GM2 gangliosidosis: A compendium. in *Advances in Genetics* (eds. Desnick, R. J. & Kaback, M. M.) vol. 44 199–224 (Academic Press Inc., 2001).
77. Hechtman, P. *et al.* More than one mutant allele causes infantile Tay-Sachs disease in French-Canadians. *Am J Hum Genet* **47**, 815–822 (1990).
78. McDowell, G. A., Mules, E. H., Fabacher, P., Shapira, E. & Blitzer, M. G. The presence of two different infantile Tay-Sachs disease mutations in a Cajun population. *Am J Hum Genet* **51**, 1071–1077 (1992).
79. Kaufman, M. *et al.* Tay-Sachs disease and HEXA mutations among Moroccan Jews. *Hum Mutat* **10**, 295–300 (1997).
80. Boles, D. J. & Proia, R. L. The molecular basis of HEXA mRNA deficiency caused by the most common Tay- Sachs disease mutation. *Am J Hum Genet* **56**, 716–724 (1995).
81. Gasperi, D., Sosa, M. A. G., Zelnik, N., Leshinsky, E. & Kolodny, E. H. Late-onset GM2 gangliosidosis: Ashkenazi Jewish family with an exon 5 mutation (Tyr180→His) in the Hex A α-chain gene. *American Academy of Neurology* **47**, 547–552 (1996).
82. Cao, Z., Petroulakis, E., Salo, T. & Triggs-Raine, B. Benign HEXA mutations, C739T(R247W) and C745T(R249W), cause β- hexosaminidase A pseudodeficiency by reducing the α-subunit protein levels. *Journal of Biological Chemistry* **272**, 14975–14982 (1997).
83. Kytzia, H. J., Hinrichs, U., Maire, I., Suzuki, K. & Sandhoff, K. Variant of GM2-gangliosidosis with hexosaminidase A having a severely changed substrate specificity. *EMBO J* **2**, 1201–1205 (1983).
84. Tanaka, A. *et al.* GM2-gangliosidosis B1 variant: Analysis of β-hexosaminidase α gene abnormalities in seven patients. *Am J Hum Genet* **46**, 329–339 (1990).
85. Ribeiro, M. G., Pinto, R. A., Dos Santos, M. R., Maia, M. & Sá Miranda, M. C. Biochemical characterization of β-hexosaminidase in different biological specimens from eleven patients with GM2-gangliosidosis B1 variant. *J Inherit Metab Dis* **14**, 715–720 (1991).
86. Drousiotou, A. *et al.* Sandhoff disease in yprus: Population screening by biochemical and DNA analysis indicates a high frequency of carriers in the Maronite community. *Hum Genet* **107**, 12–17 (2000).
87. Fitterer, B. *et al.* Incidence and carrier frequency of Sandhoff disease in Saskatchewan determined using a novel substrate with detection by tandem mass spectrometry and molecular genetic analysis. *Mol Genet Metab* **111**, 382–389 (2014).

88. Neote, K., McInnes, B., Mahuran, D. J. & Gravel, R. A. Structure and distribution of an Alu-type deletion mutation in Sandhoff disease. *Journal of Clinical Investigation* **86**, 1524–1531 (1990).
89. Dlott, B., D'Azzo, A., Quon, D. V. K. & Neufeld, E. F. Two mutations produce intron insertion in mRNA and elongated β-subunit of human β-hexosaminidase. *Journal of Biological Chemistry* **265**, 17921–17927 (1990).
90. McInnes, B. *et al.* An unusual splicing mutation in the HEXB gene is associated with dramatically different phenotypes in patients from different racial backgrounds. *Journal of Clinical Investigation* **90**, 306–314 (1992).
91. Zhang, Z., Wakamatsu, N., Mules, E. H., Thomas, G. & Gravel, R. A. Impact of premature stop codons on mRNA levels in infantile sandhoff disease. *Hum Mol Genet* **3**, 139–145 (1994).
92. Degasperi, R. *et al.* Substitution of Alanine543 with a Threonine Residue at the Carboxy Terminal End of the β-Chain Is Associated with Thermolabile Hexosaminidase B in a Jewish Family of Oriental Ancestry. *Biochem Mol Med* **56**, 31–36 (1995).
93. Hara, A. *et al.* Adult Sandhoff's disease: R505Q and 1207V substitutions in the HEXB gene of the first Japanese case. *J Neurol Sci* **155**, 86–91 (1998).
94. Hou, Y., McInnes, B., Hinek, A., Karpati, G. & Mahuran, D. A Pro504 → Ser substitution in the β-subunit of β-hexosaminidase A inhibits α-subunit hydrolysis of G(M2) ganglioside, resulting in chronic Sandhoff disease. *Journal of Biological Chemistry* **273**, 21386–21392 (1998).
95. Chen, B., Rigat, B., Curry, C. & Mahuran, D. J. Structure of the GM2A gene: Identification of an exon 2 nonsense mutation and a naturally occurring transcript with an in-frame deletion of exon 2. *Am J Hum Genet* **65**, 77–87 (1999).
96. Xie, B., Wang, W. & Mahuran, D. J. A Cys138-to-Arg substitution in the GM2 activator protein is associated with the AB variant form of GM2 gangliosidosis. *Am J Hum Genet* **50**, 1046–1052 (1992).
97. Matsuda, J. & Suzuki, K. *Lysosomal Storage Disorders*. *Journal of Chemical Information and Modeling* (Springer, 2007).
98. Van Hout, H. Den *et al.* Recombinant human α-glucosidase from rabbit milk in Pompe patients. *Lancet* **356**, 397–398 (2000).
99. Cox, T. *et al.* Novel oral treatment of Gaucher's disease with N-butyldeoxynojirimycin (OGT 918) to decrease substrate biosynthesis. *Lancet* **355**, 1481–1485 (2000).
100. Neufeld, E. F. Lysosomal storage diseases. *Annu Rev Biochem* **60**, 257–280 (1991).
101. Furbish, F. S., Blair, H. E., Shiloach, J., Pentchev, P. G. & Brady, R. O. Enzyme replacement therapy in Gaucher's disease: large-scale purification of glucocerebrosidase suitable for human administration. *Proc Natl Acad Sci U S A* **74**, 3560–3563 (1977).
102. Barton, N. W. *et al.* Replacement Therapy for Inherited Enzyme Deficiency — Macrophage-Targeted Glucocerebrosidase for Gaucher's Disease. *New England Journal of Medicine* vol. 324 1464–1470 Preprint at https://doi.org/10.1056/nejm199105233242104 (1991).
103. Tropak, M. B. *et al.* Construction of a hybrid β-hexosaminidase subunit capable of forming stable homodimers that hydrolyze GM2 ganglioside in vivo. *Mol Ther Methods Clin Dev* **3**, 15057 (2016).

104. Schwering, C. *et al.* Development of the "Hamburg Best Practice Guidelines for ICV−Enzyme Replacement therapy (ERT) in CLN2 Disease" Based on 6 Years Treatment Experience in 48 Patients. *J Child Neurol* **36**, 635–641 (2021).
105. Ou, L., Przybilla, M. J., Koniar, B. & Whitley, C. B. RTB lectin-mediated delivery of lysosomal α-L-iduronidase mitigates disease manifestations systemically including the central nervous system. *Mol Genet Metab* **123**, 105–111 (2018).
106. Condori, J. *et al.* Enzyme replacement for GM1-gangliosidosis: Uptake, lysosomal activation, and cellular disease correction using a novel β-galactosidase: RTB lectin fusion. *Mol Genet Metab* **117**, 199–209 (2016).
107. Liu, L., Lee, W. S., Doray, B. & Kornfeld, S. Engineering of GlcNAc-1-Phosphotransferase for Production of Highly Phosphorylated Lysosomal Enzymes for Enzyme Replacement Therapy. *Mol Ther Methods Clin Dev* **5**, 59–65 (2017).
108. Platt, F. M. & Lachmann, R. H. Treating lysosomal storage disorders: Current practice and future prospects. *Biochim Biophys Acta Mol Cell Res* **1793**, 737–745 (2009).
109. Hoogerbrugge, P. M. *et al.* Allogeneic bone marrow transplantation for lysosomal storage diseases. *The Lancet* **345**, 1398–1402 (1995).
110. Escolar, M. L. *et al.* Transplantation of Umbilical-Cord Blood in Babies with Infantile Krabbe's Disease. *New England Journal of Medicine* **352**, 2069–2081 (2005).
111. Mistry, P. K. *et al.* Effect of oral eliglustat on splenomegaly in patients with Gaucher disease type 1: The ENGAGE randomized clinical trial. *JAMA - Journal of the American Medical Association* **313**, 695–706 (2015).
112. Marshall, J. *et al.* Substrate Reduction Therapy for Sandhoff Disease through Inhibition of Glucosylceramide Synthase Activity. *Molecular Therapy* **27**, 1495–1506 (2019).
113. Chiricozzi, E. *et al.* Chaperone Therapy for GM2 Gangliosidosis: Effects of Pyrimethamine on β-Hexosaminidase Activity in Sandhoff Fibroblasts. *Mol Neurobiol* **50**, 159–167 (2014).
114. Maegawa, G. H. B. *et al.* Pyrimethamine as a potential pharmacological chaperone for late-onset forms of GM2 gangliosidosis. *Journal of Biological Chemistry* **282**, 9150–9161 (2007).
115. Osher, E. *et al.* Pyrimethamine increases β-hexosaminidase A activity in patients with Late Onset Tay Sachs. *Mol Genet Metab* **102**, 356–363 (2011).
116. Osher, E. *et al.* Effect of cyclic, low dose pyrimethamine treatment in patients with Late Onset Tay Sachs: An open label, extended pilot study. *Orphanet J Rare Dis* **10**, 1–7 (2015).
117. Udwadia-Hegde, A. & Hajirnis, O. Temporary Efficacy of Pyrimethamine in Juvenile-Onset Tay-Sachs Disease Caused by 2 Unreported HEXA Mutations in the Indian Population. *Child Neurol Open* **4**, 2329048X1668788 (2017).
118. Guidotti, J. E. *et al.* Adenoviral gene therapy of the Tay-Sachs disease in hexosaminidase A-deficient knock-out mice. *Hum Mol Genet* **8**, 831–838 (1999).
119. Dogbevia, G., Grasshoff, H., Othman, A., Penno, A. & Schwaninger, M. Brain endothelial specific gene therapy improves experimental Sandhoff disease. *Journal of Cerebral Blood Flow and Metabolism* **40**, 1338–1350 (2020).
120. Gray-Edwards, H. *et al.* Adeno-Associated Virus Gene Therapy in a Sheep Model of Tay-Sachs Disease. *Hum Gene Ther* **29**, 312–326 (2018).

121. McCurdy, V. J. *et al.* Widespread correction of central nervous system disease after intracranial gene therapy in a feline model of Sandhoff disease. *Gene Ther* **22**, 181–189 (2015).
122. Woodley, E. *et al.* Efficacy of a Bicistronic Vector for Correction of Sandhoff Disease in a Mouse Model. *Mol Ther Methods Clin Dev* **12**, 47–57 (2019).
123. Niemir, N. *et al.* Intravenous administration of scAAV9-Hexb normalizes lifespan and prevents pathology in sandhoff disease mice. *Hum Mol Genet* **27**, 954–968 (2018).
124. Beegle, J., Hendrix, K., Maciel, H., Nolta, J. A. & Anderson, J. S. Improvement of motor and behavioral activity in Sandhoff mice transplanted with human CD34+ cells transduced with a HexA/HexB expressing lentiviral vector. *Journal of Gene Medicine* **22**, 1–13 (2020).
125. Lahey, H. G. *et al.* Pronounced Therapeutic Benefit of a Single Bidirectional AAV Vector Administered Systemically in Sandhoff Mice. *Molecular Therapy* **28**, 2150–2160 (2020).
126. Martino, S. *et al.* A direct gene transfer strategy via brain internal capsule reverses the biochemical defect in Tay-Sachs disease. *Hum Mol Genet* **14**, 2113–2123 (2005).
127. Walia, J. S. *et al.* Long-term correction of Sandhoff disease following intravenous delivery of rAAV9 to mouse neonates. *Molecular Therapy* **23**, 414–422 (2015).
128. Choudhury, S. R. *et al.* Widespread central nervous system gene transfer and silencing after systemic delivery of novel AAV-AS vector. *Molecular Therapy* **24**, 726–735 (2016).
129. Karumuthil-Melethil, S. *et al.* Novel Vector Design and Hexosaminidase Variant Enabling Self-Complementary Adeno-Associated Virus for the Treatment of Tay-Sachs Disease. *Hum Gene Ther* **27**, 509–521 (2016).
130. Lawson, C. A. & Martin, D. R. Animal models of GM2 gangliosidosis: utility and limitations. *Appl Clin Genet* **9**, 111–120 (2016).
131. Cavender, C. *et al.* Natural history study of glycan accumulation in large animal models of GM2 gangliosidoses. *PLoS One* **15**, 1–25 (2020).
132. Sango, K. *et al.* Mouse models of Tay-Sachs and Sandhoff diseases differ in neurolgoical phenotype and ganglioside metabolism. *Nat Genet* **11**, 170–176 (1995).
133. Cohen-Tannoudji, M. *et al.* Disruption of murine Hexa gene leads to enzymatic deficiency and to neuronal lysosomal storage, similar to that observed in Tay-Sachs disease. *Mammalian Genome* **6**, 844–849 (1995).
134. Phaneuf, D. *et al.* Dramatically different phenotypes in mouse models of human Tay-Sachs and Sandhoff diseases. *Hum Mol Genet* **5**, 1–14 (1996).
135. Miklyaeva, E. I. *et al.* Late onset Tay-Sachs disease in mice with targeted disruption of the Hexa gene: Behavioral changes and pathology of the central nervous system. *Brain Res* **1001**, 37–50 (2004).
136. Liu, Y. *et al.* Mouse model of G M2 activator deficiency manifests cerebellar pathology and motor impairment. *Medical Sciences* **94**, 8138–8143 (1997).
137. Seyrantepe, V. *et al.* Murine Sialidase Neu3 facilitates GM2 degradation and bypass in mouse model of Tay-Sachs disease. *Exp Neurol* **299**, 26–41 (2018).
138. Demir, S. A., Timur, Z. K., Ateş, N., Martínez, L. A. & Seyrantepe, V. GM2 ganglioside accumulation causes neuroinflammation and behavioral alterations in a mouse model of early onset Tay-Sachs disease. *J Neuroinflammation* **17**, 1–18 (2020).
139. Bradbury, A. M. *et al.* A review of gene therapy in canine and feline models of lysosomal storage disorders. *Hum Gene Ther Clin Dev* **26**, 27–37 (2015).

140. Martin, D. R. *et al.* An inversion of 25 base pairs causes feline GM2 gangliosidosis variant 0. *Exp Neurol* **187**, 30–37 (2004).
141. Torres, P. A. *et al.* Tay-Sachs disease in Jacob sheep. *Mol Genet Metab* **101**, 357–363 (2010).
142. Qin, W. *et al.* Efficient CRISPR/cas9-mediated genome editing in mice by zygote electroporation of nuclease. *Genetics* **200**, 423–430 (2015).
143. Müllenbach, R., Lagoda, P. & Welter, C. An Efficient Salt-Chloroform Extraction of DNA from blood and tissues. *Trend in Genetics* **5**, 391 (1989).
144. Miedel, C. J., Patton, J. M., Miedel, A. N., Miedel, E. S. & Levenson, J. M. Assessment of spontaneous alternation, novel object recognition and limb clasping in transgenic mouse models of amyloid-β and tau neuropathology. *Journal of Visualized Experiments* **2017**, 1–8 (2017).
145. Allen Institute for Brain Science. Allen Mouse Brain Atlas: Saggital Mouse Brain Reference. mouse.brain-map.org (2011).
146. Richards, M. R., Guo, T., Hunter, C. D. & Cairo, C. W. Molecular dynamics simulations of viral neuraminidase inhibitors with the human neuraminidase enzymes: Insights into isoenzyme selectivity. *Bioorg Med Chem* **26**, 5349–5358 (2018).
147. Lalonde, R. & Strazielle, C. Brain regions and genes affecting limb-clasping responses. *Brain Res Rev* **67**, 252–259 (2011).
148. McManamny, P. *et al.* A mouse model of spinal and bulbar muscular atrophy. *Hum Mol Genet* **11**, 2103–2111 (2002).
149. Lorden, J. F., Mckeon, T. W., Baker, H. J., Cox, N. & Walkley, S. U. Characterization of the rat mutant dystonic (dt): A new animal model of dystonia musculorum deformans. *Journal of Neuroscience* **4**, 1925–1932 (1984).
150. Treuting, P. M., Frevert, C. W., Liggitt, D. & Dintzis, S. M. *The Nervous System*. *Comparative Anatomy and Histology : a Mouse and Human Atlas* (Elsevier Science, 2011). doi:10.1016/B978-012369454-6/50055-8.
151. Seibenhener, M. L. & Wooten, M. C. Use of the open field maze to measure locomotor and anxiety-like behavior in mice. *Journal of Visualized Experiments* **96**, 1–6 (2015).
152. Lister, R. G. Ethologically-based animal models of anxiety disorders. *Pharmacol Ther* **46**, 321–340 (1990).
153. Prut, L. & Belzung, C. The open field as a paradigm to measure the effects of drugs on anxiety-like behaviors: A review. *Eur J Pharmacol* **463**, 3–33 (2003).
154. Kulesskaya, N. & Voikar, V. Assessment of mouse anxiety-like behavior in the light-dark box and open-field arena: Role of equipment and procedure. *Physiol Behav* **133**, 30–38 (2014).
155. Modigliani, R. *et al.* Diarrhea and Autonomic Dysfunction in a Patient with Hexosaminidase B Deficiency (Sandhoff disease). *Gastroenterology* **106**, 775–781 (1994).
156. Wang, S. Z. *et al.* A novel HEXB mutation and its structural effects in juvenile Sandhoff disease. *Mol Genet Metab* **95**, 236–238 (2008).
157. Beccari, T., Hoade, J., Orlacchio, A. & Stirling, J. L. Cloning and sequence analysis of a cDNA encoding the α-subunit of mouse β-N-acetylhexosaminidase and comparison with the human enzyme. *Biochemical Journal* **285**, 593–596 (1992).

158. Brown, C. A. & Mahuran, D. J. β-Hexosaminidase isozymes from cells cotransfected with α and β cDNA constructs: Analysis of the α-subunit missense mutation associated with the adult form of Tay-Sachs disease. *Am J Hum Genet* **53**, 497–508 (1993).
159. Albohy, A., Li, M. D., Zheng, R. B., Zou, C. & Cairo, C. W. Insight into substrate recognition and catalysis by the human neuraminidase 3 (NEU3) through molecular modeling and site-directed mutagenesis. *Glycobiology* **20**, 1127–1138 (2010).
160. Li, S. C., Li, Y. T., Moriya, S. & Miyagi, T. Degradation of GM1 and GM2 by mammalian sialidases. *Biochemical Journal* **360**, 233–237 (2001).
161. Papini, N. *et al.* The Plasma Membrane-associated Sialidase MmNEU3 Modifies the Ganglioside Pattern of Adjacent Cells Supporting Its Involvement in Cell-to-Cell Interactions. *Journal of Biological Chemistry* **279**, 16989–16995 (2004).
162. Anastasia, L. *et al.* NEU3 sialidase strictly modulates GM3 levels in skeletal myoblasts C2C12 thus favoring their differentiation and protecting them from apoptosis. *Journal of Biological Chemistry* **283**, 36265–36271 (2008).
163. Miyagi, T. & Yamamoto, K. Sialidase NEU3 and its pathological significance. *Glycoconj J* **39**, 677–683 (2022).
164. Abo-ouf, H. *et al.* Deletion of tumor necrosis factor-α ameliorates neurodegeneration in sandhoff disease mice. *Hum Mol Genet* **22**, 3960–3975 (2013).
165. White, E. J., Trigatti, B. L. & Igdoura, S. A. Suppression of NK and CD8+ T cells reduces astrogliosis but accelerates cerebellar dysfunction and shortens life span in a mouse model of Sandhoff disease. *J Neuroimmunol* **306**, 55–67 (2017).
166. Kyrkanides, S. *et al.* Peripheral blood mononuclear cell infiltration and neuroinflammation in the HexB−/− mouse model of neurodegeneration. *J Neuroimmunol* **203**, 1–7 (2008).
167. Ou, L. *et al.* A novel gene editing system to treat both Tay–Sachs and Sandhoff diseases. *Gene Ther* **27**, 226–236 (2020).